

2013-12-13

Indirect Measurement of Fractional Impedances

Freeborn, Todd

Freeborn, T. (2013). Indirect Measurement of Fractional Impedances (Doctoral thesis, University of Calgary, Calgary, Canada). Retrieved from <https://prism.ucalgary.ca>. doi:10.11575/PRISM/26504
<http://hdl.handle.net/11023/1195>

Downloaded from PRISM Repository, University of Calgary

THE UNIVERSITY OF CALGARY

Indirect Measurement of Fractional Impedances

by

Todd Freeborn

A THESIS

SUBMITTED TO THE FACULTY OF GRADUATE STUDIES IN PARTIAL
FULFILLMENT OF THE REQUIREMENTS FOR THE DEGREE OF
DOCTOR OF PHILOSOPHY

DEPARTMENT OF ELECTRICAL AND COMPUTER ENGINEERING

CALGARY, ALBERTA

DECEMBER, 2013

© Todd Freeborn 2013

ABSTRACT

This thesis investigates the measurement of fractional-order parameters that describe the electrical impedance of tissues and devices without requiring direct impedance measurements. Concepts from fractional calculus are imported to develop fractional circuit theory and derive the voltage and current excited step responses and magnitude responses of the single-dispersion Cole impedance model which is widely used in biomedicine and biology. Using these responses a numerical graph-fitting and non-linear least squares fitting routine have been applied to MATLAB simulations to assess the accuracy of this approach to extract the fractional impedance parameters that describe this model. Experimentally collected data from fruit tissues and ideal Cole models validate these methods.

These fractional calculus concepts are further applied to develop the circuit theory to describe the current excited step response and magnitude response of the double-dispersion Cole impedance model. MATLAB and PSPICE simulations of assess the accuracy of this approach to extract the fractional impedance parameters that describe this model. Experimentally collected data from the current-excited step response and voltage excited magnitude response of apples validates these methods.

Finally, the fractional circuit theory is applied to develop the expression for the voltage-excited step-response of a fractional model for a supercapacitor which is then used with non-linear least squares method extract the impedance parameters that characterize the model. This method is validated experimentally using results collected from low capacity supercapacitors with manufacturer ratings of 0.33 F, 1 F, and 1.5 F and high capacity supercapacitors with 1500 F and 3000 F manufacturer ratings.

ACKNOWLEDGEMENTS

This thesis has been possible due to the guidance and support offered by many people throughout my time in graduate studies. First, I would like to take this moment to truly thank my supervisor, Dr. Brent Maundy, for all the time he has given me through the years in the pursuit of my PhD. Thank you for introducing me to the field of fractional circuits and systems and giving me the space and independence to put my small mark on this field. I could not have asked for a better supervisor.

I also cannot thank Dr. Ahmed Elwakil from the Department of Electrical and Computer Engineering at the University of Sharjah in the United Arab Emirates enough. Without the reviews and insightful guidance offered regarding my research I could never have completed this work. Our discussions regarding fractional circuits and systems and more generally research have definitely shaped my approach to research and how important I view this emerging field. Also, the chance to work together at the University of Sharjah in January 2013 is an experience I will always be grateful for.

The support of my parents, Don and Sherry Freeborn, has been vitally important to all of my academic pursuits. Thanks for being a constant and unwavering source of support for all these years and thanks for listening even when it sounded like I was speaking another language.

I am also very grateful for the graduate student scholarships offered by the provincial and federal governments. Without the financial support of the Alberta Innovates - Technology Futures and NSERC post-graduate scholarships I would never have been able to undertake this research.

For my grandparents,

Doug and Elva Freeborn.

Thanks for the push to get my doctorate,
even though it doesn't make me a "real" doctor.

TABLE OF CONTENTS

Abstract	ii
Acknowledgments	iii
Dedication	iv
Table of Contents	v
List of Tables	viii
List of Figures	ix
1 INTRODUCTION	1
1.1 Fractional Calculus	1
1.1.1 Fractional Laplace Transform Operator	3
1.2 Fractional Models and Applications	5
1.2.1 Cole Impedance Models	6
1.2.2 Fractional Plant Models	9
1.2.3 Electrode Tissue Interface Model	11
1.2.4 Fractional Respiratory Model	13
1.2.5 Fractional Supercapacitor Models	14
1.3 Extraction Methods	16
1.4 Research Objectives	17
1.5 Thesis Overview	18
2 SINGLE DISPERSION COLE IMPEDANCE MODEL	20
2.1 Numerical Extraction from Step Response	21
2.1.1 Comparison to Step Response when $\alpha = 1$	22
2.1.2 Extraction from Voltage-Excited Step Response	24
2.1.3 Extraction from Ideal Simulated Datasets	29
2.1.4 PSPICE and Experimental Results	31

2.1.5	Limitations	34
2.2	Least Squares Extraction from Step Response	36
2.2.1	Voltage Excited Step Response	38
2.2.2	Current Excited Step Response	40
2.2.2.1	Simulation Results	42
2.2.2.2	Experimental Results	44
2.3	Least Squares Extraction from Magnitude Response	45
2.3.1	Effects of Low and High Frequency Gain Errors	48
2.3.2	Least Squares Extraction Method	51
2.3.2.1	Simulation Results	51
2.3.2.2	Experimental Results	53
2.4	Contribution	55
3	DOUBLE DISPERSION COLE IMPEDANCE MODEL	57
3.1	Least Squares Extraction from Current Excited Step Response	58
3.1.1	Simulation Results	61
3.1.2	Experimental Results	63
3.2	Least Squares Extraction from Magnitude Response	65
3.2.1	MATLAB Simulation Results	68
3.2.2	PSPICE Simulation Results	71
3.2.3	Experimental Results	76
3.3	Contribution	78
4	FRACTIONAL SUPERCAPACITOR IMPEDANCE MODEL	80
4.1	Fractional Capacitors	81
4.1.1	Measurement with a Wien Bridge	82
4.2	Charging and Discharging of Supercapacitors	84
4.3	Simulation Results	86
4.4	Experimental Results	89
4.4.1	1 F Supercapacitor Comparison	94
4.4.2	Voltage Dependence	97
4.4.3	High Capacity Supercapacitors	99
4.5	Fractional Multivibrator	101
4.6	Contribution	105
5	CONCLUSIONS AND FUTURE WORK	106
5.1	Conclusion	106

5.2	Contribution	107
5.3	Future Work	108
BIBLIOGRAPHY		109
A	EXTRACTION OF IMPEDANCE PARAMETERS IN MATLAB	123
A.1	Cole Impedance Models	123
A.1.1	Voltage-Excited Single Dispersion Step Response Numerical Ex- traction	123
A.1.2	Voltage-Excited Single Dispersion Step Response NLSF Extraction	127
A.1.3	Current-Excited Single-Dispersion Step Response NLSF Extraction	129
A.1.4	Current-Excited Double-Dispersion Step Response NLSF Extraction	131
A.1.5	Magnitude Single-Dispersion NLSF Extraction	134
A.1.6	Magnitude Double-Dispersion NLSF Extraction	136
A.2	Supercapacitor Model	139
A.2.1	Voltage-Excited Step Response NLSF Extraction	139
B	SIMPLIFIED CURRENT-EXCITED STEP-RESPONSE DERIVATION	141
B.1	MATLAB Simulated Extractions	143
C	APPROXIMATED CONSTANT PHASE ELEMENT	146
D	SUPERCAPACITOR STEP-RESPONSE TEST CIRCUITS	151

LIST OF TABLES

2.1	Numerically calculated slopes in V/decade using (2.14) for values of α from 0.2 to 1.0 in steps of 0.2 while varying C from $0.001 \mu\text{F}$ to $1 \mu\text{F}$ in decade steps with $R = R_\infty = R_1 = 1 \text{ k}\Omega$ and an input step of 1 V.	26
2.2	Numerical calculation of V_M , t_{VM} , and ΔT_M using (2.5) while varying values of C for $\alpha = 0.8$ and $R = R_\infty = R_1 = 1 \text{ k}\Omega$	28
2.3	Numerically extracted Cole impedance parameters and relative errors from simulated step responses using previously extracted fruit parameters.	29
2.4	Theoretical and numerically extracted Cole impedance parameters with relative errors from PSPICE simulated step response for an ideal capacitor ($\alpha = 1$).	32
2.5	Measured and numerically extracted Cole impedance parameters with relative errors from experimentally collected step response.	33
2.6	Relative errors of parameters extracted from simulated step responses for different measured values of $v_o(0)$	37
2.7	Absolute relative errors from simulated responses of fruit tissues from $1 \mu\text{s}$ to 1 s.	39
2.8	NLSF extracted Cole impedance parameters from experimentally collected step responses of fruit.	40
2.9	Average relative error of impedance parameters extracted from 100 MATLAB simulations of the single dispersion step response with 0.5%, 1%, and 2% random noise.	43
2.10	Parameters from (2.30) for the filter and integrator circuits of Fig. 2.17(a) and (b), respectively.	47
2.11	Relative extracted errors from direct and NLSF methods applied to simulated apricot, apple, kiwi and potato frequency responses in the circuit of Fig. 2.17(a).	52

2.12	Impedance parameters extracted with direct and NLSF methods from experimentally collected apricot and apple frequency responses in the circuit of Fig. 2.17(a)	54
3.1	Average relative error of impedance parameters extracted from 100 MATLAB simulations of the double dispersion step response with 0.5%, 1%, and 2% random noise.	62
3.2	Single and double dispersion impedance parameters extracted from step responses of apples 1 and 2 using NLSF.	64
3.3	Magnitude response coefficients of the circuit in Fig. 3.8 given by (3.7). . .	66
3.4	Average relative error of double dispersion Cole impedance parameters extracted from 100 MATLAB simulations of (3.7) with 30 dB to 80 dB SNR Gaussian white noise.	69
3.5	Values to realize 10 th order approximated fractional capacitors with values $C = 3.086 \mu\text{F}$, $\alpha = 0.507$ and $C = 89.29 \mu\text{F}$, $\alpha = 0.766$ centered at $f = 60$ kHz.	74
4.1	Theoretical extractions of capacitance and series resistance of a fractional capacitor in a classic Wien Bridge circuit.	84
4.2	Manufacturer part numbers for 0.33, 1, and 1.5 F rated supercapacitors from Panasonic, Elna, and Cooper-Bussmann.	92
4.3	Fractional parameters extracted using NLSF method from supercapacitors with (a) 0.33, (b) 1, and (c) 1.5 F rated capacitance.	93
4.4	Fractional impedance parameters extracted from 330 mF panasonic supercapacitor from initial voltages of 0.5 V to 4 V in 0.5 V steps.	98
B.1	Average relative errors and extraction times of impedance parameters using (B.3) and (B.2) from 1000 MATLAB simulated step responses of an apricot with 50 dB SNR Gaussian white noise.	144
C.1	Component values to realize 4 th order approximations of fractional order capacitors with a center frequency of 1 kHz.	148
D.1	Components, part-numbers, and descriptions of components to populate high capacity supercapacitor test PCBs.	152

LIST OF FIGURES

1.1	First order and 1/2 order derivatives of the function $f(x) = \cos(x)$	3
1.2	Bode plots of s^α when $\alpha = 0.2, 0.4, 0.6, 0.8$, and 1.	5
1.3	Theoretical (a) single dispersion and (b) double dispersion Cole impedance models.	6
1.4	Lumped circuits for modelling (a) bark and (b) wood to compare against a fractional circuit model.	10
1.5	Fractional impedance model to fit root/stem/electrode interface of willows grown to monitor root growth.	11
1.6	Fractional order model to analyze moisture gradients of wood.	11
1.7	(a) Tissue-electrode circuit model for a unit surface area and (b) simplified distributed fractional order model.	12
1.8	Fractional order impedance model of the respiratory system of humans proposed.	13
1.9	Theoretical fractional impedance model of a supercapacitor.	15
1.10	Impedance loci used to graphically extract the single dispersion Cole impedance parameters.	16
2.1	Theoretical single-dispersion Cole impedance model.	20
2.2	Theoretical circuits to apply a (a) voltage-step and (b) current-step input to the single dispersion Cole impedance model.	21
2.3	Comparison of MATLAB simulated output voltage of step (a) voltage-excited and (b) current-excited Cole impedance when $\alpha = 1$ using Mittag-Leffler functions and traditional expressions, shown as black circles and solid lines, respectively.	24
2.4	Comparison of slope of the step response of Fig. 2.2(a) for varying values of α from 0.6 to 1.0 in steps of 0.1 with $R = R_\infty = R_1 = 1 \text{ k}\Omega$ and $C = 1 \text{ }\mu\text{F}$, respectively.	26

2.5	Comparison of location of V_M of the step response of Fig. 2.2(a) for varying values of C from $0.001\ \mu\text{F}$ to $1\ \mu\text{F}$ in decade steps with fixed resistors and α values of $1\ \text{k}\Omega$ and 0.8 , respectively.	27
2.6	Pseudo-algorithm to numerically extract the Cole impedance parameters from the step response data.	30
2.7	MATLAB simulated step responses using theoretical and extracted Cole impedance parameters of an apricot as a solid line and black circles, respectively, with $R = 1\ \text{k}\Omega$ and $V_{cc} = 5\ \text{V}$	32
2.8	PSPICE and MATLAB simulated step responses using theoretical and numerically extracted Cole impedance parameters as solid and dashed lines, respectively, with $R = 1\ \text{k}\Omega$ and $V_{cc} = 5\ \text{V}$	33
2.9	Experimental and MATLAB simulated step responses using numerically extracted Cole impedance parameters as solid and dashed lines, respectively, with $R = 0.996\ \text{k}\Omega$ and $V_{cc} = 5\ \text{V}$	34
2.10	Lower divider, charging, and upper divider regions common to all step responses of the circuit in Fig. 2.2.	35
2.11	Minimum sampling time required for R_∞ extraction within 5% for $0.5 \leq \alpha \leq 1$ and $1\ \text{pF} \leq C \leq 1\ \mu\text{F}$ when $R = R_\infty = R_1 = 1\ \text{k}\Omega$	36
2.12	Experimental (solid) and MATLAB simulated (dashed) step responses of Fig. 2.2(a) when $(R_\infty, R_1, \alpha, C) = (1.753\ \text{k}\Omega, 32\ \text{k}\Omega, 1, 1\ \mu\text{F})$	40
2.13	Experimental (solid) and MATLAB simulated (dashed) step responses using an (a) apple and (b) tomato in the circuit of Fig. 2.2(a).	41
2.14	MATLAB simulated step responses of single dispersion Cole impedance model excited by a step current of $0.1\ \text{mA}$ when $R_\infty = 406\ \Omega$, $R_1 = 12.894\ \text{k}\Omega$, $C = 62.34\ \text{nF}$, and $\alpha = 0.739$. Ideal simulations with 0.5% noise are given as a solid line with the simulations using the extracted parameters given as circles.	44
2.15	Test circuit to apply a current-step input to a single dispersion Cole impedance with the AD844 operating as a current conveyor.	45
2.16	(a) Experimentally collected step responses of apple 1 (solid) and apple 2 (dashed) compared to MATLAB simulated responses using extracted impedance parameters (black circles) and (b) absolute relative errors of apple 1 and 2 simulated responses compared to the experimental.	46
2.17	Circuits for (a) filter and (b) integrator extraction of the Cole model parameters.	47

2.18	Effect of relative errors of (a) G_1 and $-G_2$ (filter circuit) and (b) $-G_1$ and G_2 (integrator circuit) up to 3.5% on relative errors of extracted ω_{3dB} , $\omega_{\phi max}$, α and τ from simulated frequency response using known impedance parameters of an apricot and load resistor $R_L = 1 \text{ k}\Omega$	50
2.19	Simulated frequency responses using parameters extracted using non-linear fitting (black circles) and direct methods (dashed) from an ideal frequency response using known apricot parameters (solid).	52
2.20	Simulated frequency responses using parameters extracted using non-linear fitting (black circles) and direct methods (dashed) from an ideal frequency response using known apricot parameters with white gaussian noise (solid).	53
2.21	Test circuit to collect the magnitude response of a single-dispersion Cole impedance.	54
2.22	Simulated frequency responses using parameters extracted using non-linear fitting (black circles) and direct methods (dashed) from experimentally collected frequency response of an apricot (solid) as the Cole impedance in the circuit of Fig. 2.17(a) with $R_L = 1 \text{ k}\Omega$	55
3.1	Theoretical double-dispersion Cole impedance model.	57
3.2	Theoretical circuit to apply a step-current input to the double-dispersion Cole impedance model.	58
3.3	MATLAB simulated step response double dispersion Cole impedance model excited by a step current of 0.1 mA when $R_\infty = 406 \text{ }\Omega$, $R_1 = 12.894 \text{ k}\Omega$, $R_2 = 2.5 \text{ k}\Omega$, $C_1 = 62.34 \text{ nF}$, $C_2 = 100 \text{ }\mu\text{F}$, $\alpha_1 = 0.739$, $\alpha_2 = 0.55$. Ideal simulations with 0.5% noise are given as a solid line with the simulations using the extracted parameters given as circles.	59
3.4	Evolution of the average relative error of 100 MATLAB simulations with 15 randomly generated initial guesses applied to the NLSF of the double dispersion step response datasets with impedance parameters $R_\infty = 406 \text{ }\Omega$, $R_1 = 12.894 \text{ k}\Omega$, $R_2 = 2.5 \text{ k}\Omega$, $C_1 = 62.34 \text{ nF}$, $C_2 = 100 \text{ }\mu\text{F}$, $\alpha_1 = 0.739$, $\alpha_2 = 0.55$ and 0.5% random noise.	61
3.5	Test circuit to apply a current-step input to a double dispersion Cole impedance with the AD844 operating as a current conveyor.	63
3.6	(a) Experimental step response of Apple 1 compared to simulated responses using extracted single (rectangles) and double (black circles) dispersion parameters and (b) absolute relative errors.	64

3.7	(a) Experimental step response of Apple 2 compared to simulated responses using extracted single (rectangles) and double (black circles) dispersion parameters and (b) absolute relative errors.	65
3.8	Theoretical circuit for the collection of the magnitude response of the double dispersion Cole impedance.	66
3.9	MATLAB simulated magnitude response of (3.7) when $[R_\infty, R_1, R_2, \alpha_1, \alpha_2, C_1, C_2] = [885 \Omega, 899 \Omega, 626 \Omega, 0.5414, 0.7653, 19 \text{ nF}, 5.1 \mu\text{F}]$ and $R_L = 100 \Omega, 200 \Omega$, and 500Ω	67
3.10	Evolution of the average relative error of 100 MATLAB simulations with 20 randomly generated initial guesses applied to the NLSF of the magnitude datasets with impedance parameters $R_\infty = 42.9 \Omega$, $R_1 = 71.6 \Omega$, $R_2 = 16.5 \Omega$, $\alpha_1 = 0.507$, $\alpha_2 = 0.766$, $C_1 = 3.086 \mu\text{F}$, $C_2 = 89.29 \mu\text{F}$ and 60 dB SNR Gaussian white noise.	69
3.11	MATLAB simulated (a) magnitude and (b) error plots of a double dispersion Cole impedance (solid) with impedance parameters $R_\infty = 42.9 \Omega$, $R_1 = 71.6 \Omega$, $R_2 = 16.5 \Omega$, $\alpha_1 = 0.507$, $\alpha_2 = 0.766$, $C_1 = 3.086 \mu\text{F}$, $C_2 = 89.29 \mu\text{F}$ when $R_L = 100 \Omega$ with 60 dB SNR Gaussian white noise compared to the response using the extracted parameters (circles).	70
3.12	(a) Evolution of the average relative error of 100 MATLAB simulations with 60 randomly generated initial guesses applied to the NLSF with magnitude datasets randomly generated such that $R_{\infty,1,2} \leq 1 \text{ k}\Omega$, $0.5 \leq \alpha_{1,2} \leq 1$, $0.1 \text{ nF} \leq C_{1,2} \leq 1 \text{ mF}$ with 60 dB SNR Gaussian white and (b) simulated dataset with parameters $[R_\infty, R_1, R_2, \alpha_1, \alpha_2, C_1, C_2] = [885 \Omega, 899 \Omega, 626 \Omega, 0.5414, 0.7653, 19 \text{ nF}, 5.1 \mu\text{F}]$, $R_L = 100 \Omega$ and 60 dB SNR Gaussian white noise (solid) compared to simulations using extracted parameters (circles).	72
3.13	(a) RC ladder structure to realize a n^{th} order integer approximation of a CPE and (b) the error of 10^{th} order approximated fractional capacitors with values $C = 3.086 \mu\text{F}$, $\alpha = 0.507$ (solid) and $C = 89.29 \mu\text{F}$, $\alpha = 0.766$ (dashed) centered at $f = 60 \text{ kHz}$	73
3.14	Circuit simulated in PSPICE to collect the magnitude response of a double-dispersion Cole impedance parameters implemented using RC ladder approximations of the CPEs.	74

3.15	(a) Simulated ideal (solid), PSPICE (dashed) magnitude responses when ($R_\infty = 42.9 \, \Omega$, $R_1 = 71.6 \, \Omega$, $R_2 = 16.5 \, \Omega$, $\alpha_1 = 0.507$, $\alpha_2 = 0.766$, $C_1 = 3.086 \, \mu\text{F}$, $C_2 = 89.29 \, \mu\text{F}$) and $R_L = 100 \, \Omega$ compared to the simulated response using the extracted parameters (circles) and (b) relative errors of the PSPICE simulation compared to the ideal (squares) and simulated response using the extracted parameters compared to the PSPICE response (circles).	75
3.16	Experimental circuit to collect the magnitude response of a double-dispersion Cole impedance parameters using apples as the Cole impedance model.	76
3.17	Experimentally collected step responses of (a) apple 1 (solid) and (b) apple 2 (dashed) compared to MATLAB simulated responses using extracted impedance parameters (circles and squares) and (c) relative errors of apple 1 (circles) and 2 (squares) simulated responses compared to the experimental.	77
4.1	Theoretical fractional impedance model of a supercapacitor.	80
4.2	(a) Parallel and (b) series connection of n fractional capacitors.	81
4.3	Wien bridge circuit to determine the capacitance of series resistance of a capacitor.	82
4.4	Circuit to apply a step-voltage input to the fractional model of a supercapacitor.	84
4.5	MATLAB simulations of the charging of Fig. 4.4 using (4.13) for $\alpha = 0.25$, 0.5 , 0.75 , and 1 when $C_\alpha = 1 \, \text{F}$, $R_s = 30 \, \Omega$, $R = 180 \, \Omega$, $V_{cc} = 5 \, \text{V}$	86
4.6	Average relative error of extracted parameters from 1000 MATLAB simulated step responses when $C_\alpha = 1 \, \text{F/s}^{1-\alpha}$, $R_s = 30 \, \Omega$, and $\alpha = 0.5$, 0.75 , and 1 with 40 to 80 dB SNR Gaussian white noise.	88
4.7	MATLAB simulated step responses with 60 dB SNR Gaussian white noise (dots) and simulated response using estimated parameters (squares) for $\alpha = 0.25$, 0.5 , 0.75 , and 1 when $C_\alpha = 1 \, \text{F/s}^{1-\alpha}$, $R_s = 30 \, \Omega$	88
4.8	(a) Test circuit and (b) physical implementation to apply a step-voltage input to a supercapacitor to collect the output step response.	89
4.9	Buffered step input $\hat{v}_{in}(t)$ (solid) and charging supercapacitor (dashed) waveforms to validate that the OPA544 op amp is operating in its linear region.	90
4.10	Experimentally collected step responses of (a) 0.33, (b) 1, and (c) 1.5 F Panasonic, Elna, and Cooper-Bussmann brand supercapacitors.	91
4.11	Experimentally collected step response of the 1 F, Panasonic(1) supercapacitor (solid) and the MATLAB simulated response using the estimated fractional (black circles) and integer (dashed) parameters.	94

4.12	Absolute relative error of the (a) 0.33, (b) 1, and (c) 1.5 F simulated step responses using the estimated parameters in Table 4.3 compared to the experimental results of Fig. 4.10.	95
4.13	(a) Step responses collected from (b) 1 F rated capacitors from Cooper-Bussmann with part numbers KR-5R5V105-R, PM-5R0V105-R, and PB-5R0V105-R as solid, circle, and square lines, respectively, and	96
4.14	Experimental step responses collected from 0.33 F Panasonic supercapacitor from initial voltages of $v(0) = 0.5$ V to 4 V in 0.5 V steps when $V_{cc} = 5$ V.	97
4.15	Experimental (solid) and simulated (dashed) response to voltage pulses collected from 0.33 F Panasonic supercapacitor.	99
4.16	BCAP1500-P270-K05 and BCAP3000-P270-K05 supercapacitors from Maxwell Technologies Inc. with rated capacitances of 1500 and 3000 F, respectively.	100
4.17	Experimental step responses collected from 1500 F (BCAP1500-P270-K05) and 3000 F (BCAP3000-P270-K05) rated capacitors from Maxwell Technologies (solid) compared to MATLAB simulated responses using extracted fractional parameters (circles).	100
4.18	(a) Theoretical and (b) physically implemented fractional multivibrator circuit using a supercapacitor as the fractional element.	102
4.19	MATLAB simulated response of the multivibrator waveforms $v^-(t)$ (solid) and $v_c(t)$ (dashed) using the extracted fractional parameters of 1 F, Panasonic(2) supercapacitor when $V_{cc} = 5$ V.	103
4.20	Experimental waveforms $v_o(t)$ and $v^-(t)$ using the 1 F, Panasonic(2) supercapacitor collected from the multivibrator circuit of Fig. 4.18.	104
B.1	Theoretical circuit to apply a step-current input to the single-dispersion Cole impedance model.	141
B.2	MATLAB simulations of (B.2) and (B.3) when $R_\infty = R_1 = 1$ k Ω , $C = 1$ μ F and α is varied from 0.5 to 1 as solid lines and black circles, respectively.	143
B.3	MATLAB simulated step response of (B.3) using an apricot parameters ($R_\infty = 406$ Ω , $R_1 = 12.49$ k Ω , $C = 62.34$ nF, $\alpha = 0.739$) with 50 dB SNR Gaussian white noise and using extracted parameters as a solid line and black circles, respectively.	145
C.1	RC ladder structure to realize a n^{th} order integer approximation of a CPE with pseudo-capacitance C_α	147

C.2	Magnitude and phase response of the approximated fractional order capacitor (dashed) compared to the ideal (solid) with capacitance of $12.6\ \mu\text{F}$ and order $\alpha = 0.5$ after scaling to a center frequency of $f_c = 1\ \text{kHz}$	148
D.1	(a) Designed and (b) manufactured PCBs to build high capacity supercapacitor step-response test fixture.	152
D.2	BCAP1500-P270-K05 supercapacitor from Maxwell Technologies Inc. installed between the high capacity supercapacitor test PCBs.	153

CHAPTER 1

INTRODUCTION

1.1 Fractional Calculus

Fractional calculus, the branch of mathematics regarding differentiations and integrations to non-integer orders, is a field that is over 300 years old [1]. Its origins dating back to a correspondence from 1695 between Leibniz and L'Hopital, with L'Hopital inquiring about Leibniz's notation, $\frac{d^n y}{dx^n}$, and the meaning if $n = 1/2$, and a reply from Leibniz, "It will lead to a paradox, a paradox from which one day useful consequences will be drawn, because there are no useless paradoxes" [2]. Time has proven Leibniz quite the prophet as the applications of these fractional derivatives and integrals has seen explosive growth in many fields of science and engineering during the past few decades. These applications are in fields that include materials theory [3–5], bioengineering [6], control theory [7, 8], electromagnetics [9], power electronics [10], integrator [11, 12] and differentiator circuits [13], oscillators [14], multivibrator circuits [15], and filter theory [16–18] with potentially many others [19, 20].

A fractional derivative of order α , with lower terminal a , is given by the Caputo derivative [21] as

$${}_a D_t^\alpha f(t) = \frac{1}{\Gamma(n - \alpha)} \int_a^t \frac{f^{(n)}(\tau)}{(t - \tau)^{\alpha+1-n}} d\tau \quad (1.1)$$

where $\Gamma(\cdot)$ is the gamma function and $n - 1 \leq \alpha \leq n$. Though other definitions of the

fractional derivative exist such as the Riemann-Liouville definition [1] given by

$${}_a D_t^\alpha f(t) = \frac{d^n}{dt^n} \left[\frac{1}{\Gamma(n-\alpha)} \int_a^t \frac{f(\tau)}{(t-\tau)^{\alpha+1-n}} d\tau \right] \quad (1.2)$$

or the Grünwald-Letnikov definition given by

$${}_a D^\alpha f(x) = \lim_{h \rightarrow 0} \frac{1}{h^\alpha} \sum_{m=0}^{\left[\frac{x-a}{h}\right]} (-1)^m \frac{\Gamma(\alpha+1)}{m! \Gamma(\alpha-m+1)} f(x-mh) \quad (1.3)$$

While there are no physical analogies to fractional derivatives and integrals like slope or area under a curve they can begin to be visualized by examining integer-order derivatives of sinusoidal functions and generalizing them to the fractional order. Take for example the function $f(x) = \cos(x)$ given as a solid line in Fig. 1.1. Differentiating $f(x)$ yields $df/dx = \sin(x)$ which can also be represented in terms of the cosine function as $df/dx = \cos(x - \pi/2)$, given in Fig. 1.1 as a dashed line. Taking the second derivative of $f(x)$ yields $d^2f/dx^2 = -\cos(x) = \cos(x - \pi)$, and further generalizing this process to the n^{th} order yields

$$\frac{d^n}{dx^n} \cos(x) = \cos\left(x - n\frac{\pi}{2}\right) \quad (1.4)$$

where n is an integer. Therefore the integer order derivatives cause a phase shift of $n \cdot \pi/2$ rad/s or $n \cdot 90^\circ$ to the cosine function. Following this logic, if the order n is expanded to the set of real numbers, then the phase shift introduced to the cosine function by the fractional derivative is no longer limited to multiples of 90° . Therefore, a fractional derivative of order $n = 0.5$, that is $d^{0.5}f(x)/dx^{0.5}$ yields a phase shift of 45° to the cosine function, given in Fig. 1.1 as black circles. Now, while the fractional derivatives of other functions cannot be calculated as simply or intuitively as the sine and cosine functions, this special case provides an intuitive entry point to fractional calculus and fractional derivatives.

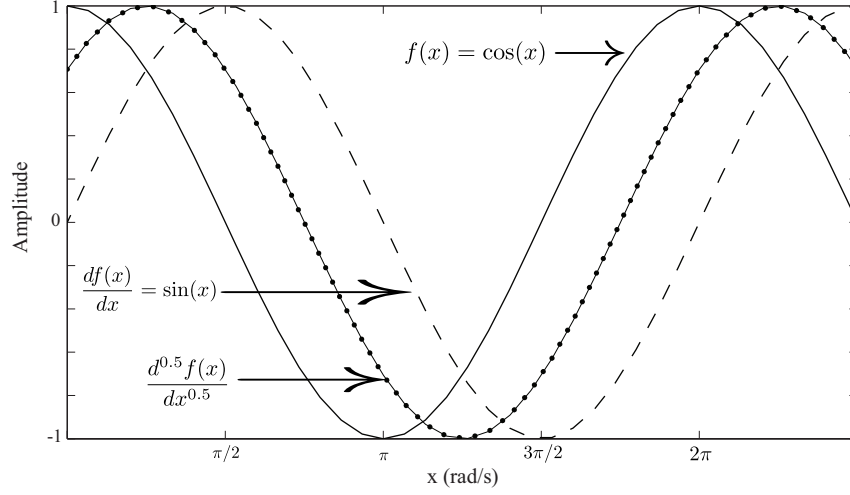


Figure 1.1: First order and 1/2 order derivatives of the function $f(x) = \cos(x)$.

1.1.1 Fractional Laplace Transform Operator

In the design and analysis of electronic circuits the Laplace transform is a very useful tool, transforming the circuit from the time domain to the frequency domain. With this transformation the analysis of circuits can be conducted algebraically rather than by solving differential equations. This transformation when applied to a time domain function, $f(t)$, is given by

$$\mathcal{L}\{f(t)\} = F(s) = \int_{0^-}^{\infty} f(t)e^{-st} dt$$

where $F(s)$ is the transformed function in the frequency domain and s is the Laplace transform operator. Applying this transformation to the standard circuit elements of a capacitor, resistor, and inductor, with zero initial conditions, yields their impedance characteristics in the frequency domain described as

$$\begin{aligned} Z_C(s) &= \frac{1}{sC} \\ Z_R(s) &= R \\ Z_L(s) &= sL \end{aligned}$$

where $Z_{C,R,L}$ are the impedance of the capacitor, resistor, and inductor, respectively, in the frequency domain. While the Laplace transform operator in circuit analysis has traditionally been raised to an integer order, it is mathematically valid to raise to a non-integer order, s^α , where $n - 1 < \alpha < n$, effectively representing a fractional-order system. Applying the Laplace transform to the fractional derivative of (1.1) with lower terminal $a = 0$ yields

$$\mathcal{L}\{ {}_0D_t^\alpha f(t) \} = s^\alpha F(s) - \sum_{k=0}^{n-1} s^{\alpha-k-1} f^{(k)}(0) \quad (1.5)$$

Note, that we use the Caputo definition of a fractional derivative over other approaches because the initial conditions for this definition take the same form as the more familiar integer-order differential equations. Therefore, it becomes possible to define a general fractance device with impedance proportional to s^α [22] where the traditional circuit elements are special cases of the general device when the order is -1 , 0 , and 1 for a capacitor, resistor, and inductor, respectively. Another special case of the general fractance device is referred to as a Constant Phase Element (CPE), with impedance $Z_{CPE} = 1/(j\omega)^\alpha C$ or $1/s^\alpha C$ in the s -domain, where C is the pseudo-capacitance with units $F/s^{1-\alpha}$ and $0 \leq \alpha \leq 1$ the order. These units were originally proposed in [23] where $[s]$ is the unit of time not to be confused with s , the Laplace transform operator. However, throughout this work we will refer to the units of the CPE as $[F]$ for simplicity. The name of CPEs are in reference to the phase angle, ϕ_{CPE} , which is independent of frequency and dependent only on the order given as $\phi_{CPE} = \alpha\pi/2$. While $\alpha \in \mathfrak{R}$ is mathematically possible, the values from experimentally collected data are typically in the range of $0 < \alpha < 1$. For reference, the bode plots of s^α when $\alpha = 0.2, 0.4, 0.6, 0.8$, and 1 are given in Fig. 1.2. These devices have also been called fractional capacitors, in reference to their order that takes a value between the traditional circuit elements of a resistor and capacitor. It is for this reason that we use a capacitor as the schematic representation of CPEs in this work. The use of fractional-order elements in different fields of electrical engineering is steadily increasing including:

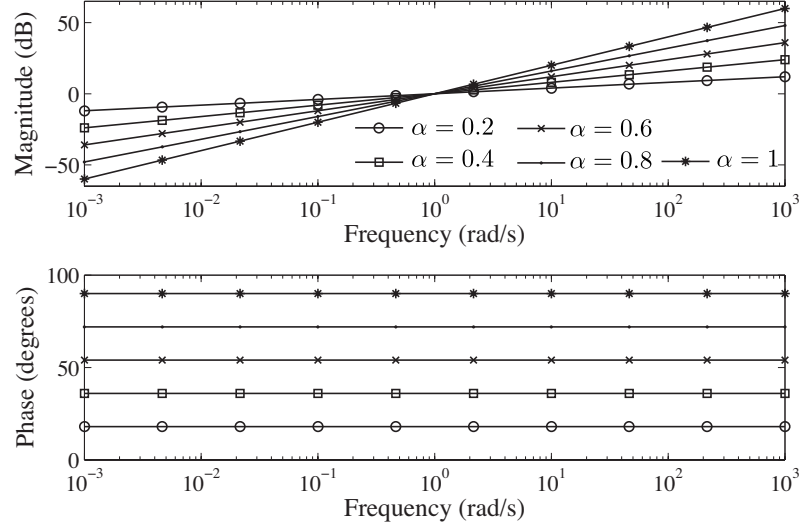


Figure 1.2: Bode plots of s^α when $\alpha = 0.2, 0.4, 0.6, 0.8$, and 1.

- Modelling RF inductors with a frequency dependent resistor that varies by \sqrt{f} [24];
- Modelling the losses of coils using a fractional impedance [25];
- Generalizing the Smith chart to the fractional domain for plotting and matching fractional impedances in the RF and microwave regime [26];
- Expanding the freedom and versatility of electric circuits by introducing fractional orders [27, 28];
- Generalizing the integer-order cable model of the neuron system to the fractional domain [29].

1.2 Fractional Models and Applications

Constant phase elements have shown numerous applications in the field of bioimpedance, which measures the passive electrical properties of biological materials. These measurements give information about the electrochemical processes in tissues and can be used to characterize the tissue or monitor for physiological changes [30]. There are many fractional models currently used in literature to model biological tissues, electrode-tissue interfaces,

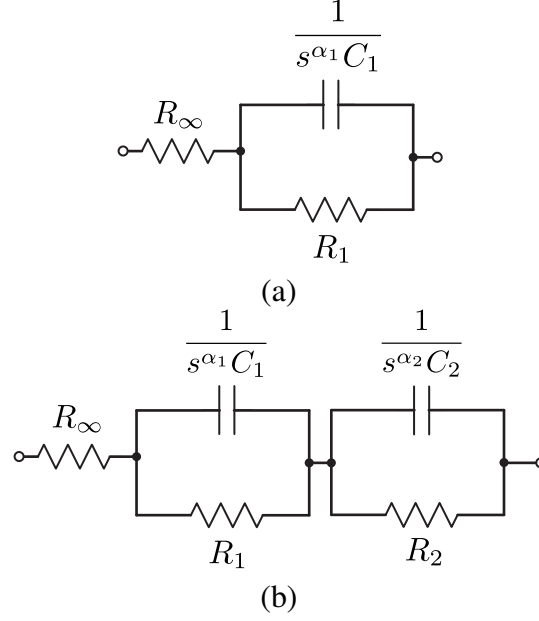


Figure 1.3: Theoretical (a) single dispersion and (b) double dispersion Cole impedance models.

respiratory impedance, and supercapacitors with many diverse applications.

1.2.1 Cole Impedance Models

The most famous and well known fractional model is the Cole impedance model, introduced by Kenneth Cole in 1940 [31]. This model is used for characterizing biological tissues and biochemical materials. In literature, this model has also been commonly referred to as the Cole-Cole model or Cole-Cole impedance model. However, the Cole-Cole model is actually a similar model introduced by the Cole brothers in 1941 regarding dielectric permittivity [32]. Therefore, care needs to be taken when describing the model to prevent confusion between work with dielectric permittivity and impedance. The Cole model, shown in Fig. 1.3(a), is composed of three hypothetical circuit elements. A high-frequency resistor R_∞ , a resistor R_1 and a CPE. The impedance of this model is then given by

$$Z(s) = R_\infty + \frac{R_1}{1 + s^{\alpha_1} R_1 C_1} = Z' + jZ'' \quad (1.6)$$

Noting that $s^\alpha = (j\omega)^\alpha = \omega^\alpha [\cos(\alpha\pi/2) + j\sin(\alpha\pi/2)]$. This model has become very popular because of its simplicity and good fit with measured data, illustrating the behaviour of impedance as a function of frequency. However, while this model is effective at representing experimentally collected bioimpedance data, it does not provide an explanation of the underlying mechanisms. Physiologically, the resistances in this model are contributed by the numerous intracellular, extracellular, and cellular membrane resistances within the tissue; with capacitance contributed by the membrane capacitances of the numerous tissue cells. The parameter α is a dimensionless quantity though it is possible to regard it in several ways, including, as a distribution of relaxation times caused by the heterogeneity of cell sizes and shapes, a measure of the deviation from an ideal capacitor in the equivalent circuit, or as a measure of physical processes like the Warburg diffusion [30].

Now, while these models do not provide an explanation of the underlying mechanisms there has been a large and expanding body of research regarding their use in many diverse fields of biology and biomedicine. The single dispersion model and its parameters have been investigated for applications in biomedicine that include:

- Characterizing muscle, liver, lung, and spleen tissues excised from sheep [33];
- Estimating the hemocrit value or total volume of red blood cells in a sample of human blood [34] or assessing the quality of red blood cell suspensions under storage [35];
- Monitoring tissue ischemia, the condition of insufficient oxygen and nutrient supply, from pH value estimated from the impedance parameters [36];
- Monitoring intra/extra-cellular volume or detecting tissue structural alterations through the α parameter, also referred to as the bioimpedance width [37];
- Monitoring the hydration process of patients during hemodialysis as a potential indicator of hypotension crisis [38];

- Accurate modelling of different types of human skulls for simulation of their properties for bioelectric related research [39];
- Usefulness of the impedance parameters for estimating tissue response to chronic microelectrode arrays [40];
- Detection of occlusal non-caviated carious for dentistry [41];
- Body composition analysis for total body water, extracellular fluid content, intracellular fluid content, and fat mass [42].

Many investigations regarding the Cole parameters and their relation to cancerous tissues have been conducted with applications that include:

- Aiding in the diagnosis of cervical cancer in women [43];
- Classifier based diagnostic tool for healthy and cancerous hepatic tissue in humans [44];
- Identifying cancer [45] and the features of surrounding areas in breast tissue [46];
- Minimally invasive detection of bladder cancer [47];
- As a diagnostic and prognostic factor for survival in cancer patients [48].

An expanded model, the double dispersion Cole model, is used to accurately represent the impedance over a larger frequency range or for more complex materials. This model, shown in Fig. 1.3(b), is composed of an additional parallel combination of a resistor and CPE in series with the single dispersion Cole model with total impedance given by

$$Z(s) = R_{\infty} + \frac{R_1}{1 + s^{\alpha_1} R_1 C_1} + \frac{R_2}{1 + s^{\alpha_2} R_2 C_2} \quad (1.7)$$

The double dispersion Cole model and its parameters have been investigated for applications in:

- Characterizing intestinal tissue excised from sheep [33];
- Monitoring necrosis of human tumor xenografts during and/or after hyperthermia treatment [49];
- Investigating age-related changes of human dentine to create non-destructive test methods applied to early caries and micro-leakage identification [50].

1.2.2 Fractional Plant Models

Fractional impedance models are not only important in biomedicine but have shown useful applications in biology, specifically in regards to plant physiology. The single dispersion Cole model and its parameters having been investigated for:

- Characterizing the tissues of different fruits and vegetables including apples, apricots [51], plums [52], potatoes, kiwis [51,53], garlic, tomatoes, and pears; with potential to measure the maturity or give an estimate of lifespan for storage purposes [54];
- Relationship between the rooting ability and Cole parameters of shoots and leaves of olive cuttings [55];
- Effects of drying and freezing-thawing treatments on eggplant pulp samples [56];
- Non-destructive method for detection of incipient mould development on wood surfaces [57];
- Fit the impedance data collected from the bark and wood of current and one year old Scots pine shoots [58].

In [58] the single dispersion Cole model provided a more accurate fit with experimental data than two other integer circuit models for bark and wood, even when both integer models had more parameters (5 and 9, respectively) than the fractional model (3). For comparison, the integer order models are given in Figs. 1.4(a) and (b). This study concluded that the

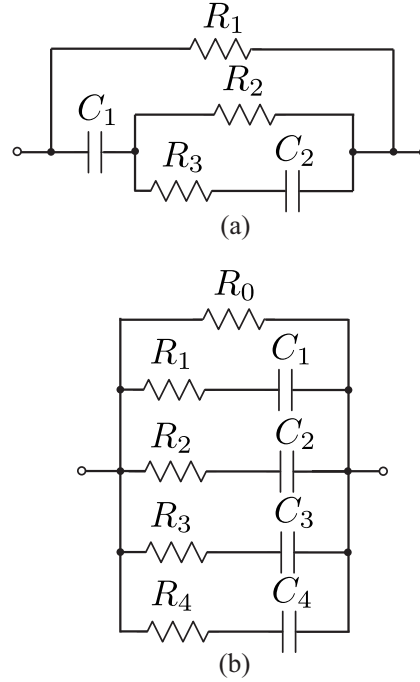


Figure 1.4: Lumped circuits for modelling (a) bark and (b) wood to compare against a fractional circuit model.

fractional model is better suited to model tissues with numerous types of cells with different sizes and morphologically different structures [58]. The double dispersion Cole model has also been investigated as an indicator of frost hardiness in Scots pine shoots [59].

The Cole impedance models are not the only fractional impedance models useful in matching the impedance data collected from plant tissues. The model, shown in Fig. 1.5, is composed of three resistors and three CPEs with impedance given by

$$Z(s) = R_{\infty} + \frac{R_1}{1 + s^{\alpha_1} R_1 C_1} + \frac{R_2}{1 + s^{\alpha_2} R_2 C_2} + \frac{1}{s^{\alpha_3} C_3} \quad (1.8)$$

is used to fit the impedance data collected from root/stem/electrode interface of willows to monitor the root growth through the change in the impedance parameters [60]. This method was investigated as a method of measuring root growth with the resistances $(R_1 + R_2)$ showing the highest correlation with the root fresh mass. This study also concluded that the speed and non-destructive nature of the measurements warranted further study on the

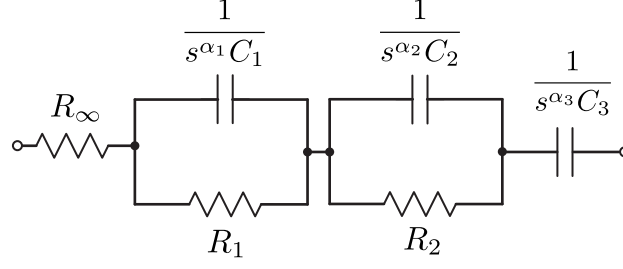


Figure 1.5: Fractional impedance model to fit root/stem/electrode interface of willows grown to monitor root growth.

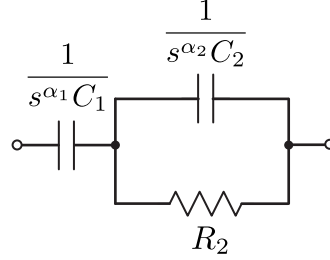


Figure 1.6: Fractional order model to analyze moisture gradients of wood.

effects of soil type, moisture content, and electrode position on the impedance parameters.

The model given in Fig. 1.6 composed of two CPEs and a resistor with impedance given by

$$Z(s) = \frac{1}{s^{\alpha_1} C_1} + \frac{R_2}{1 + s^{\alpha_2} R_2 C_2} \quad (1.9)$$

is used to fit the impedance data collected from a wood sample to estimate the internal moisture gradients [61]. For this study, a portable device with applications to optimize wood drying, condition surveys of wood buildings and construction, and estimates of pulpwood moisture gradients was developed [61]. This portable device as well as others developed to extract the Cole parameters from plants and trees without requiring the use of an impedance analyzer [62, 63] creates the potential for extensive field studies in wood research not possible using traditional laboratory equipment.

1.2.3 Electrode Tissue Interface Model

Modeling the electrode-tissue interface is important for all systems involving biopotential recordings and stimulations. This is even more important for pacemakers because device

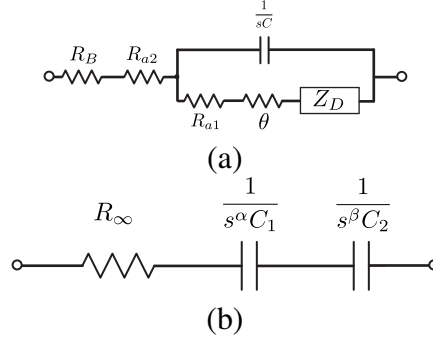


Figure 1.7: (a) Tissue-electrode circuit model for a unit surface area and (b) simplified distributed fractional order model.

failures are often the result of properties of the electrode-tissue interface rather than component failure intrinsic to the device [64] with reported failures by commercial devices highlighting the need for more accurate models to ensure patient safety [65]. An equivalent fractional order circuit model of the electrode-tissue interface in living hearts proposed in [64], is shown in Fig. 1.7(a), that describes the impedance for a unit surface area. This model was derived from experimentally collected data from perfused living rat hearts and is composed of 6 elements to describe the behaviour of the tissue-electrode interface where R_B is the bulk tissue resistance, R_{a1} and R_{a2} are the electrode access resistances, θ is the electrochemical charge transfer resistance, C is the dipole layer capacitance, and Z_D is a spatially confined Warburg impedance (CPE with $\alpha = 0.5$). It was recently proposed in [65] that the experimental data of the model in Fig. 1.7(a) could also be represented by the fractional order model given in Fig. 1.7(b); reducing the model to 3 elements, a resistance in series with two CPEs with impedance given by the expression

$$Z(s) = R_\infty + \frac{1}{s^\alpha C_1} + \frac{1}{s^\beta C_2} \quad (1.10)$$

Though in reducing the electrode-tissue interface from that shown in Fig. 1.7(a) to that in Fig. 1.7(b) we lose the physiological description of each contributing element of the impedance though the simplified model provides a good fit to the experimental data. Fractional models are also useful in simulations of the electrode-tissue interface and are relevant

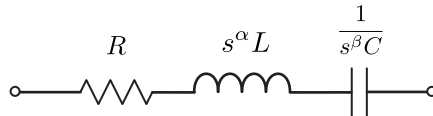


Figure 1.8: Fractional order impedance model of the respiratory system of humans proposed.

to biosensors, chronic indwelling electrodes, and cardiac pacemakers [64–66].

1.2.4 Fractional Respiratory Model

Fractional order models have been shown useful in modeling the mechanical impedance of the respiratory system in dogs [67], cats [68], and humans [69]. An electrical equivalent representation of the mechanical impedance of the human respiratory system, given in Fig. 1.8, is composed of series connection of 3 elements. The impedance of this system is given by the expression

$$Z(s) = R + s^\alpha L + \frac{1}{s^\beta C} \quad (1.11)$$

where R is a Newtonian resistance, L the inertance, and C the compliance. This model is unique in that it introduces a fractional element, with impedance $Z_L = s^\alpha L$, different than the CPE's previously described. Where the order of the previous CPE's places them between the traditional elements of a resistor and capacitor, the order of this element places it between a resistor and inductor. It is for this reason that we use an inductor as the schematic representation of this element in Fig. 1.8 and could also refer to this element as a fractional inductor.

This model has been verified in both frequency and time domains to reasonably fit the experimentally collected data using the forced oscillation technique to measure the respiratory impedance. These impedance parameters are potentially useful in tuning controllers to deliver the reference pressure value and obtain optimal ventilation for a patient requiring minimal breathing effort yielding improvements to ventilatory assisting devices [69].

It has been shown in [70] that changes in the mechanical properties of lung parenchyma

can be detected in the impedance parameters between healthy patients and those with chronic pulmonary disease. This model is able to capture the viscoelastic changes of soft tissues in the lungs. It has further been shown in [71] that the fractional order behaviour observed in the respiratory input impedance is dependent on not only the tissue viscoelasticity, but also on the intrinsic geometry and morphology of the respiratory tree. The fractional model of Fig. 1.8 has also been used to investigate the respiratory mechanics in total liquid ventilation [72]. With the fractional values acknowledged to best explain the frequency-dependence of the input impedance with useful applications for the design of a pressure controller for total liquid ventilators and monitoring patient respiratory parameters during treatment.

1.2.5 Fractional Supercapacitor Models

Supercapacitors also referred to as ultracapacitors or electric double layer capacitors, are high energy storage devices with many practical uses in energy storage for wind turbines [73], photovoltaic systems [74, 75], energy harvesting [76], hybrid and electric vehicles [77], and biomedical sensors [78]. Traditionally, these capacitors have been modelled using RC networks to describe their behaviour over wide frequency bands, with larger frequency bands requiring a greater number of parameters [79]. However, recent work has employed the concept of fractional impedances to model and describe the behaviour of these components [80, 81]. These fractional models have been developed to describe the impedance in low and medium frequencies [82, 83], long-term transients [84], and step response characteristics [85, 86] of supercapacitors; showing much better fit with experimental data over their integer order counterparts and requiring fewer model parameters.

A very simple fractional-order supercapacitor model, shown in Fig. 1.9, is composed

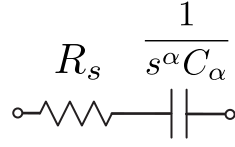


Figure 1.9: Theoretical fractional impedance model of a supercapacitor.

of a series resistor, R_s , and CPE. The impedance of this fractional model is given by

$$Z_c(s) = R_s + \frac{1}{C_\alpha s^\alpha} \quad (1.12)$$

This model is a simplification of the model derived from the porous electrode behaviour of supercapacitors and represents the low and high frequency behaviour of the supercapacitors when $\alpha = 1$ and $\alpha = 0.5$, respectively [87]. This model has been used in [82] to model the impedance in the frequency range from 10 mHz to 1000 Hz and [83] in the frequency range 50 mHz to 215 mHz with $\alpha \approx 1$ and 450 mHz to 100 Hz with $\alpha \approx 0.5$. This model has been selected over other fractional models because of its simplicity and good fit with experimental data at low and high frequencies. Using this model, supercapacitors belong to a family of devices known as fractional capacitors, of which traditional capacitors are a small subset, possessing fractional impedances. Now, while all capacitors have been shown to possess fractional characteristics [23] and should be modelled with an impedance $Z(s) = 1/s^\alpha C_\alpha$, the value of α is very near to 1 for commercially available low-value capacitors. There has been much work to realize low-value fractional capacitors using photolithographic manufacturing [3,88] and electrolyte processes [89,90] with applications in controls [8], oscillators [14,15], power electronics [10], and analog filter design [18,91].

Typically, the impedance parameters of capacitors are measured using equipment such as LCR meters. However, these pieces of equipment operate on the assumption that the circuit element can be modelled using integer order impedances which yields incorrect results when trying to measure fractional impedances. As a result, the determination of the fractional parameters to describe supercapacitors has required direct measurement of

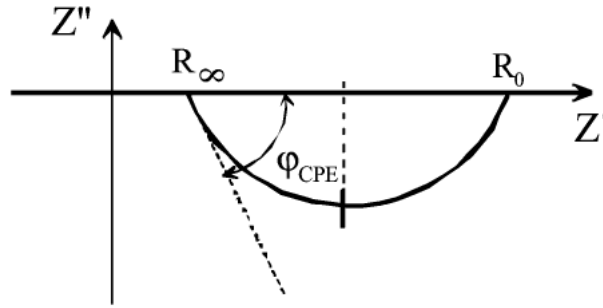


Figure 1.10: Impedance loci used to graphically extract the single dispersion Cole impedance parameters.

the impedance [83] or frequency response [86] requiring either an impedance or network analyzer. Therefore, there exists a need for both equipment and techniques to measure the fractional characteristics of a circuit element directly.

1.3 Extraction Methods

To characterize a particular tissue or material requires the determination of the fractional impedance parameters that completely describe the impedance behaviour as a function of frequency. For example, using the single or double dispersion Cole models this requires the determination of the four $(R_\infty, R_1, C, \alpha)$ or seven $(R_\infty, R_1, R_2, C_1, C_2, \alpha_1, \alpha_2)$ parameters, respectively. Early methods extracted the parameters graphically from an impedance plot relating the imaginary impedance, Z'' , to the real impedance, Z' . An example impedance loci used to extract the single dispersion Cole impedance parameters is shown in Fig. 1.10. From the circular arc the theoretical low frequency resistance, R_o , and high frequency resistance, R_∞ , can be directly measured (see Fig. 1.10) where $R_1 = R_o - R_\infty$. The order, α , can be calculated from the measured angle ϕ_{CPE} through the relation $\phi_{CPE} = \alpha\pi/2$. While the frequency at which $|Z''|$ has its maximum is equal to $1/\tau$ and the dispersion time constant is given as $\tau = [(R_o - R_\infty)C]^{1/\alpha}$, enabling the calculation of C with the previously measured parameters (R_o, R_∞, α) . The double dispersion Cole parameters can be extracted in a similar fashion, with two circular arcs appearing in the impedance loci as a result of

the two dispersions.

With the rise of computers and very powerful numerical fitting software such as LEVM / LEVMW [92] and MATLAB [93], the majority of parameters are now estimated using non-linear least squares routines fitting experimental data to the desired model. Parameters are selected such that the least squares error between the experimental data and estimated response are minimized. While these fitting processes were initially applied to impedance data, research has been expanded to extract the parameters without requiring direct measurement of the impedance. Instead, parameters are extracted only from the real part of the impedance (Z') [94, 95], the imaginary (Z''), or the modulus [42, 95] components of the impedance. Methods without requiring fitting routines have also been investigated to extract the parameters from the magnitude response [51, 52] and the time domain response to a triangle-wave current input [96].

1.4 Research Objectives

Fractional order circuit models provide a better fit for experimentally collected impedance data of both biological tissues and supercapacitors over their integer-order counterparts. These fractional models, while lacking in providing an explanation of the underlying mechanisms responsible for producing their behaviour, are still very useful showing a wide array of applications in biomedicine and biology. The practical application of these models warrants significant continued research into not only their use as prognostic and diagnostic tools, but also into techniques for their measurement. Traditionally, to collect the impedance data requires an impedance analyzer which is expensive and not portable, though portable hardware to accomplish this same task has been reported in [47, 61, 97, 98]. However, these instruments use direct measurements of the impedance. By implementing indirect measurement techniques there is the potential to further decrease the cost of instruments by reducing the amount of required hardware; with potential to significantly reduce the barriers to conduct research especially with regards to real-time monitoring with

portable devices [99].

This research is dedicated to the investigation of alternative methods to extract fractional impedance characteristics from biological tissues and supercapacitors without requiring direct impedance measurements. This is accomplished by using concepts from fractional calculus to further the development of fractional circuit theory and model the responses of these materials in the time and frequency domains. Leading to the development of methods to extract the fractional impedance parameters indirectly from the step and magnitude responses of the materials or devices.

1.5 Thesis Overview

This thesis is divided into three areas of research focus regarding the extraction of fractional impedance parameters, without requiring direct impedance measurements, from fractional circuit models. These three fractional models are the single and double dispersion Cole impedance models applied to biological tissues and a fractional model applied to supercapacitors.

Chapter 2 applies concepts from fractional calculus to develop the fractional circuit theory required to model the current and voltage excited step response and magnitude response of the single-dispersion Cole impedance model. From the step-excited responses a numerical curve fitting method is developed and applied to extract the impedance parameters that describe this model. To further overcome the accuracy limitations, which are highlighted in MATLAB simulations, a non-linear least squares method is applied to the current and voltage excited step responses with the improvements verified from experimentally collected fruit tissue datasets. Finally, the least-squares method is applied to the magnitude response of this model to again improve the accuracy with results verified in simulation and from experimental data collected from fruit tissues.

Chapter 3 extends the circuit theory introduced in Chapter 2 to the double-dispersion Cole impedance model. Fractional calculus is applied to develop the fractional circuit

theory to model the current-excited step response and magnitude response of this fractional impedance model. Using these models, non-linear least squares methods are applied to both frequency and time domain datasets of the double dispersion Cole impedance model to extract the fractional impedance parameters that characterize this model. The extractions are validated by both simulations and experimentally collected results from fruit tissues.

Chapter 4 presents the impact of using integer-order techniques to measure a CPE or supercapacitor and how parameters extracted with these methods inaccurately represent the transient characteristics of these devices. Fractional circuit theory is applied to a fractional-impedance supercapacitor model to describe the voltage-excited step response of this device. Using this fractional model a non-linear least squares method is applied to extract the fractional impedance parameters that accurately describe their transient behaviour. This process is verified using experimentally collected step responses from both low and high capacity supercapacitors.

Chapter 5 concludes the thesis and suggests possibilities for future research based off of the direction of this work.

CHAPTER 2

SINGLE DISPERSION COLE IMPEDANCE MODEL

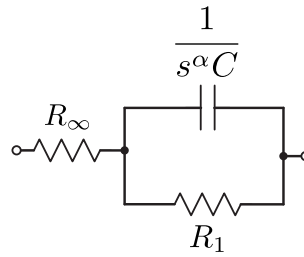


Figure 2.1: Theoretical single-dispersion Cole impedance model.

The single-dispersion Cole impedance model shown in Fig. 2.1, previously introduced in Section 1.2.1, has been extensively used in both biology and biomedicine to characterize and investigate biological tissues for many diverse applications. This model has an impedance given by

$$Z(s) = R_\infty + \frac{R_1}{1 + s^\alpha R_1 C} \quad (2.1)$$

Typically, when characterizing a tissue using this model the impedance parameters (R_∞, R_1, α, C) are extracted from the impedance data directly measured using an impedance analyzer. This requires hardware to apply a sinusoidal input signal at various frequencies to excite the tissue and the measurement of the magnitude and phase of the corresponding response for further data processing. However, it is possible to extract these same parameters without requiring direct impedance measurements. In this chapter indirect methods to extract the impedance parameters from the voltage and current excited step responses and the magnitude response of the single-dispersion Cole impedance model are presented. For these methods the underlying circuit theory and process are presented and validated

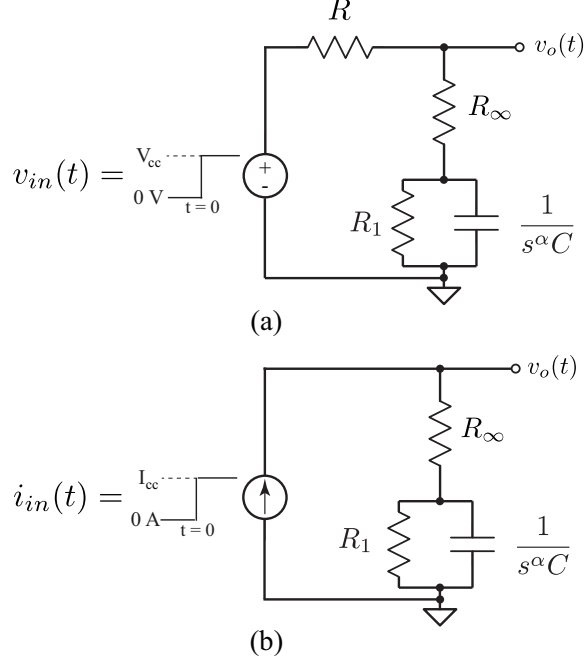


Figure 2.2: Theoretical circuits to apply a (a) voltage-step and (b) current-step input to the single dispersion Cole impedance model.

by both simulations and experimentally collected results from both ideal circuits and fruit tissues.

2.1 Numerical Extraction from Step Response

In [100] we presented a method to numerically extract the single dispersion Cole impedance model parameters from collected step response dataset without requiring direct measurement of the impedance. Two simple circuits that can be used to obtain the step responses of the Cole impedance model to either a voltage or current step-input are given in Figs. 2.2(a) and (b), respectively.

It can be shown that the transfer function of Fig. 2.2(a) assuming zero initial conditions is

$$\frac{V_o(s)}{V_{in}(s)} = \frac{s^\alpha \frac{R_\infty}{R+R_\infty}}{s^\alpha + \frac{R+R_\infty+R_1}{CR_1(R+R_\infty)}} + \frac{\frac{R_\infty+R_1}{CR_1(R+R_\infty)}}{s^\alpha + \frac{R+R_\infty+R_1}{CR_1(R+R_\infty)}} \quad (2.2)$$

which if $V_{in}(s)$ is a step function of magnitude V_{cc} , that is $V_{in}(s) = V_{cc}/s$, (2.2) becomes

$$V_o(s) = V_{cc} \left[\frac{s^{\alpha-1} \frac{R_{\infty}}{R+R_{\infty}}}{s^{\alpha} + \frac{R+R_{\infty}+R_1}{CR_1(R+R_{\infty})}} + \frac{s^{-1} \frac{R_{\infty}+R_1}{CR_1(R+R_{\infty})}}{s^{\alpha} + \frac{R+R_{\infty}+R_1}{CR_1(R+R_{\infty})}} \right] \quad (2.3)$$

Applying the Laplace transform formula for the Mittag-Leffler function [21]

$$\mathcal{L} \left\{ \frac{k! s^{\alpha-\beta}}{(s^{\alpha} \mp a)^{k+1}} \right\} = t^{\alpha k + \beta - 1} E_{\alpha, \beta}^{(k)} (\pm a t^{\alpha}) \quad (2.4)$$

on (2.3) yields a time domain equation of the form,

$$v_o(t) = V_{cc} \left[\frac{R_{\infty}}{R+R_{\infty}} E_{\alpha, 1} \left(-t^{\alpha} \frac{R+R_{\infty}+R_1}{CR_1(R+R_{\infty})} \right) + \frac{R_{\infty}+R_1}{CR_1(R+R_{\infty})} t^{\alpha} E_{\alpha, \alpha+1} \left(-t^{\alpha} \frac{R+R_{\infty}+R_1}{CR_1(R+R_{\infty})} \right) \right] \quad (2.5)$$

where $v_o(t)$ is the time domain expression of the output voltage and $E_{\alpha, \beta}(\cdot)$ is the two-term Mittag-Leffler function defined as [21]

$$E_{\alpha, \beta} = \sum_{k=0}^{\infty} \frac{z^k}{\Gamma(\alpha k + \beta)} \quad (2.6)$$

where $\Gamma(\cdot)$ is the gamma function. Applying this same procedure to the circuit of Fig. 2.2(b), when $I_{in}(s)$ is a step function of magnitude I_{cc} , yields the time domain expression of the output voltage due to a step current input given by

$$v_o(t) = I_{cc} \left[R_{\infty} E_{\alpha, 1} \left(\frac{-t^{\alpha}}{R_1 C} \right) + \frac{R_{\infty}+R_1}{CR_1} t^{\alpha} E_{\alpha, \alpha+1} \left(\frac{-t^{\alpha}}{R_1 C} \right) \right] \quad (2.7)$$

2.1.1 Comparison to Step Response when $\alpha = 1$

From the definition of the two-term Mittag-Leffler function we can determine the time-domain expressions from (2.5) and (2.7) at the boundary between traditional and fractional

calculus, that is the case when $\alpha = 1$. Knowing that

$$E_{1,1}(z) = e^z \quad (2.8)$$

$$E_{1,2}(z) = \frac{e^z - 1}{z} \quad (2.9)$$

and substituting both (2.8) and (2.9) into (2.5) and (2.7) we obtain the more familiar expressions for the case when $\alpha = 1$. The expression for the output voltage of the step-voltage excited circuit of Fig. 2.2(a) can be shown as

$$v_o(t) = \frac{V_{cc}}{R + R_{\infty} + R_1} \left[R_{\infty} + \frac{R_1}{R + R_{\infty}} \left(R_{\infty} + R \left(1 - e^{-t \frac{R + R_{\infty} + R_1}{CR_1(R + R_{\infty})}} \right) \right) \right] \quad (2.10)$$

and the output voltage of the step-current excited circuit of Fig. 2.2(b) can be shown as

$$v_o(t) = I_{cc} \left[R_{\infty} + R_1 \left(1 - e^{-\frac{t}{CR_1}} \right) \right] \quad (2.11)$$

For further verification we compare MATLAB simulations of (2.5) and (2.7) when $\alpha = 1$ to (2.10) and (2.11), respectively. Using a MATLAB script to calculate the Mittag-Leffler function [101] the time domain output voltages for both the step-voltage and step-current excited circuits are shown in Figs. 2.3(a) and (b), respectively. For these simulations the values of all resistors were set to 1 k Ω with a capacitor of 1 μ F with step inputs of 1 V and 1 mA for the voltage and current excited responses, respectively. Figure 2.3(a) clearly indicates that the waveforms generated by (2.5) for $\alpha = 1$ and (2.10), shown as black circles and solid lines, are in perfect agreement. With those same results reflected in Fig. 2.3(b) for the waveforms using (2.7) for $\alpha = 1$ and (2.11) shown as a dashed and solid lines, respectively. Verifying in simulation that the expressions derived from fractional calculus with the Mittag-Leffler functions are equivalent to those derived with traditional calculus when $\alpha = 1$.

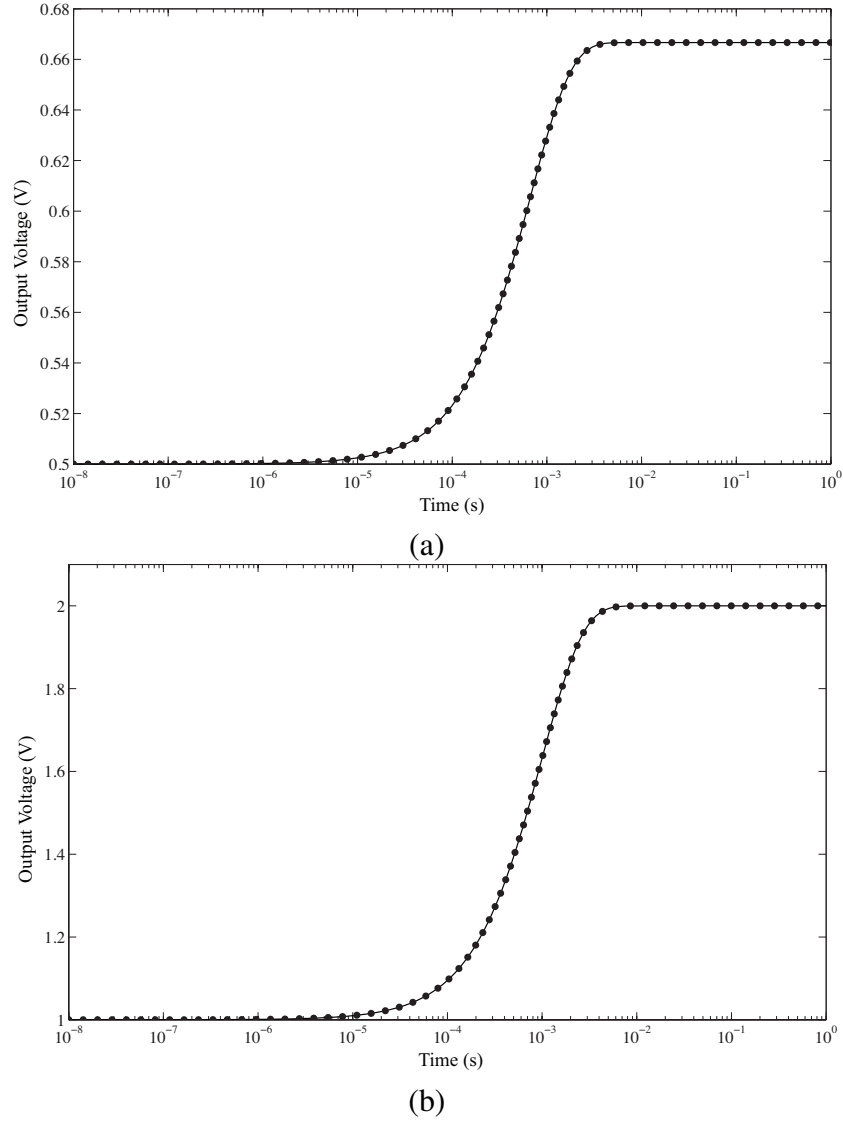


Figure 2.3: Comparison of MATLAB simulated output voltage of step (a) voltage-excited and (b) current-excited Cole impedance when $\alpha = 1$ using Mittag-Leffler functions and traditional expressions, shown as black circles and solid lines, respectively.

2.1.2 Extraction from Voltage-Excited Step Response

With expressions to describe the step response of the voltage excited Cole impedance of Fig. 2.2(a) using (2.5), it is possible to use properties of the step-responses to extract the impedance parameters that describe the model. First, at times both very soon and very far

after the step is applied notice that

$$v_o(0^+) = \lim_{t \rightarrow 0^+} v_o(t) = \frac{R_\infty}{R + R_\infty} V_{cc} \quad (2.12)$$

$$v_o(\infty) = \lim_{t \rightarrow \infty} v_o(t) = \frac{R_\infty + R_1}{R + R_\infty + R_1} V_{cc} \quad (2.13)$$

Equations (2.12) and (2.13) show that the output voltage at times very near and very far from the input step are independent of the charging time related to C and α and only dependent on the voltage divider networks created by R , R_∞ , and R_1 . This is verified when we observe the step response in Fig. 2.3(a) where it can be observed that for times less than $10 \mu s$ the step voltage approaches 0.5 V and for times above 10 ms it approaches 0.66 V , which knowing $R = R_\infty = R_1 = 1 \text{ k}\Omega$ and $V_{cc} = 1 \text{ V}$, exactly match those predicted by (2.12) and (2.13). Therefore, by measuring $v_o(t)$ at times very near and very long after the voltage step is applied, we can use the relationships of (2.12) and (2.13) to calculate the values of R_∞ and R_1 in the Cole impedance knowing R and V_{cc} .

Another property of the step response of (2.5) that is useful for the extraction is that the slope of the rise time, when plotted on a log time scale, is independent of C for a fixed R_∞ , R_1 and R , showing a dependency on only the value of α . This slope m , with units of V/decade, is calculated as

$$m = \frac{V_{90\%} - V_{10\%}}{\log_{10} \left(\frac{t_{V_{90\%}}}{t_{V_{10\%}}} \right)} \quad (2.14)$$

where $V_{90\%}$ and $V_{10\%}$ are the voltages at 90% and 10%, respectively, of the total rise time of the step response of (2.5) and $t_{V_{90\%}}$ and $t_{V_{10\%}}$ are their corresponding times after the step input was applied. The numerically calculated slopes using (2.14) for the step responses simulated with (2.5) for values of α from 0.2 to 1.0 in steps of 0.2 while varying C from $0.001 \mu F$ to $1 \mu F$ in decade steps are given in Table 2.1. For all of these calculations the values were fixed such that $R = R_\infty = R_1 = 1 \text{ k}\Omega$ with an input step of 1 V . For each value of α we note that the calculated slope is the same regardless of the value of C . This change of slope for resistor values of $1 \text{ k}\Omega$, a $1 \mu F$ capacitor, and 1 V step for values of α from

C (μF)	α				
	0.2	0.4	0.6	0.8	1.0
1	9.4276	4.5380	2.8226	1.9000	1.3395
0.1	9.4276	4.5380	2.8226	1.9000	1.3395
0.01	9.4276	4.5380	2.8226	1.9000	1.3395
0.001	9.4276	4.5380	2.8226	1.9000	1.3395

Table 2.1: Numerically calculated slopes in V/decade using (2.14) for values of α from 0.2 to 1.0 in steps of 0.2 while varying C from 0.001 μF to 1 μF in decade steps with $R = R_\infty = R_1 = 1 \text{ k}\Omega$ and an input step of 1 V.

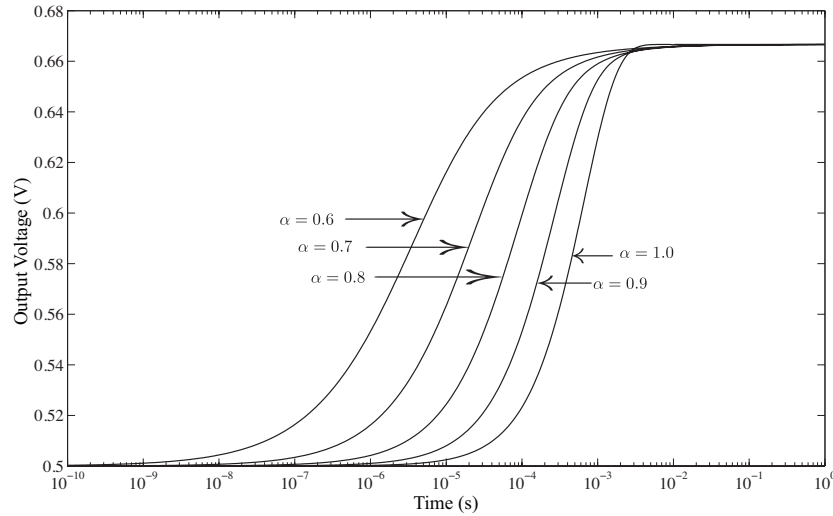


Figure 2.4: Comparison of slope of the step response of Fig. 2.2(a) for varying values of α from 0.6 to 1.0 in steps of 0.1 with $R = R_\infty = R_1 = 1 \text{ k}\Omega$ and $C = 1 \mu\text{F}$, respectively.

0.6 to 1.0 in steps of 0.1 is presented in Fig. 2.4. From this figure, note that the slope of each simulated step response increases with the value of α reinforcing that this slope is independent of C and dependent on α for fixed R , R_∞ , and R_1 . Therefore, by measuring the slope of the step response over its 10% – 90% rise time, knowing R and having previously determined R_∞ and R_1 , we can extract the value of α by comparing the collected dataset to a simulated step response while varying α until the slope of the rise time of the simulation matches the collected data.

Finally, the last step response property useful in extracting the last impedance parameter, C , is that the position of the rise time is dependent on C for fixed values of R , R_∞ , R_1 and α . Therefore, the value of C acts as a time scaling factor shifting the position of this

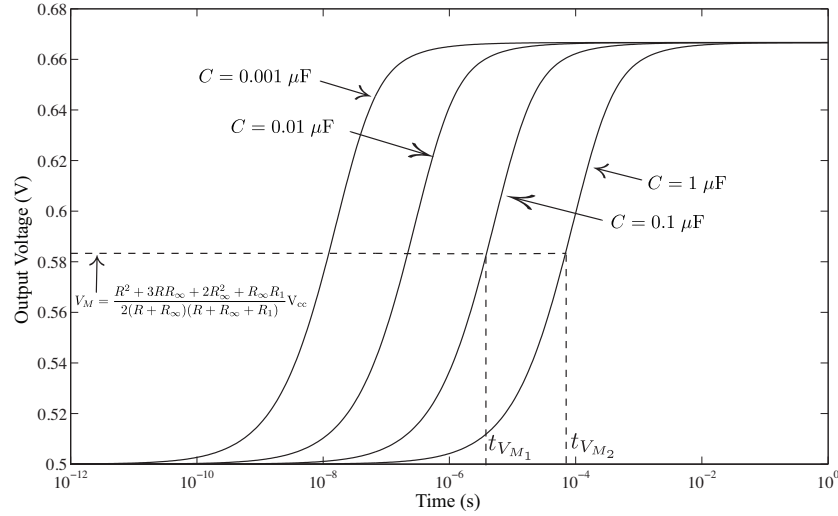


Figure 2.5: Comparison of location of V_M of the step response of Fig. 2.2(a) for varying values of C from $0.001 \mu\text{F}$ to $1 \mu\text{F}$ in decade steps with fixed resistors and α values of $1 \text{ k}\Omega$ and 0.8 , respectively.

rise time to higher or lower times with α determining the slope of the rise time for fixed R , R_∞ , and R_1 . From Fig. 2.5, with fixed values of $\alpha = 0.8$ and $R = R_\infty = R_1 = 1 \text{ k}\Omega$, decreasing C results in decreasing the location of the rise time without changing the slope. By comparing the midpoint voltage, that is the voltage that is half-way between the lower and upper limits, calculated as

$$V_M = \frac{R^2 + 3RR_\infty + 2R_\infty^2 + R_\infty R_1}{2(R + R_\infty)(R + R_\infty + R_1)} V_{cc} \quad (2.15)$$

observe that t_{V_M} decreases with decreasing C . From Fig. 2.5 each step response has a slope, calculated using (2.14), of 1.9 V/decade while t_{V_M} decreases from $68.928 \mu\text{s}$ to $3.8761 \mu\text{s}$, $0.21797 \mu\text{s}$, and 12.257 ns when decreasing the capacitance from $1 \mu\text{F}$ to $0.1 \mu\text{F}$, $0.01 \mu\text{F}$, and $0.001 \mu\text{F}$, respectively. How a change in C impacts the location of t_{V_M} is further quantified by observing that this shift per capacitance is linear when calculated as

$$\Delta T_M = \frac{\log_{10} \left(\frac{t_{V_{M2}}}{t_{V_{M1}}} \right)}{\log_{10} \left(\frac{C_2}{C_1} \right)} \quad (2.16)$$

Capacitance C (μF)	Midpoint Voltage V_M (V)	Midpoint Time t_{V_M} (s)	Shift Constant ΔT_M
1	0.5833	6.8928×10^{-5}	0.125
0.1	0.5833	3.8761×10^{-6}	0.125
0.01	0.5833	2.1797×10^{-7}	0.125
0.001	0.5833	1.2257×10^{-8}	-

Table 2.2: Numerical calculation of V_M , t_{V_M} , and ΔT_M using (2.5) while varying values of C for $\alpha = 0.8$ and $R = R_\infty = R_1 = 1 \text{ k}\Omega$.

where $t_{V_{M1,2}}$ are the midpoint voltage times for any two step responses with fixed α , R , R_∞ , and R_1 where $t_{V_{M2}} > t_{V_{M1}}$ to maintain a positive value, and $C_{1,2}$ are the corresponding capacitances of each step response. A comparison of the numerically calculated V_M , t_{V_M} , and ΔT_M values for each simulated step response in Fig. 2.5 are given in Table 2.2. Note that ΔT_M for each row is calculated using the values in that current row and one immediately below, but could also be calculated using a row and any row below it yielding the same ΔT_M . Having previously extracted the other Cole impedance parameters, C is extracted by calculating ΔT_M from two simulated step responses using known capacitances, C_1 and C_2 where $C_2 > C_1$ and the previously extracted impedance parameters. Then, knowing ΔT_M , C is calculated in two steps

$$n = \frac{\log_{10}(t_{V_m}/t_{C_1})}{\Delta T_M} \quad (2.17)$$

$$C = C_1 \cdot 10^n \quad (2.18)$$

where t_{V_m} is the closest sampled time above the midpoint voltage V_m from the collected step response and t_{C_1} is the time from the simulated step response using the known capacitance C_1 at the same voltage of t_{V_m} . Note, since it would be very difficult to ensure that the step response is sampled at exactly V_M we can use the first sampled value above V_M in the calculation, as long as we use this same voltage value and corresponding time when comparing against the simulated step response.

Fruit	Extracted Value Relative Error (%)			
	R_∞ (k Ω)	R_1 (k Ω)	α	C (nF)
Apricot 1	0.406	12.488	0.739	63
	-7.08×10^{-9}	7.55×10^{-4}	-4.34×10^{-5}	5.28×10^{-4}
Apple 1	2.72	26.915	0.633	122
	-7.34×10^{-8}	-7.34×10^{-3}	-1.57×10^{-3}	1.60×10^{-2}
Kiwi 1	0.260	4.765	0.669	265
	-6.70×10^{-8}	2.15×10^{-3}	-6.64×10^{-4}	7.05×10^{-3}
Potato 1	0.323	6.805	0.731	98
	-8.28×10^{-9}	6.86×10^{-4}	-1.23×10^{-4}	1.43×10^{-3}

Table 2.3: Numerically extracted Cole impedance parameters and relative errors from simulated step responses using previously extracted fruit parameters.

In summary, the useful properties for the impedance parameter extraction from this investigation of the voltage-excited step response are:

1. Lower and upper voltage limits depend on only R , R_∞ , and R_1 ;
2. Slope of the rise time on a log scale is dependent only on α ;
3. Position in time of the midpoint voltage is dependent only on C .

Using these properties the impedance parameters R_∞ , R_1 , C , and α can be extracted from a collected dataset using those regions of the step response described above that are dependent on only a single parameter to extract that parameter. The pseudo-algorithm to extract these parameters is shown in Fig. 2.6.

2.1.3 Extraction from Ideal Simulated Datasets

Implementing in MATLAB the process described in Section 2.1.2, and shown in Fig. 2.6, the impedance parameters from simulated step response datasets were extracted when the impedance parameters of fruits previously extracted in [51] were used. The extracted values as well as their relative errors when compared to the values presented in [51] are given in Table 2.3. For the simulated step responses $R = 1$ k Ω and $V_{cc} = 5$ V. The simulated dataset using the theoretical impedance parameters for Apricot 1 [51] is given in Fig. 2.7 as a solid

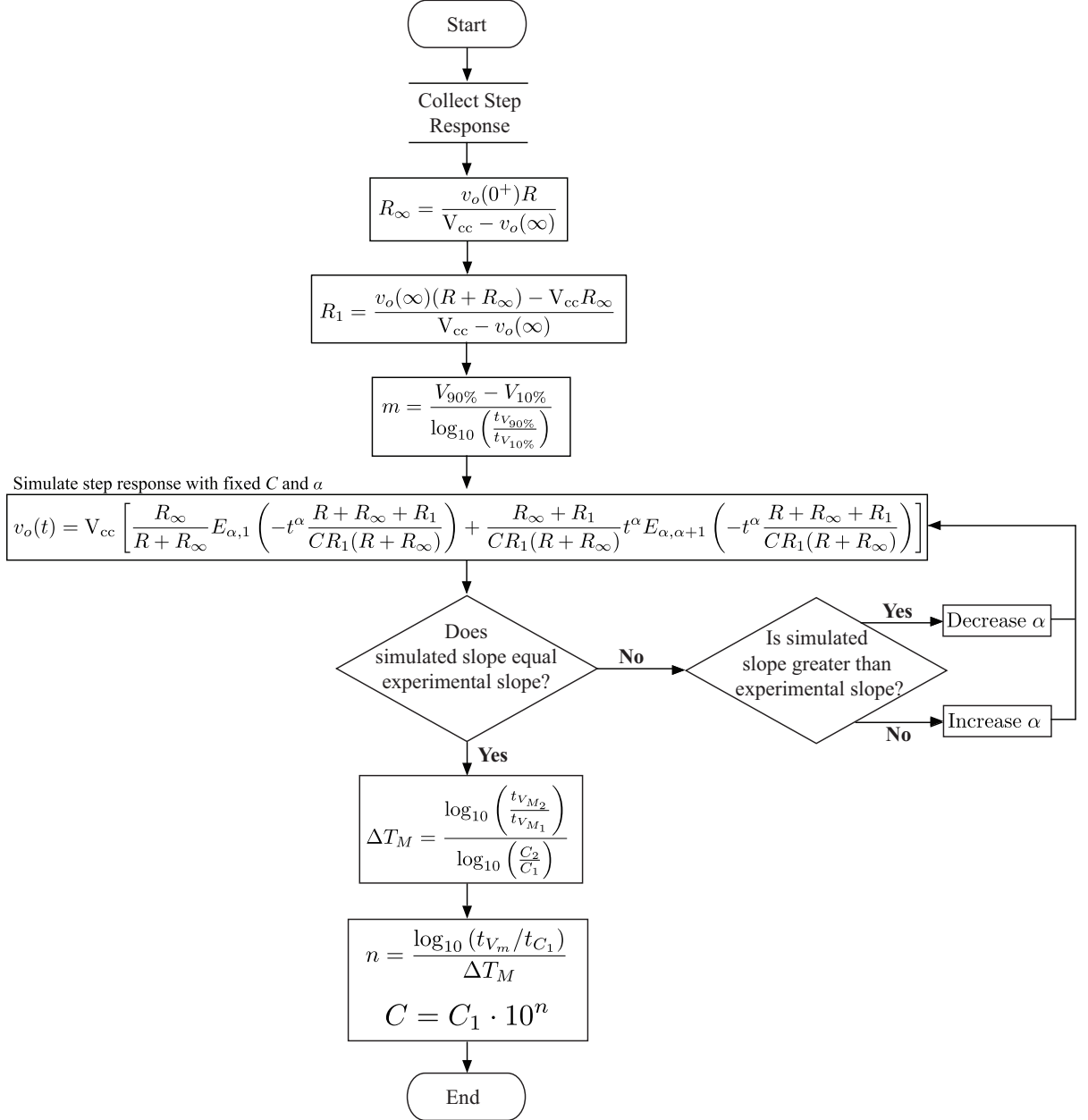


Figure 2.6: Psuedo-algorithm to numerically extract the Cole impedance parameters from the step response data.

line. From this dataset R_∞ was calculated using a value of $v_o(t)$ when $t < 0.1$ ns, the region where $v_o(t)$ is very close to its lower limit. Rearranging (2.12) to the form

$$R_\infty = \frac{v_o(0^+)R}{V_{cc} - v_o(0^+)} \quad (2.19)$$

and using $v_o(0) \approx v_o(0.5011 \text{ ps}) = 1.4438 \text{ V}$ yields $R_\infty = 0.406 \text{ k}\Omega$. Next, R_1 is calculated by rearranging (2.13) to the form

$$R_1 = \frac{v_o(\infty)(R + R_\infty) - V_{cc}R_\infty}{V_{cc} - v_o(\infty)} \quad (2.20)$$

and using $v_o(\infty) \approx v_o(100 \text{ s}) = 4.6401 \text{ V}$, the region where $v_o(t)$ is very close to its upper limit, we calculate $R_1 = 12.488 \text{ k}\Omega$. Next, using the slope calculated with (2.14), 1.202 V/decade , the value of α was numerically determined to be 0.739 . Now, two step responses using $C_1 = 1 \text{ nF}$ and $C_2 = 10 \text{ nF}$ with the previously extracted R_∞ , R_1 , and α are generated and sampled at the first value greater than $V_M = 3.042 \text{ V}$ in the dataset. These sampled values are taken at 3.1207 V at times of 7.3312 ns and $0.16533 \mu\text{s}$ for C_1 and C_2 , respectively. Using these collected values ΔT_M is calculated with (2.16) yielding 1.3532 . With ΔT_M and $v_o(1.9953 \mu\text{s}) = 3.1207 \text{ V}$ from the generated dataset in Fig. 2.7 we determine C , using (2.18) as $C = 63 \text{ nF}$. All of these extracted values show very good agreement with the theoretical values, with very small relative errors, given in Table 2.3. The step response using these extracted values is given in Fig. 2.7 as black circles showing perfect agreement with the simulated dataset given as the solid line. This verifies that we can extract all the impedance parameters (R_∞ , R_1 , α , and C) numerically from the simulated step-response data using the proposed process in Section 2.1.2.

2.1.4 PSPICE and Experimental Results

Building on the extraction of the impedance parameters from ideal datasets, we extract the Cole impedance parameters from the circuit of Fig. 2.2(a) implemented with a standard capacitor ($\alpha = 1$) and $R = 1 \text{ k}\Omega$ in both PSPICE and realized with discrete components. The impedance parameters used in the PSPICE simulation are given in Table 2.4. For this transient simulation a step voltage of 5 V with a rise time of 5 ns , pulse width of 1 ms , and period of 2 ms was applied. The output voltage, $v_o(t)$, collected from 10 ns to 1 ms is

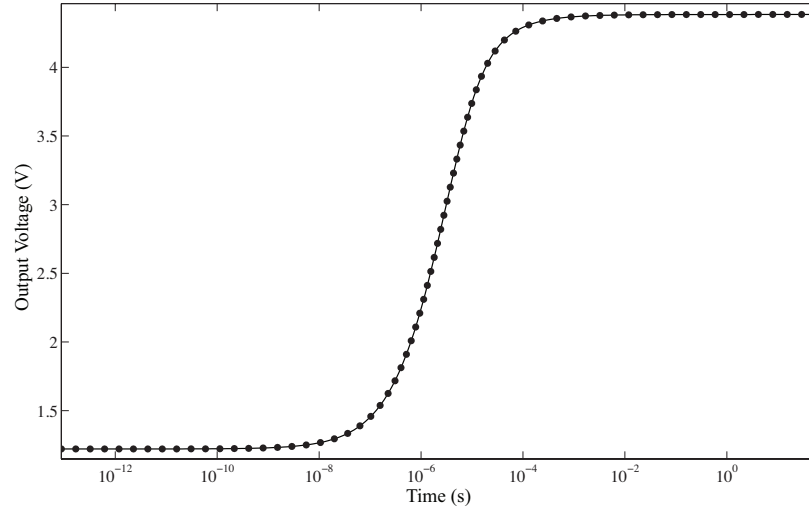


Figure 2.7: MATLAB simulated step responses using theoretical and extracted Cole impedance parameters of an apricot as a solid line and black circles, respectively, with $R = 1 \text{ k}\Omega$ and $V_{cc} = 5 \text{ V}$.

	Impedance Parameters			
	$R_{\infty} \text{ (k}\Omega\text{)}$	$R_1 \text{ (k}\Omega\text{)}$	α	$C \text{ (nF)}$
PSPICE	1.786	25.475	1.000	40.75
Extracted	1.786	25.460	1.000	40.79
Relative Error (%)	-6.88×10^{-3}	5.82×10^{-2}	2.38×10^{-5}	-8.88×10^{-2}

Table 2.4: Theoretical and numerically extracted Cole impedance parameters with relative errors from PSPICE simulated step response for an ideal capacitor ($\alpha = 1$).

shown in Fig. 2.8 as a solid line. The same algorithm implemented in MATLAB and previously applied to the ideal datasets was applied to the PSPICE dataset with the extracted parameters, as well as their relative errors, are given in Table 2.4. Again, the numerically extracted Cole impedance parameters show very close agreement with the theoretical values. Using the extracted parameters from Table 2.4, the step response of the circuit was simulated using (2.5), shown in Fig. 2.8 as a dashed line. It shows near perfect agreement with the PSPICE simulated results, further verifying that the algorithm can be used to extract the Cole parameters from step response data.

Finally the Cole impedance of Fig. 2.2(a) was realized using the components listed in Table 2.5 with $R = 0.996 \text{ k}\Omega$. Using this experimental setup a voltage pulse with 20 ns edge times, 500 ms pulse width, and period of 1 s generated by an Agilent 33250A

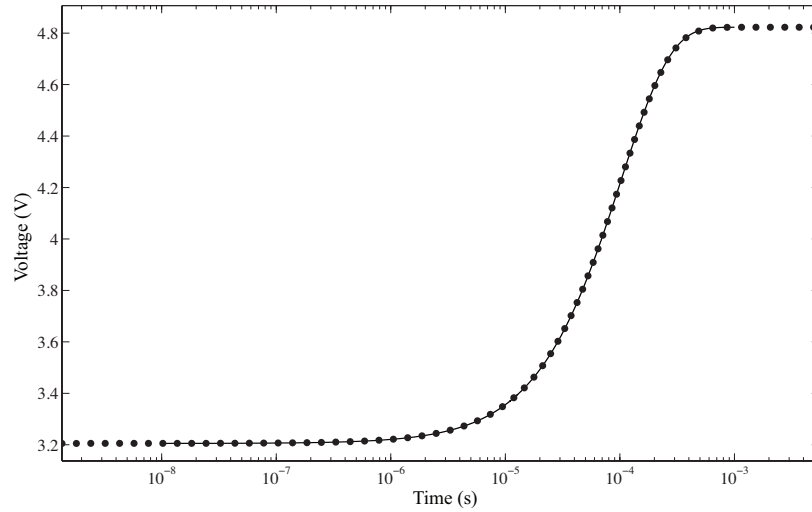


Figure 2.8: PSPICE and MATLAB simulated step responses using theoretical and numerically extracted Cole impedance parameters as solid and dashed lines, respectively, with $R = 1 \text{ k}\Omega$ and $V_{cc} = 5 \text{ V}$.

	Impedance Parameters			
	$R_{\infty} \text{ (k}\Omega\text{)}$	$R_1 \text{ (k}\Omega\text{)}$	α	$C \text{ (nF)}$
Measured	1.742	31.99	1.000	47
Extracted	1.796	34.73	1.000	45
Relative Error (%)	-3.138	-8.595	2.22×10^{-14}	4.243

Table 2.5: Measured and numerically extracted Cole impedance parameters with relative errors from experimentally collected step response.

waveform generator was applied to the circuit under test. The resulting response of the circuit was collected using a Tektronix 745D digital oscilloscope with maximum sampling rate of 2 GS/s and averaging 20 collected samples is given in Fig. 2.9(b) as the solid line labeled v_o . Averaging was used to reduce the noise in the collected waveform in order to achieve more accurate impedance parameters through the numerical extraction. The MATLAB algorithm was applied to the experimentally collected dataset in Fig. 2.9(b), with the numerically extracted Cole impedance parameters given in Table 2.5 along with their relative errors compared to the measured component values. Comparing the measured and extracted values we find that they are relatively close, with less than $\pm 10\%$ error for all components. Two main sources of error that contribute to the extracted parameters deviating from the measured values more than in simulation are noise and non-ideal $v_{in}(t)$.

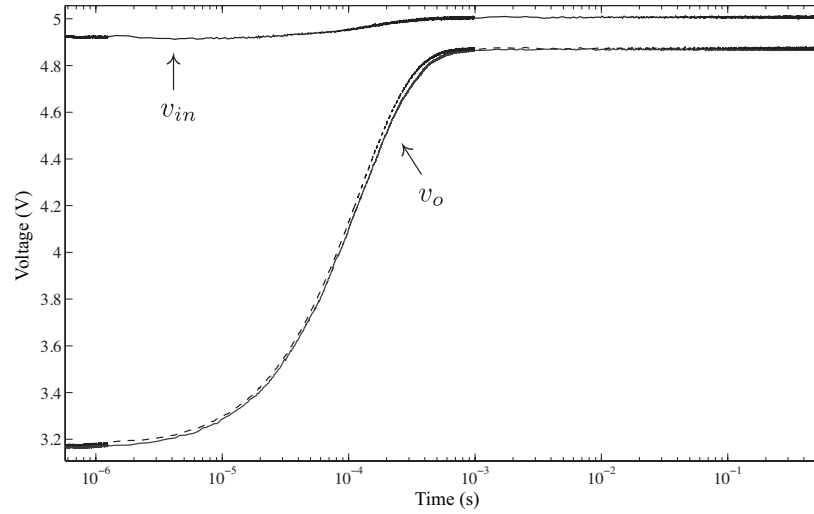


Figure 2.9: Experimental and MATLAB simulated step responses using numerically extracted Cole impedance parameters as solid and dashed lines, respectively, with $R = 0.996 \text{ k}\Omega$ and $V_{cc} = 5 \text{ V}$.

Even though averaging was used to reduce the noise on the measured output voltage, we still see some noise contribution in Fig. 2.9(b) contributing errors to all of the impedance parameters. Also, $v_{in}(t)$ in Fig. 2.9(b) is not a perfect 5 V signal, as was the case in both the MATLAB and PSPICE simulations, which introduces error into both the calculated R_∞ and R_1 values and later α and C in subsequent calculations. Nevertheless, the step response simulated using (2.5) and the extracted parameters, shown in Fig. 2.9(b) as the dashed line, shows good agreement with the experimentally collected response. This confirms that the process described in Section 2.1.2 can be implemented and successfully used to numerically extract the Cole impedance parameters (R_∞ , R_1 , α , and C) from the experimentally collected step response of the circuit in Fig. 2.2(a).

2.1.5 Limitations

There are two serious limitations introduced by both the signal generator and oscilloscope when measuring the voltage excited step response of the Cole impedance test circuit in Fig. 2.2(a). First, note that the voltage-excited step response in Fig. 2.10 exhibits 3 distinct regions: 1) at very low times, when the CPE is uncharged, a constant voltage results from

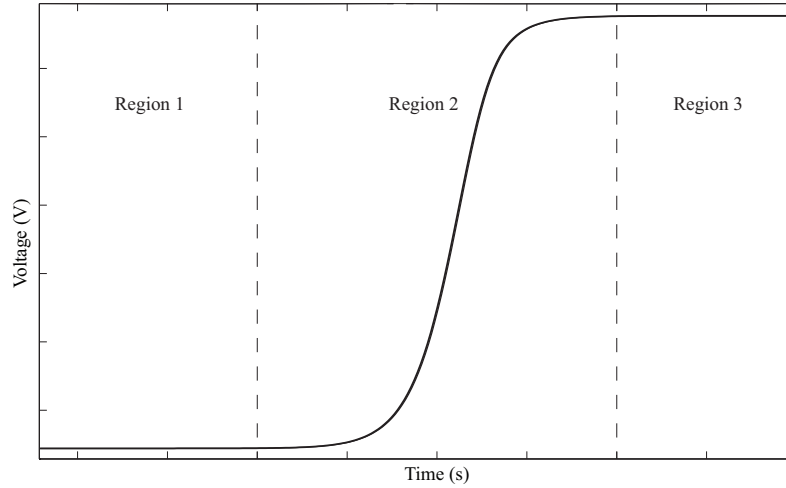


Figure 2.10: Lower divider, charging, and upper divider regions common to all step responses of the circuit in Fig. 2.2.

the voltage divider formed by R and R_∞ , 2) the increasing voltage region when the CPE is charging, and 3) at high times, another constant voltage region from the voltage divider network of R , R_∞ , and R_1 when the CPE is fully charged. When applying a step input to the circuit, the rise time of this generated signal must be fast enough that it reaches its steady state value before the capacitor begins to charge, that is while it is still in Region 1. Otherwise, if the signal reaches its steady state value during the charging region, Region 2, it will not be possible to capture an accurate value of the Region 1 voltage divider. Without this value it is impossible to calculate an accurate value of R_∞ . The same is true when measuring this step response using an oscilloscope, which must sample the output voltage quickly enough to provide a value within Region 1, or else introduce significant error into the extracted R_∞ value which propagates into all further calculations.

With the numerical extraction of the impedance parameters requiring a value in Region 1, it becomes important to know what impacts the location in time of Region 2. From Section 2.1.2 we previously noted that both α and C impact the location in time and duration of Region 2. With the length of the Region 2 increasing with decreasing α while the location decreases in time with decreasing C . Therefore, lower values of both α and C require much faster signal generators and oscilloscopes to be able to capture the three distinct regions of

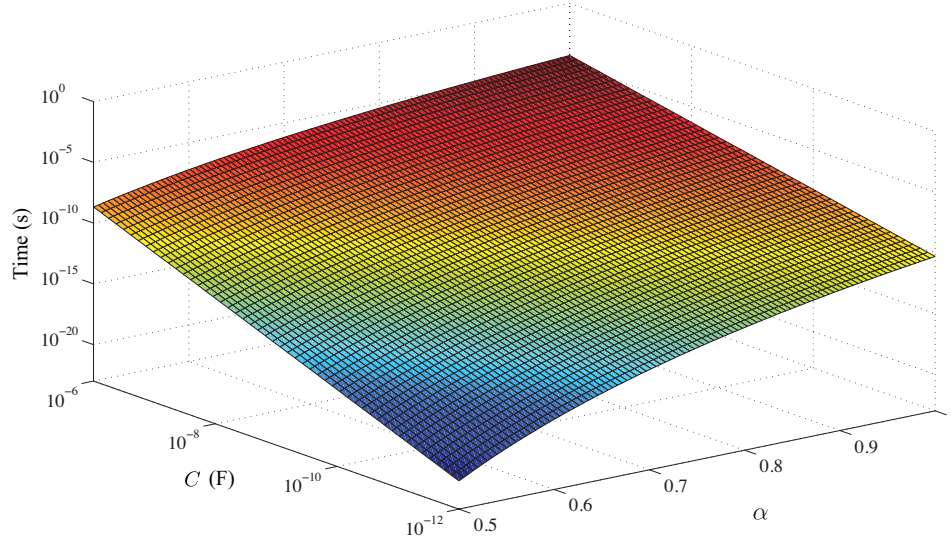


Figure 2.11: Minimum sampling time required for R_∞ extraction within 5% for $0.5 \leq \alpha \leq 1$ and $1 \text{ pF} \leq C \leq 1 \text{ }\mu\text{F}$ when $R = R_\infty = R_1 = 1 \text{ k}\Omega$.

the step response. A simulation showing the minimum time to keep the calculated value of R_∞ within 5% of its value is shown in Fig. 2.11. This figure was generated for fixed $R = R_\infty = R_1 = 1 \text{ k}\Omega$ while varying C from 1 pF to 1 μF and α from 0.5 to 1. Therefore, the signal generator must have a rise time and the oscilloscope a sampling time equal to or lower than this value in order for the numerical extraction to give an R_∞ value within 5%.

2.2 Least Squares Extraction from Step Response

It is clear that the measurement of $v_o(0)$ and $v_o(\infty)$ has a significant impact on the accuracy of the extracted Cole impedance parameters. Since their exact values cannot be measured from a response that does not extend from $t = 0$ to $t = \infty$, their measured values will only ever be an approximation. These approximate values introduce errors into the extracted R_∞ and R_1 that propagate into the extracted α and C ; which require accurate R_∞ and R_1 values for their calculation. For example, the effect of these errors on the extracted parameters from (2.5) simulated with $R = R_\infty = R_1 = 1 \text{ k}\Omega$, $\alpha = 0.75$, $C = 100 \text{ nF}$, $V_{cc} = 5 \text{ V}$, and the output voltage sampled at times $v_o(0) \approx v_o(1 \text{ ps})$, $v_o(1 \text{ ns})$, and $v_o(1 \text{ }\mu\text{s})$, respectively, are given in Table 2.6.

$v_o(0)$ measured after	Relative Error (%)			
	R_∞	R_1	α	C
1 ps	0.00109	0.000383	0.00140	−0.00114
1 ns	0.193	−1.92	0.456	−2.71
1 μ s	29.1	−29.1	33.3	−78.6

Table 2.6: Relative errors of parameters extracte from simulated step responses for different measured values of $v_o(0)$.

As the error in the $v_o(0)$ value increases due to measurements being made farther in time from the ideal $t = 0$, the errors of the extracted parameters get significantly larger with the largest effect seen in the error of the extracted C value reaching an error of -78.6% when the output voltage used in the calculation was $v_o(0) \approx v_o(1 \mu s)$. This highlights how sensitive this extraction process is to the accuracy of the value collected to approximate $v_o(0)$; which serves as the foundation for the extraction of all further impedance parameters. The problem becomes worse with lower α and C values, which decrease both the rise time and location of the midpoint voltage [100], which increases the hardware complexity by requiring a high precision step input generator.

The limitation of the direct extraction method can be overcome using a non-linear least squares fitting (NLSF) method, which we initially proposed in [102]. Fitting routines to extract fractional information from time-domain responses have also been previously employed for general experimental data [103] and for the fractional behaviour of nested and ladder circuits [104]. The non-linear least squares fitting used in this work is a numerical method that attempts to solve the problem

$$\begin{aligned} \min_x \|T(x) - ydata\|_2^2 &= \min_x \sum_{i=1}^n (T(x)_i - ydata_i)^2 \\ \text{s.t. } x &> 0 \end{aligned} \quad (2.21)$$

where x is the vector of impedance parameters (R_∞ , R_1 , α , C), $T(x)$ is the time domain step response (2.5) calculated using x , $ydata$ is the collected step response to fit to (2.5), $T(x)_i$ and $ydata_i$ are the simulated response and collected response at time t_i , and n is

the total number of data points in the collected step response. This routine aims to find the impedance parameters that would ideally reduce the least squares error to zero. The accuracy of the parameters extracted from the collected dataset using the NLSF method is not limited by the accuracy of R_∞ and R_1 , determined by 2 datapoints in the direct method, because every collected datapoint is used to find the parameters that result in the best fit. This fitting was implemented in MATLAB using the *lsqcurvefit* function to estimate the parameters using the trust-region-reflective algorithm [105]. To begin, the NLSF method requires an initial guess, x_0 , to apply and iteratively solve towards a solution x^* . Using the default settings in MATLAB, the solver will quit its search if any of these conditions are satisfied:

1. The number of function evaluations exceeds $100 \cdot m$, where m is the number of impedance parameters in x ;
2. The number of iterations of the algorithm exceeds 400;
3. The change in the value of x is less than 1×10^{-6} ;
4. The change in the function value is less than 1×10^{-6} .

After quitting due to meeting any of the ending criteria the solver returns a possible solution.

2.2.1 Voltage Excited Step Response

Both the direct and NLSF methods were applied to the ideal step responses of the circuit in Fig. 2.2(a), given by (2.5), using fruit impedance parameters from [51] with $R = 1 \text{ k}\Omega$. These MATLAB simulations were carried out for a $1 \mu\text{s}$ to 1 s time set with the relative errors using each method compared to the ideal impedance parameters given in Table 2.7. From these results the NLSF shows up to 5 orders of magnitude less error than the direct method. Therefore, a high level of accuracy can be maintained using the NLSF method

Fruit	Absolute Relative Error (%) $\left[\frac{\text{NLSF}}{\text{Direct}} \right]$			
	R_∞	R_1	α	C
Apple	1.93×10^{-3}	1.23×10^{-4}	1.60×10^{-3}	1.15×10^{-2}
	1.78×10^2	5.77×10^0	3.38×10^1	8.76×10^1
Apricot	1.38×10^{-3}	3.40×10^{-4}	3.54×10^{-3}	1.87×10^{-2}
	5.74×10^1	5.71×10^0	3.18×10^1	7.52×10^1
Kiwi	1.82×10^0	9.98×10^{-2}	9.00×10^{-3}	1.00×10^{-1}
	8.02×10^2	4.38×10^1	4.77×10^1	8.18×10^1
Potatoe	7.08×10^{-3}	2.93×10^{-4}	8.80×10^{-4}	6.97×10^{-3}
	3.42×10^2	1.62×10^0	3.68×10^1	8.57×10^1

Table 2.7: Absolute relative errors from simulated responses of fruit tissues from 1 μ s to 1 s.

while relaxing the hardware requirements since it is enough to gather data over 6 decades (from 1 μ s to 1 s). Recall from Table 2.6 that this is not possible with the direct extraction method.

The Cole impedance of Fig. 2.2(a) was realized using discrete components $R = 1.007$ k Ω , $R_\infty = 1.753$ k Ω , $R_1 = 32$ k Ω , $C = 1$ μ F, and $\alpha = 1$. Using this setup a voltage step input of 5 V was applied using a Agilent 33250A waveform generator. A pulse with 15 ns edge time, 500 ms pulse width, and period of 1 s was generated and applied to the circuit under test with the resulting response measured using a Tektronix 745D digital oscilloscope. The collected step response is shown in Fig. 2.12 as the solid line. The NLSF was applied to the experimentally collected dataset with relative errors of (4.91, 7.11, 3.46×10^{-7} , 2.22×10^{-6})% for (R_∞ , R_1 , α , C), respectively. The response simulated using the estimated parameters (dashed line in Fig. 2.12) shows very good agreement with the experimentally collected response.

To further verify the NLSF method, the circuit of Fig. 2.2(a) was implemented using an apple and a tomato as the Cole impedances with $R = 1.007$ k Ω . The values extracted from the step response, collected from 1 μ s to 500 ms, from both fruits are given in Table 2.8. The collected step response of the circuit realized with the apple and tomato are shown in Figs. 2.13(a) and (b), respectively, as solid lines with the MATLAB simulated response

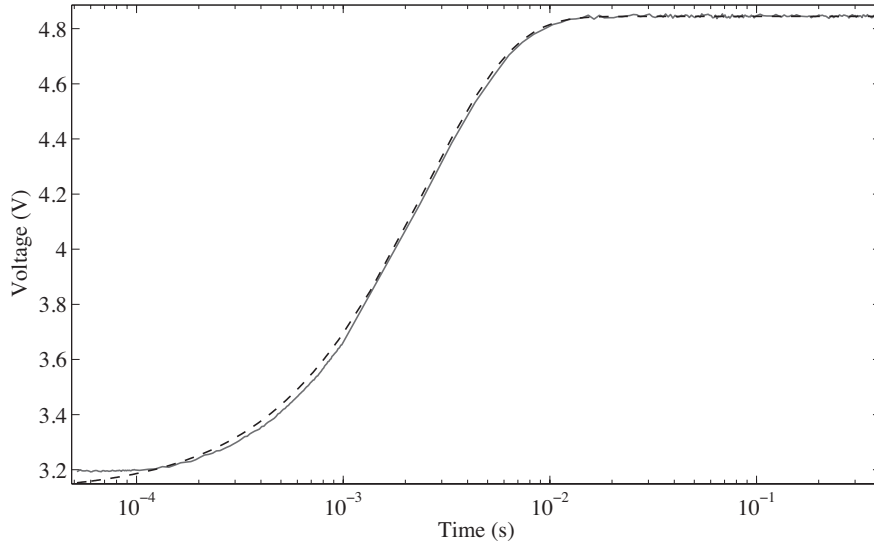


Figure 2.12: Experimental (solid) and MATLAB simulated (dashed) step responses of Fig. 2.2(a) when $(R_\infty, R_1, \alpha, C) = (1.753 \text{ k}\Omega, 32 \text{ k}\Omega, 1, 1 \mu\text{F})$.

Fruit	Impedance Parameters			
	R_∞ (k Ω)	R_1 (k Ω)	α	C (nF)
Apple	2.206	29.88	0.8814	4.769
Tomato	0.0246	19.64	0.6145	372.5

Table 2.8: NLSF extrace Cole impedance parameters from experimentally collected step responses of fruit.

using the NLSF estimated parameters shown as dashed lines.

2.2.2 Current Excited Step Response

A simplified expression for the time domain output voltage, $v_o(t)$, of the Cole impedance induced by a current-step of amplitude I_{cc} , as shown in the circuit given in Fig. 2.2(b), compared to (2.7) given in Section 2.1 was presented in [106] and [107]. The s -domain expression of the output voltage when the input current step has an amplitude of I_{cc} , that is $I_{in}(s) = I_{cc}/s$ is given by

$$\begin{aligned}
 V_o(s) &= \frac{I_{cc}}{s} \left[R_\infty + \frac{R_1}{1 + s^\alpha R_1 C} \right] \\
 &= \frac{I_{cc}}{s} \left[R_\infty + \frac{1/C}{s^\alpha + 1/R_1 C} \right]
 \end{aligned}$$

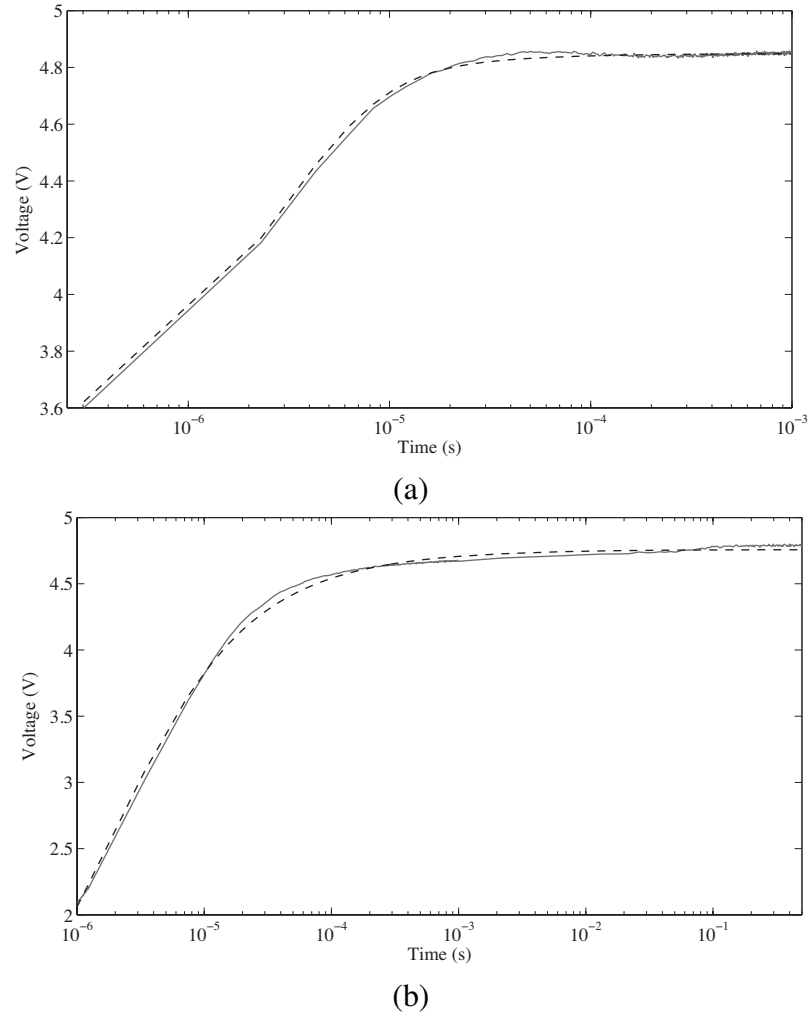


Figure 2.13: Experimental (solid) and MATLAB simulated (dashed) step responses using an (a) apple and (b) tomato in the circuit of Fig. 2.2(a).

$$= I_{cc} \left[\frac{R_{\infty}}{s} + \frac{1}{C} \cdot \frac{s^{-1}}{s^{\alpha} + 1/R_1 C} \right] \quad (2.22)$$

Applying the Laplace transform formula for the Mittag-Leffler function given by (2.4) to (2.22) yields the time domain expression of the output voltage given by

$$v_o(t) = I_{cc} \left[R_{\infty} + \frac{t^{\alpha}}{C} E_{\alpha, \alpha+1} \left(\frac{-t^{\alpha}}{RC} \right) \right] \quad (2.23)$$

This simplification reduces the number of Mittag-Leffler terms from two to one for the simulation of each step response. The derivations of (2.7) and (2.23) are presented in

Appendix B to confirm their equivalency, as well as detail the advantages of using (2.23) over (2.7).

A MATLAB simulated example of (2.23) when $R_\infty = 406 \, \Omega$, $R_1 = 12.894 \, \text{k}\Omega$, $C = 62.34 \, \text{nF}$, $\alpha = 0.739$, and $I_{cc} = 0.1 \, \text{mA}$ is given in Fig. 2.14 as a solid line. From this step-response we note that there are three distinct regions common to the step response of all single-dispersion Cole impedance models to a current step input: 1) at very low times, when the CPE is uncharged, a constant voltage results from the current applied to R_∞ , 2) the increasing voltage region when the CPE is charging, and 3) at high times, another constant voltage region results from the current applied to $R_\infty + R_1$; when the CPEs are fully charged.

Similar to the voltage-excited step response, the impedance parameters can be extracted from the current-excited step response by applying a NLSF to fit the collected data to (2.23). Initial guesses to use in the solver can be estimated from (2.23), noting that at $t = 0$ and $t = \infty$ the voltage will be $v_o(0) = I_{cc}R_\infty$ and $v_o(\infty) = I_{cc}(R_\infty + R_1)$. Since the collected step response will not extend from $t = 0$ to $t = \infty$ but is instead finite in the range $0 < t_1 < t_n < \infty$, where t_1 and t_n are the smallest and largest time datapoints, respectively, boundaries when generating R_∞ and R_1 for the initial guesses can be generated such that

$$R_\infty \leq \frac{v_o(t_1)}{I_{cc}} \quad (2.24)$$

$$R_1 \geq \frac{v_o(t_n)}{I_{cc}} - R_\infty \quad (2.25)$$

Finally the range of values reported in the literature are used to create the bounds to generate the initial guesses such that $0 \leq \alpha \leq 1$ and $0.1 \, \text{nF} \leq C \leq 1 \, \text{mF}$.

2.2.2.1 Simulation Results

Previously, when extracting the impedance parameters from the ideal voltage-excited step response only a single initial guess was applied to the solver yielding accurate results. How-

Noise (%)	Relative Error (%)			
	R_∞	R_1	C	α
0.5	0.480	0.033	0.693	0.095
1.0	1.07	0.062	1.43	0.20
2.0	1.94	0.132	2.85	0.40

Table 2.9: Average relative error of impedance parameters extracted from 100 MATLAB simulations of the single dispersion step response with 0.5%, 1%, and 2% random noise.

ever, the addition of noise to an ideal dataset increases the likelihood of the solver finding a local minima that satisfies the ending criteria of the solver without being the global solution. One method to overcome this problem is to run the solver multiple times, each time using a new randomly generated x_0 . With the intent that one or more of the randomly generated initial guesses will be close in proximity to the global solution and return it as the solution when the ending criteria are met. Therefore, by solving (2.21) from each x_0 and selecting the solution set that yields the lowest least squares error increases the likelihood of finding the global solution. The accuracy of extracting the single dispersion impedance parameters from step response data using this approach is assessed by extracting the parameters from 100 MATLAB simulations of (2.23) with random noise levels of 0.5%, 1%, and 2% with 5 applied initial guesses. For all simulations, the datasets were generated from $t_1 = 0.1 \mu\text{s}$ to $t_n = 10 \text{ s}$ with 50 logarithmically spaced datapoints using impedance parameters $R_\infty = 406 \Omega$, $R_1 = 12.894 \text{ k}\Omega$, $C = 62.34 \text{ nF}$, $\alpha = 0.739$, previously extracted from an apricot [51], to an input step of $I_{cc} = 0.1 \text{ mA}$. The impact of increasing levels of noise in the collected step response dataset on the relative errors of the extracted parameters are given in Table 2.9; with errors less than 3% for all parameters at all levels of random noise. The level of noise has the greatest impact on the extraction of the C parameter. An example of a simulated dataset with 2% noise (solid line) compared to the simulation using the extracted parameters (circles) is given in Fig. 2.14. From this dataset the output voltages at $0.1 \mu\text{s}$ and 10 s are $v_o(0.1 \mu\text{s}) = 0.0524 \text{ V}$ and $v_o(10 \text{ s}) = 1.2813 \text{ V}$, respectively. Therefore, from (2.24) and (2.25) the boundaries for the generation of the initial guesses are $R_\infty \leq 524 \Omega$

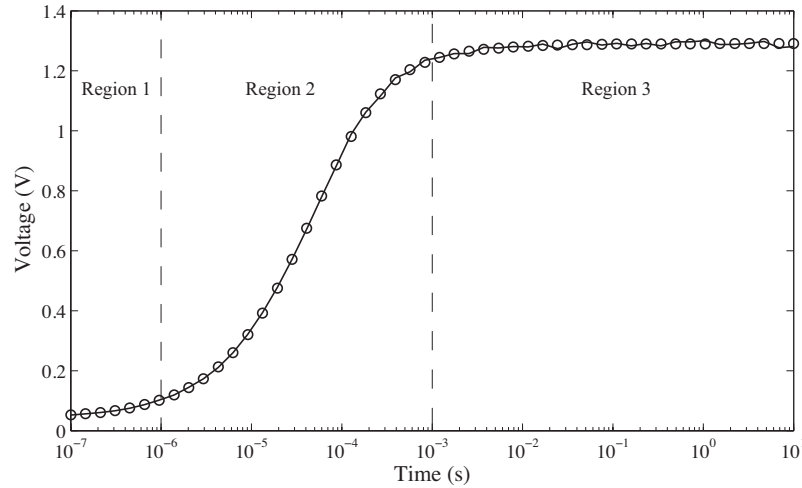


Figure 2.14: MATLAB simulated step responses of single dispersion Cole impedance model excited by a step current of 0.1 mA when $R_\infty = 406 \, \Omega$, $R_1 = 12.894 \, \text{k}\Omega$, $C = 62.34 \, \text{nF}$, and $\alpha = 0.739$. Ideal simulations with 0.5% noise are given as a solid line with the simulations using the extracted parameters given as circles.

and $R_1 \geq 12.289 \, \text{k}\Omega$. Applying the NLSF with 5 initial guesses yields relative errors of $[0.223, 0.077, 2.67, 0.264]\%$ for $[R_\infty, R_1, C, \alpha]$, respectively. The simulated dataset using the extracted parameters shows less than 1.3% relative error with the simulated noisy dataset over the entire time scale.

2.2.2.2 Experimental Results

The AD844 is a current-mode operational amplifier that can be operated as a second-generation current conveyor [108] when configured as shown in Fig. 2.15. In this configuration, when an input voltage-step of amplitude V_{cc} is applied it is converted to a current-step of amplitude $I_{cc} = V_{cc}/(R + R_i)$ where R_i is the internal resistance of the AD844, and is approximately $50 \, \Omega$. Using this circuit a voltage-step was applied to the AD844 by an Agilent 33250A signal generator to create a step-current of $I_{cc} = 1\text{V}/(9.92\text{k}\Omega + 50\Omega) \approx 0.1 \, \text{mA}$ which was applied to 2 apples, used as the Cole impedances in Fig. 2.15. The responses, $v_o(t)$, collected using a Tektronix 745D digital oscilloscope, composed of 51 logarithmically spaced datapoints from $0.2 \, \mu\text{s}$ to 0.07s , are given in Fig. 2.16(a) as solid and dashed lines. From the experimental step responses parameters of $[R_\infty, R_1, C, \alpha]$ were

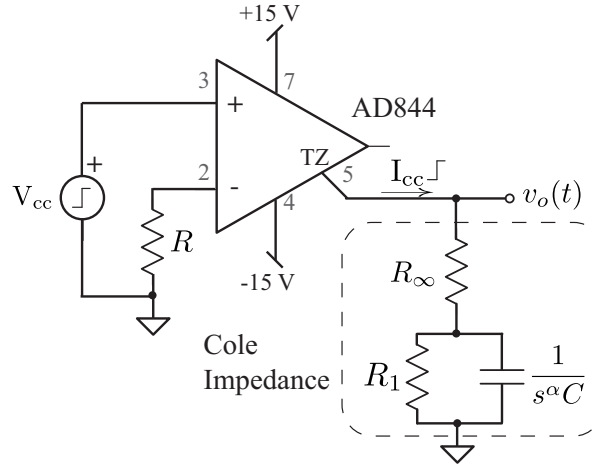


Figure 2.15: Test circuit to apply a current-step input to a single dispersion Cole impedance with the AD844 operating as a current conveyor.

extracted as [4.64 k Ω , 42.9 k Ω , 69.1 nF, 0.646] and [6.99 k Ω , 50.3 k Ω , 38.1 nF, 0.701] for apple 1 and 2, respectively. The MATLAB simulated responses using these parameters are given in Fig. 2.16(a) as black circles. These simulated responses show very good agreement with the experimental results, with the relative errors between the experimental and simulated datapoints given in Fig. 2.16(b) as solid and dashed lines for apple 1 and apple 2, respectively. The simulated results show less than 2% relative error over the entire collected datasets.

2.3 Least Squares Extraction from Magnitude Response

In [51] and [52] a Cole impedance is used as a component in the extraction circuits, shown in Figs. 2.17(a) and (b), respectively, exhibiting the frequency responses described by

$$T_1(s) = \frac{V_o(s)}{V_{in}(s)} = \frac{1}{G_1} \frac{1 + (\tau s)^\alpha}{1 + \frac{G_2}{G_1} (\tau s)^\alpha} \quad (2.26)$$

$$T_2(s) = \frac{V_o(s)}{V_{in}(s)} = -\frac{G_1 + G_2 (\tau s)^\alpha}{1 + (\tau s)^\alpha} \quad (2.27)$$

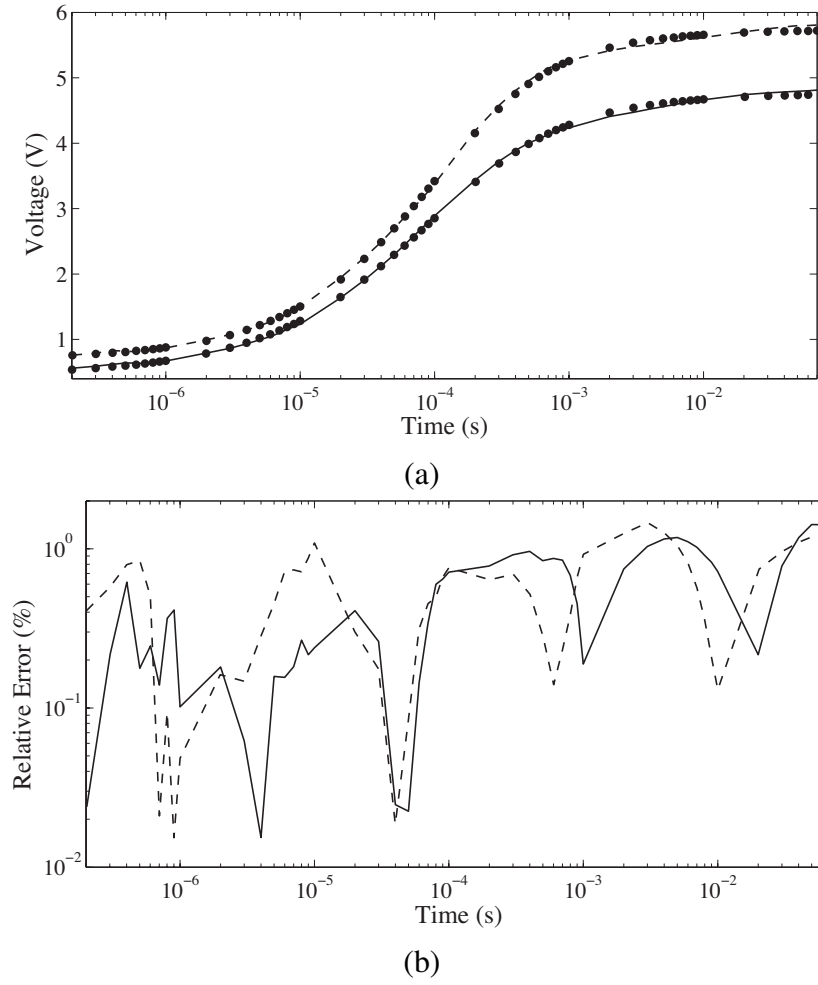


Figure 2.16: (a) Experimentally collected step responses of apple 1 (solid) and apple 2 (dashed) compared to MATLAB simulated responses using extracted impedance parameters (black circles) and (b) absolute relative errors of apple 1 and 2 simulated responses compared to the experimental.

where $T_1(s)$ and $T_2(s)$ are the filter and integrator transfer functions, respectively. $G_{1,2}$ are the low and high frequency gains, respectively, related to R_o and R_∞ through the relations

$$G_{1,2} = 1 + \frac{R_{o,\infty}}{R_L} \quad (2.28)$$

$$G_{1,2} = \frac{R_{o,\infty}}{R_L} \quad (2.29)$$

where (2.28) and (2.29) are the gains for the filter and integrator circuits, respectively. From the collected frequency responses R_o and R_∞ can be extracted knowing $G_{1,2}$ and R_L . While

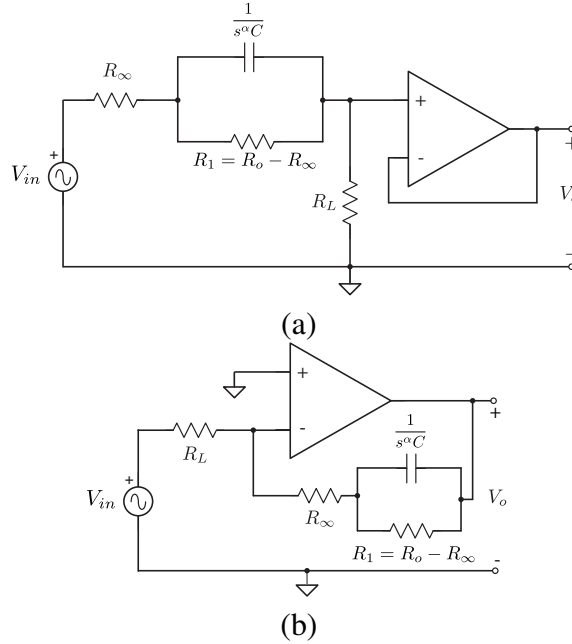


Figure 2.17: Circuits for (a) filter and (b) integrator extraction of the Cole model parameters.

Parameter	Filter	Integrator
a	$\frac{G_1 - 2G_2}{\sqrt{G_1 G_2}}$	$\frac{\sqrt{G_1 G_2} (G_1 - 2G_2)}{G_1^2 - 2G_2^2}$
b		$\frac{G_1 (3G_1 - 4G_2)}{(G_1 - 2G_2)^2}$
$ T(j\omega_{3dB}) $	$\frac{1}{\sqrt{2}G_2}$	$\frac{G_1}{\sqrt{2}}$
$ T(j\omega_{\phi max}) $	$\frac{1}{\sqrt{G_1 G_2}}$	$\sqrt{G_1 G_2}$

Table 2.10: Parameters from (2.30) for the filter and integrator circuits of Fig. 2.17(a) and (b), respectively.

α is found numerically through the solution of the equation

$$\left(\frac{\omega_{3dB}}{\omega_{\phi max}} \right)^\alpha = a \left(\sqrt{\frac{b + \cos(\alpha\pi)}{2}} \pm \cos\left(\frac{\alpha\pi}{2}\right) \right) \quad (2.30)$$

where ω_{3dB} is the frequency at which $|T(j\omega)|$ is -3 dB below its maximum value, $\omega_{\phi max}$ is the frequency at which the phase angle exhibits a maximum value, and both a and b are products of the low and high frequency gains. The values of these parameters in (2.30) for the filter and integrator circuits are given in Table 2.10. Next, knowing α , $G_{1,2}$, and $\omega_{\phi max}$,

τ is found from

$$\tau = \frac{1}{\omega_{\phi_{max}}} \left(\sqrt{\frac{G_1}{G_2}} \right)^{1/\alpha} \quad (2.31)$$

These methods combine calculations from direct measurements and a constrained optimization routine for the extraction of the impedance parameters. However, the use of direct measurements introduces significant error into the extracted impedance parameters.

2.3.1 Effects of Low and High Frequency Gain Errors

In [109] direct measurements of $G_{1,2}$ from the frequency response were shown to have a significant impact on the accuracy of the extracted impedance parameters. Since their exact values cannot be measured from a frequency response that does not extend from $\omega = 0$ to $\omega = \infty$, it is important to understand how their errors will contribute to the extracted impedance parameters. The sensitivities of R_o and R_∞ to G_1 and G_2 , respectively, are given by

$$S_{G_1, G_2}^{R_o, R_\infty} = \frac{G_{1,2}}{1 - G_{1,2}} \quad (2.32)$$

$$S_{G_1, G_2}^{R_o, R_\infty} = 1 \quad (2.33)$$

where (2.32) and (2.33) are the sensitivities for the filter and integrator circuits, respectively. Errors in $G_{1,2}$ impact both α and τ which require $|T(j\omega_{3dB})|$ and $|T(j\omega_{\phi_{max}})|$, both functions of $G_{1,2}$, to determine ω_{3dB} and $\omega_{\phi_{max}}$ for their calculation. The filter circuit variabilities for $|T(j\omega_{3dB})|$ and $|T(j\omega_{\phi_{max}})|$ to $G_{1,2}$ are given by

$$\frac{d|T(j\omega_{3dB})|}{|T(j\omega_{3dB})|} = S_{G_1}^{|T(j\omega_{3dB})|} \frac{dG_1}{G_1} + S_{G_2}^{|T(j\omega_{3dB})|} \frac{dG_2}{G_2} \quad (2.34)$$

$$= -\frac{dG_2}{G_2} \quad (2.35)$$

$$\frac{d|T(j\omega_{\phi_{max}})|}{|T(j\omega_{\phi_{max}})|} = S_{G_1}^{|T(j\omega_{\phi_{max}})|} \frac{dG_1}{G_1} + S_{G_2}^{|T(j\omega_{\phi_{max}})|} \frac{dG_2}{G_2} \quad (2.36)$$

$$= -\left(\frac{1}{2} \frac{dG_1}{G_1} + \frac{1}{2} \frac{dG_2}{G_2} \right) \quad (2.37)$$

The variabilities of the integrator circuit to $|T(j\omega_{3dB})|$ and $|T(j\omega_{\phi max})|$ are equal in magnitude to (2.34) and (2.36), respectively, but with opposite sign. Errors in $|T(j\omega_{3dB})|$ and $|T(j\omega_{\phi max})|$ result in ω_{3dB} and $\omega_{\phi max}$ errors, since these frequencies are extracted from incorrect magnitudes. The errors in ω_{3dB} and $\omega_{\phi max}$ then contribute to errors in α when numerically calculated from (2.30). This further contributes error to τ calculated using (2.31) whose variability to $G_{1,2}$, $\omega_{\phi max}$, and α is given by

$$\frac{d\tau}{\tau} = S_{G_1}^{\tau} \frac{dG_1}{G_1} + S_{G_2}^{\tau} \frac{dG_2}{G_2} + S_{\omega_{\phi max}}^{\tau} \frac{d\omega_{\phi max}}{\omega_{\phi max}} + S_{\alpha}^{\tau} \frac{d\alpha}{\alpha} \quad (2.38)$$

$$= \frac{1}{2\alpha} \left(\frac{dG_1}{G_1} - \frac{dG_2}{G_2} \right) - \frac{d\omega_{\phi max}}{\omega_{\phi max}} - \frac{\ln\left(\frac{G_1}{G_2}\right)}{2\alpha} \frac{d\alpha}{\alpha} \quad (2.39)$$

With the errors of $\omega_{\phi max}$ and α previously shown to be a result of $G_{1,2}$ errors, then the entire error contributed to τ in (2.39) can be traced to errors in $G_{1,2}$.

The filter circuit errors contributed by a finite frequency response to G_1 and G_2 will always be positive and negative, respectively, because $|T(j\omega_1)| > |T(0)|$ and $|T(j\omega_2)| < |T(\infty)|$ where $0 < \omega_1 < \omega_2 < \infty$. The opposite is true for the integrator circuit, which exhibits a low pass frequency response, where $|T(j\omega_1)| < |T(0)|$ and $|T(j\omega_2)| > |T(\infty)|$. Therefore, the effect of errors introduced by $G_{1,2}$ on the extracted ω_{3dB} , $\omega_{\phi max}$, α and τ from the circuit of Fig. 2.17(a) for low and high frequency errors from 0 to $\pm 3.5\%$ and $\mp 3.5\%$, respectively, are shown in Fig. 2.18(a). Those errors from the circuit of Fig. 2.17(b) are shown in Fig. 2.18(b). These relative errors were computed from a MATLAB simulated frequency response of (2.26) and (2.27), respectively, using the known Cole parameters of an apricot ($R_o = 12.894 \text{ k}\Omega$, $R_{\infty} = 0.4057 \text{ k}\Omega$, $\alpha = 0.739$, $\tau = 62.34 \mu\text{s}$) [51] and $R_L = 1 \text{ k}\Omega$. The $\pm 3.5\%$ and $\mp 3.5\%$ error in G_1 and G_2 , respectively, correspond to using a frequency response from 101 Hz to 1.49 MHz for the filter circuit and 93 Hz to 7.92 MHz for the integrator. To minimize the sampling error of a discrete dataset $\omega_{\phi max}$ and ω_{3dB} were calculated from $|T(j\omega_{\phi max})|$ and $|T(j\omega_{3dB})|$, respectively, simulated to have relative errors of less than $10^{-12}\%$ from the values predicted using the measured $G_{1,2}$. From

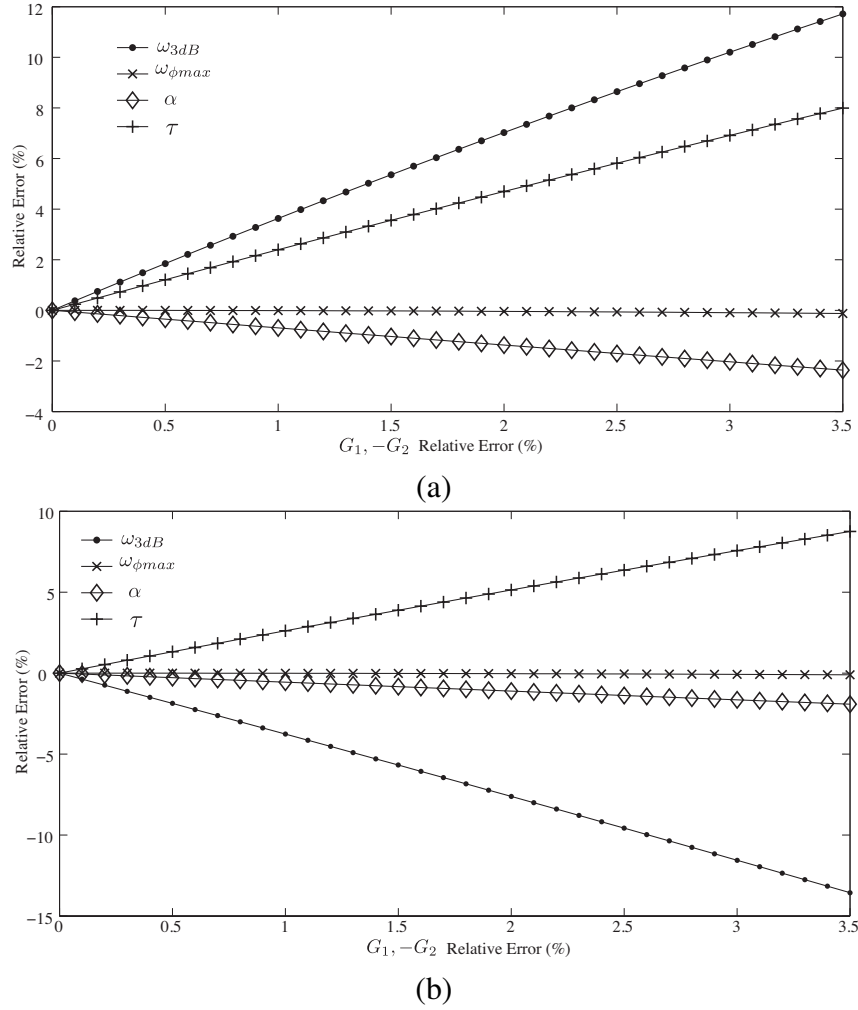


Figure 2.18: Effect of relative errors of (a) G_1 and $-G_2$ (filter circuit) and (b) $-G_1$ and G_2 (integrator circuit) up to 3.5% on relative errors of extracted ω_{3dB} , $\omega_{\phi max}$, α and τ from simulated frequency response using known impedance parameters of an apricot and load resistor $R_L = 1 \text{ k}\Omega$.

Fig. 2.18 we observe that ω_{3dB} is the parameter most impacted by errors in $G_{1,2}$ reaching maximum errors of 11.72% and -13.56% for the filter and integrator circuits, respectively. Compared to $[7.99, -0.13, -2.36] \%$ and $[8.75, -0.10, -1.91] \%$ for $[\tau, \omega_{\phi max}, \alpha]$ from the filter and integrator circuits, respectively, when the error in G_1 and G_2 was $\pm 3.5\%$ and $\mp 3.5\%$, respectively. Note, that the error of $\omega_{\phi max}$ is very close to zero for the entire range since the errors of G_1 and G_2 are equal in magnitude but opposite in sign, which using (2.36) predicts no $|T(j\omega_{\phi max})|$ error and therefore no extracted $\omega_{\phi max}$ error.

2.3.2 Least Squares Extraction Method

The limitation of the direct extraction method on the accuracy of the low and high frequency gain measurements can be overcome by using a NLSF method, similar to that previously described in Section 2.2 for the step-response extraction method. Modifying (2.21) for the magnitude response extraction requires that x is the vector of impedance parameters (G_1 , G_2 , α , τ), $T(x)$ is the transfer function (2.26) or (2.27) calculated using x , $ydata$ is the collected frequency response to fit to (2.26) or (2.27), $T(x)_i$ and $ydata_i$ are the simulated response and collected response at frequency ω_i , and n is the total number of data points in the collected frequency response. The accuracy of the parameters extracted from the collected dataset using the NLSF method is not limited by the accuracy of $G_{1,2}$, determined by 2 datapoints in the direct method, because every collected datapoint is used in the optimization routine to find the parameters within a constrained set that results in the best fit.

2.3.2.1 Simulation Results

Both the direct extraction and NLSF methods were applied to the ideal frequency response of the filter circuit in Fig. 2.17(a), given in (2.26), using fruit impedance parameters from [51] with $R_L = 1 \text{ k}\Omega$. These MATLAB simulations were from 100 Hz to 5 MHz with 201 logarithmically spaced datapoints. The relative errors of the extracted impedance parameters (G_1 , G_2 , α , τ) from ideal are given in Table 2.11. The relative errors of the parameters extracted using the NLSF are 2 to 4 orders of magnitude more accurate than the those extracted with the direct method. Similar results were also obtained when applying the NLSF extraction method to ideal frequency responses of the integrator circuit in Fig. 2.17(b). The ideal MATLAB simulated frequency response of an apricot compared to those simulated using the NLSF and direct method impedance parameters, when the direct measurements have 3.5% G_1 and -3.5% G_2 errors, are shown in Fig. 2.19. From this figure the NLSF parameters show much closer agreement with the ideal dataset than the direct ex-

Fruit	Relative Error (%) $\left[\begin{smallmatrix} \text{Direct} \\ \text{NLSF} \end{smallmatrix} \right]$			
	G_1	G_2	α	τ
Apricot	3.46	-1.36	-1.10	6.92
	1.35×10^{-3}	-6.49×10^{-4}	-8.51×10^{-4}	3.68×10^{-3}
Apple	9.43	-2.20	-2.72	21.45
	1.46×10^{-2}	-3.85×10^{-3}	-9.89×10^{-3}	5.08×10^{-2}
Kiwi	3.82	-1.47	-1.86	9.40
	1.42×10^{-3}	-9.83×10^{-4}	-1.84×10^{-3}	4.88×10^{-3}
Potato	2.67	-1.08	-1.07	5.68
	5.05×10^{-3}	-2.21×10^{-3}	-5.42×10^{-3}	1.66×10^{-2}

Table 2.11: Relative extracted errors from direct and NLSF methods applied to simulated apricot, apple, kiwi and potato frequency responses in the circuit of Fig. 2.17(a) .

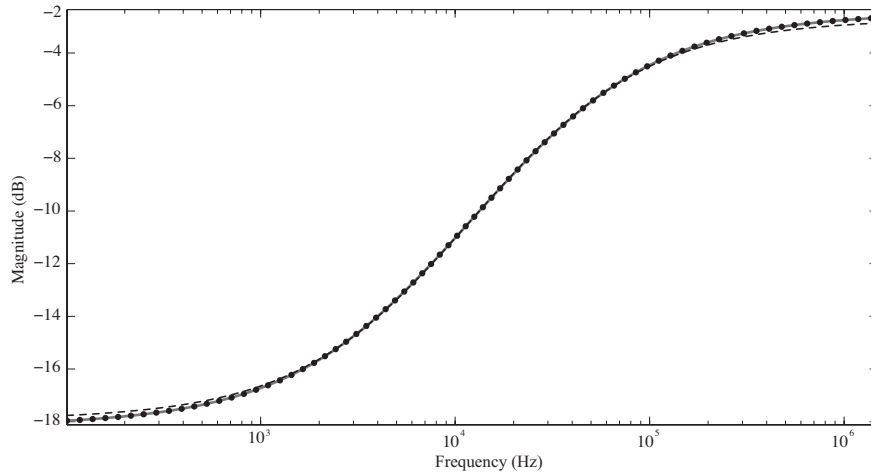


Figure 2.19: Simulated frequency responses using parameters extracted using non-linear fitting (black circles) and direct methods (dashed) from an ideal frequency response using known apricot parameters (solid).

traction method; which shows deviations from the ideal at both low and high frequencies. The low frequency deviations begin at approximately 1 kHz reaching a maximum deviation of 0.1998 dB at 101 Hz with the high frequency deviation beginning at approximately 100 kHz reaching a maximum deviation of 0.1984 dB at 1.49 MHz.

The impact of noise on the parameter extractions was investigated by applying both direct and NLSF extraction methods to 1000 MATLAB simulated frequency responses of (2.26) from 100 Hz to 5 MHz with 201 datapoints using the impedance parameters of an apricot and load resistor of 1 k Ω , with randomly generated white Gaussian noise with a

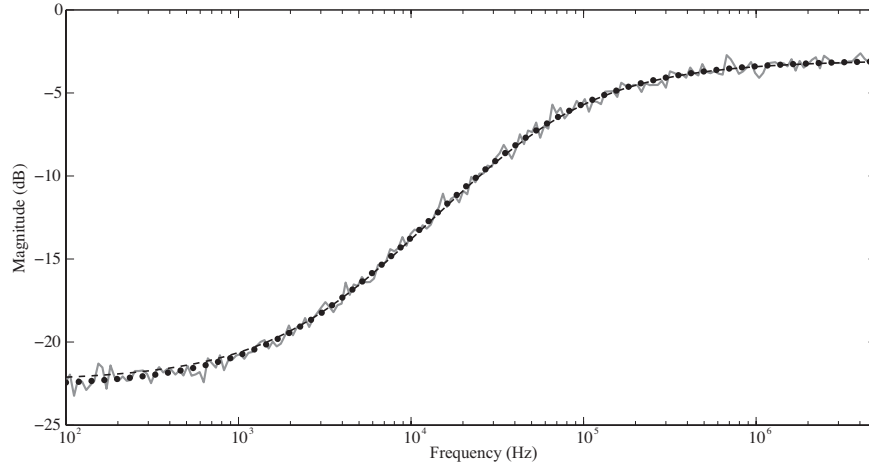


Figure 2.20: Simulated frequency responses using parameters extracted using non-linear fitting (black circles) and direct methods (dashed) from an ideal frequency response using known apricot parameters with white gaussian noise (solid).

signal-to-noise ratio (SNR) of 10 dB added to each frequency response. With mean relative errors of the extracted impedance parameters (G_1 , G_2 , α , and τ) for the direct method and NLSF of (4.15, 3.18, 4.58, 12.66)% and (0.686, 0.475, 0.614, 2.19)%, respectively. The relative errors of the parameters extracted using the NLSF show 1 order of magnitude less error than the direct method. A comparison of simulations using impedance parameters extracted from a single noisy dataset are shown in Fig. 2.20, with the least squares simulation (black circles) showing much better agreement with the apricot data (solid line) over the direct extraction simulation (dashed line).

2.3.2.2 Experimental Results

To verify the MATLAB simulations of (2.26) the circuit given in Fig. 2.17(a) was implemented using apricots and an apple as the Cole impedance terminated with $R_L = 1 \text{ k}\Omega$ and using an OP27 op amp (8 MHz gain bandwidth product) as the unity gain buffer. This test circuit is detailed in Fig. 2.21. The frequency response of these circuits was measured by a HP4395A network analyzer over the frequency band from 100 Hz to 5 MHz with a total of 201 points collected for each response. The extracted impedance parameters for each fruit are given in Table 2.12. To compare how well each method fits the experimental data the

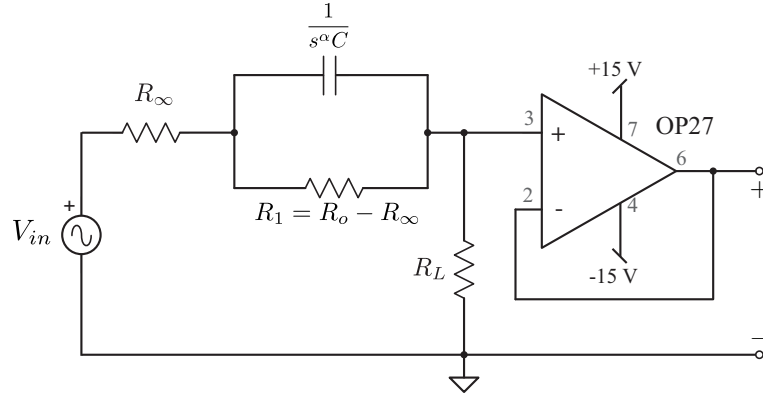


Figure 2.21: Test circuit to collect the magnitude response of a single-dispersion Cole impedance.

Fruit	Impedance Parameters Direct NLSF			
	G_1	G_2	α	τ (μ s)
Apricot 1	13.89	1.406	0.8656	31.34
	14.40	1.363	0.8008	42.18
Apricot 2	11.54	1.347	0.8280	36.11
	11.16	1.330	0.7739	40.70
Apple	30.64	3.720	0.7422	58.31
	32.22	3.776	0.7462	58.85

Table 2.12: Impedance parameters extracted with direct and NLSF methods from experimentally collected apricot and apple frequency responses in the circuit of Fig. 2.17(a) .

least squares error of the simulated response for both methods (for all fruits) was calculated as

$$\varepsilon = \sum_{i=1}^n (y_i - x_i)^2 \quad (2.40)$$

where y_i and x_i are the experimental and simulated data, respectively, at frequency ω_i and n is the total number of data points in the collected frequency response. Using this criteria on the simulated datasets from the direct method yields errors of 45.35, 43.94, and 44.42 for apricots 1, 2, and the apple, respectively, with reductions to 3.583, 3.935, and 22.81, respectively, using the NLSF. For each fruit the NLSF method extracts impedance parameters that match the experimental results much more accurately than those extracted with the filter method which is reflected in the lower least squares errors. A comparison

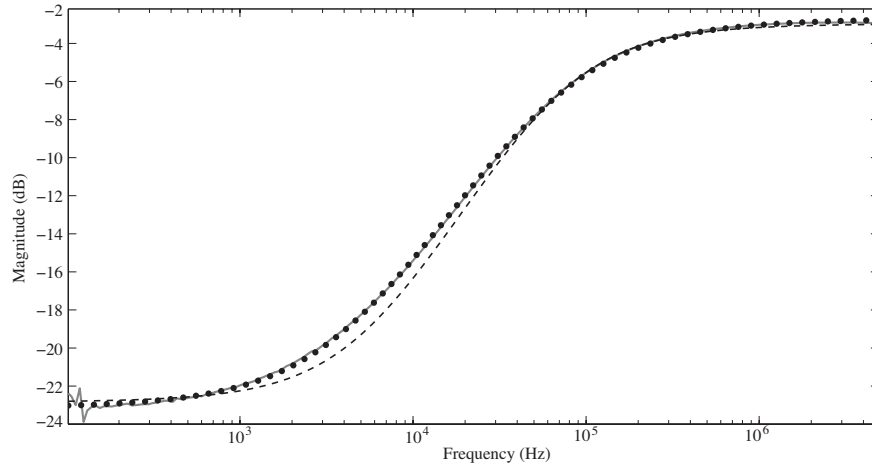


Figure 2.22: Simulated frequency responses using parameters extracted using non-linear fitting (black circles) and direct methods (dashed) from experimentally collected frequency response of an apricot (solid) as the Cole impedance in the circuit of Fig. 2.17(a) with $R_L = 1 \text{ k}\Omega$.

of (2.26) simulated using both sets of impedance parameters for Apricot 1 from Table 2.12 to the experimentally extracted frequency response is shown in Fig. 2.22. We clearly see that the response using the NLSF parameters, shown as a dashed line, shows near perfect agreement with the experimental data, shown as a solid line. While the response using the direct extraction parameters, shown as a dotted line, shows significant deviation from 600 Hz to 6 kHz when compared to the experimental.

2.4 Contribution

In conclusion, this chapter has presented methods of extracting the single-dispersion Cole impedance model parameters from the voltage and current excited step response and magnitude response, without requiring any direct impedance measurements. The summary of the results in this chapter are presented below:

- A numerical curve-fitting approach applied to the voltage-excited step response was presented and applied to ideal simulated data and experimental data using an ideal Cole model built using a traditional capacitor ($\alpha = 1$). In simulation, the extracted results showed less than 0.01% relative error from the ideal datasets while the ex-

tracted values from the experimental results showed less than 8.6% relative error for all parameters. This work was peer-reviewed and published in [100].

- A non-linear least squares method was presented and applied to the voltage-excited step response of the single-dispersion Cole impedance model to overcome potential accuracy limitations imposed by the precision of the test-hardware. Experimental results collected from an ideal Cole model (with $\alpha = 1$) show less than 7.2% relative error for all parameters while requiring a smaller collected dataset than the numerical curve-fitting method. Simulations using the parameters extracted from the experimental results collected from an apple and tomato show very good agreement with each other using the non-linear least-squares method. This work was peer reviewed and published in [102].
- The non-linear least squares method was applied to the current-excited step response of the single-dispersion Cole impedance model to verify the presented fractional circuit theory. Simulations using the parameters extracted from experimental results collected from apples show less than 2% relative error over the entire collected dataset. This work was peer reviewed and presented in [106] and [107].
- The sensitivity of an indirect extraction method from the magnitude response of the single-dispersion Cole impedance model is presented, with its limitations overcome by the application of a non-linear least squares method. This improved accuracy is verified applying the method to experimentally collected magnitude responses of two apricots and an apple, showing a much better fit using the non-linear least squares parameters. This work was peer reviewed and presented in [109].

CHAPTER 3

DOUBLE DISPERSION COLE IMPEDANCE MODEL

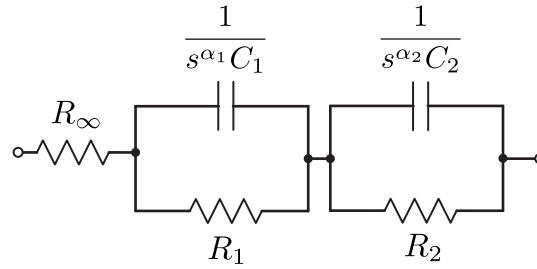


Figure 3.1: Theoretical double-dispersion Cole impedance model.

The double-dispersion Cole impedance model shown in Fig. 3.1, previously introduced in Section 1.2.1, is an expansion of the single-dispersion model used to accurately represent impedance over a larger frequency range or for more complex materials. This model has an impedance given by

$$Z(s) = R_{\infty} + \frac{R_1}{1 + s^{\alpha_1} R_1 C_1} + \frac{R_2}{1 + s^{\alpha_2} R_2 C_2} \quad (3.1)$$

Characterising a tissue or material using this model requires extracting the seven impedance parameters ($R_{\infty}, R_1, R_2, \alpha_1, \alpha_2, C_1, C_2$) to describe the model. Like the single dispersion models, these parameters have typically been extracted from the impedance data directly measured using an impedance analyzer. However, it is possible to extend the methods introduced in Chapter 2 for the single-dispersion Cole impedance parameters to extract the double-dispersion parameters without requiring direct impedance measurements. In this chapter indirect methods to extract the impedance parameters from the current excited step response and the magnitude response of the double-dispersion Cole impedance model using

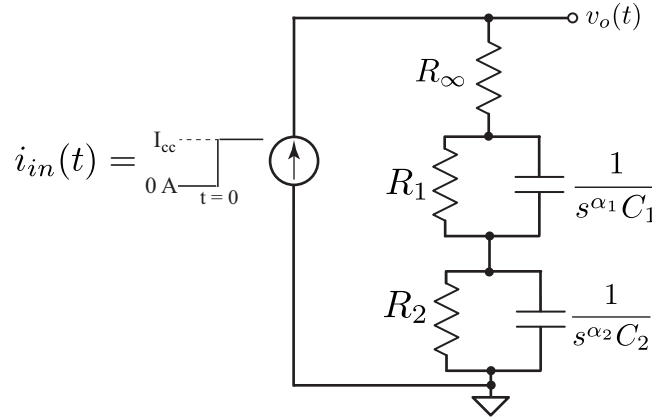


Figure 3.2: Theoretical circuit to apply a step-current input to the double-dispersion Cole impedance model.

non-linear least squares processes are presented. For these methods the underlying circuit theory and process are presented and validated by both simulations and experimentally collected results from fruit tissues.

3.1 Least Squares Extraction from Current Excited Step Response

In Section 2.2.2 a simplified expression for the output current of the single-dispersion Cole-impedance model was presented analyzing the current through the model. In [107] this method is extended to the double-dispersion model with current step of amplitude I_{cc} applied to the theoretical model of the double-dispersion Cole impedance, with the simple application circuit given in Fig. 3.2. The s -domain expression of the output voltage when the input current step has an amplitude of I_{cc} , that is $I_{in}(s) = I_{cc}/s$ is given by

$$\begin{aligned}
 V_o(s) &= \frac{I_{cc}}{s} \left[R_{\infty} + \frac{R_1}{1 + s^{\alpha_1} R_1 C_1} + \frac{R_2}{1 + s^{\alpha_2} R_2 C_2} \right] \\
 &= \frac{I_{cc}}{s} \left[R_{\infty} + \frac{1/C_1}{s^{\alpha_1} + 1/R_1 C_1} + \frac{1/C_2}{s^{\alpha_2} + 1/R_2 C_2} \right] \\
 &= I_{cc} \left[\frac{R_{\infty}}{s} + \frac{1}{C_1} \cdot \frac{s^{-1}}{s^{\alpha_1} + 1/R_1 C_1} + \frac{1}{C_2} \cdot \frac{s^{-1}}{s^{\alpha_2} + 1/R_2 C_2} \right] \quad (3.2)
 \end{aligned}$$

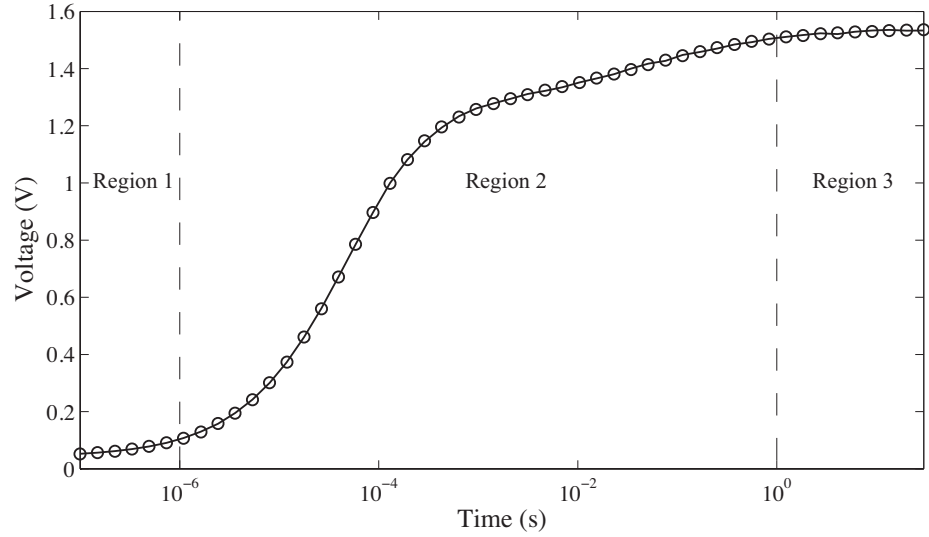


Figure 3.3: MATLAB simulated step response double dispersion Cole impedance model excited by a step current of 0.1 mA when $R_\infty = 406 \, \Omega$, $R_1 = 12.894 \, \text{k}\Omega$, $R_2 = 2.5 \, \text{k}\Omega$, $C_1 = 62.34 \, \text{nF}$, $C_2 = 100 \, \mu\text{F}$, $\alpha_1 = 0.739$, $\alpha_2 = 0.55$. Ideal simulations with 0.5% noise are given as a solid line with the simulations using the extracted parameters given as circles.

Applying the Laplace transform formula for the Mittag-Leffler function given by (2.4) to (3.2) yields the time domain expression of the output voltage given by

$$v_o(t) = I_{cc} \left[R_\infty + \frac{t^{\alpha_1}}{C_1} E_{\alpha_1, \alpha_1+1} \left(\frac{-t^{\alpha_1}}{R_1 C_1} \right) + \frac{t^{\alpha_2}}{C_2} E_{\alpha_2, \alpha_2+1} \left(\frac{-t^{\alpha_2}}{R_2 C_2} \right) \right] \quad (3.3)$$

A MATLAB simulated example of (3.3) when $R_\infty = 406 \, \Omega$, $R_1 = 12.894 \, \text{k}\Omega$, $R_2 = 2.5 \, \text{k}\Omega$, $C_1 = 62.34 \, \text{nF}$, $C_2 = 100 \, \mu\text{F}$, $\alpha_1 = 0.739$, $\alpha_2 = 0.55$, and $I_{cc} = 0.1 \, \text{mA}$ is given in Fig. 3.3 as a solid line. From this step-response we note that there are three distinct regions common to the step response of all double-dispersion Cole impedance models to a current step input: 1) at very low times, when the CPEs are uncharged, a constant voltage results from the current applied to R_∞ , 2) the increasing voltage region when the CPEs are charging, and 3) at high times, another constant voltage region results from the current applied to $R_\infty + R_1 + R_2$; when the CPEs are fully charged. The response of the double dispersion Cole impedance in Fig. 3.3 is very similar to the single dispersion model, though the behaviour in Region 2 is more complex resulting from the charging of two CPEs.

The NLSF method, previously described in Section 2.2 for the step-response extraction method of the single-dispersion model can be modified and applied to the step-response extraction of the double dispersion model. The general NLSF method is repeated here:

$$\begin{aligned} \min_x \|T(x) - ydata\|_2^2 &= \min_x \sum_{i=1}^n (T(x)_i - ydata_i)^2 \\ s.t. \quad x &> 0 \end{aligned}$$

The extraction of the double-dispersion parameters requires that x is the vector of impedance parameters $(R_\infty, R_1, R_2, \alpha_1, \alpha_2, C_1, C_2)$, $T(x)$ is step response (3.3) calculated using x , $ydata$ is the collected step response to fit to (3.3), $T(x)_i$ and $ydata_i$ are the simulated response and collected response at time t_i , and n is the total number of data points in the collected response.

Similar to the single dispersion model, initial guesses to solve for the impedance parameters from the step response dataset can be generated with knowledge of (3.3) that at $t = 0$ and $t = \infty$ the voltage will be $v_o(0) = I_{cc}R_\infty$ and $v_o(\infty) = I_{cc}(R_\infty + R_1 + R_2)$. Since the collected step response will not extend from $t = 0$ to $t = \infty$ but is instead finite in the range $0 < t_1 < t_n < \infty$, where t_1 and t_n are the smallest and largest time datapoints, respectively. Therefore, the values collected will only be an approximation of their ideal counterparts and can be used as boundaries when generating R_∞ and $R_{1,2}$ for the initial guesses such that characteristics of the step response given by (3.3) can be used to generate initial guesses for the NLSF. The boundary for R_∞ for the double dispersion Cole impedance is the same as that for the single dispersion given by (2.24), though now $R_{1,2}$ must be generated such that

$$R_\infty \leq \frac{v_o(t_1)}{I_{cc}} \quad (3.4)$$

$$R_1 + R_2 \geq \frac{v_o(t_n)}{I_{cc}} - R_\infty \quad (3.5)$$

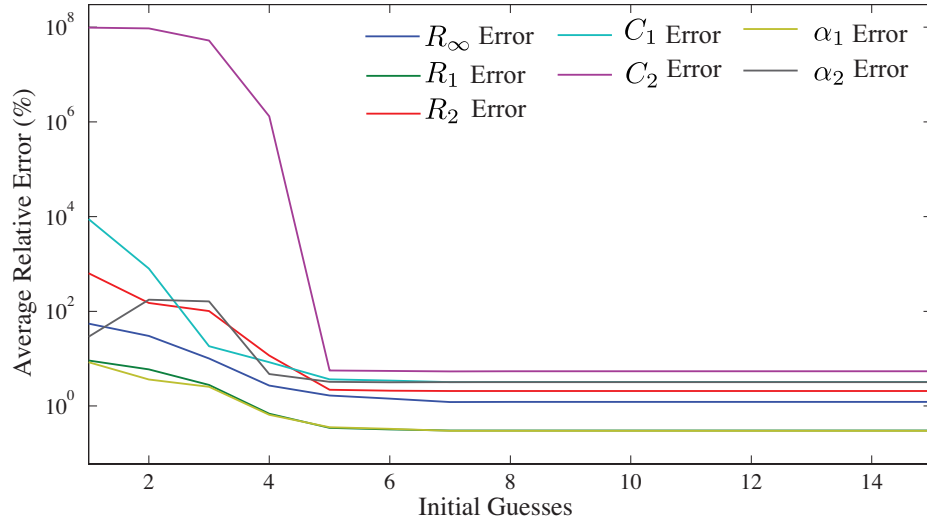


Figure 3.4: Evolution of the average relative error of 100 MATLAB simulations with 15 randomly generated initial guesses applied to the NLSF of the double dispersion step response datasets with impedance parameters $R_\infty = 406 \, \Omega$, $R_1 = 12.894 \, \text{k}\Omega$, $R_2 = 2.5 \, \text{k}\Omega$, $C_1 = 62.34 \, \text{nF}$, $C_2 = 100 \, \mu\text{F}$, $\alpha_1 = 0.739$, $\alpha_2 = 0.55$ and 0.5% random noise.

Finally the range of values reported in the literature are used to create the bounds to generate the initial guesses such that $0 \leq \alpha \leq 1$ and $0.1 \, \text{nF} \leq C_1 \leq 1 \, \text{mF}$.

3.1.1 Simulation Results

The accuracy of extracting the double dispersion impedance parameters from the step response data is assessed by extracting the parameters from 100 MATLAB simulations of (3.3) with random noise levels of 0.5%, 1%, and 2%. For all simulations, the datasets were generated from $0.1 \, \mu\text{s}$ to $30 \, \text{s}$ with 50 logarithmically spaced datapoints using impedance parameters $R_\infty = 406 \, \Omega$, $R_1 = 12.894 \, \text{k}\Omega$, $R_2 = 2.5 \, \text{k}\Omega$, $C_1 = 62.34 \, \text{nF}$, $C_2 = 100 \, \mu\text{F}$, $\alpha_1 = 0.739$, $\alpha_2 = 0.55$ to an input step of $I_{cc} = 0.1 \, \text{mA}$. To maintain the same level of accuracy (when the range of values that the solution lies within is much larger) the number of initial guesses are increased from 5 to 15 when applying the NLSF to the double dispersion datasets over the single dispersion datasets. The impact of the number of initial guesses is clear showing a significant decrease in the relative error of each parameter between the 1st and 15th applied initial guesses, shown in Fig. 3.4. Note, that the lines in

Noise (%)	Relative Error (%)						
	R_∞	R_1	R_2	C_1	C_2	α_1	α_2
0.5	1.22	0.304	2.07	3.20	5.40	0.300	3.18
1.0	2.30	0.660	3.83	5.47	6.40	0.573	5.28
2.0	2.99	1.18	7.17	14.8	9.60	1.11	9.25

Table 3.1: Average relative error of impedance parameters extracted from 100 MATLAB simulations of the double dispersion step response with 0.5%, 1%, and 2% random noise.

Fig. 3.4 are used to visually track the trend between each datapoint and are not a representation of the average relative error between these initial guesses (which is not possible to represent since the initial guesses can only ever take positive integer values). After solving using the first initial guess the extracted parameters show relative errors of $[54.7, 9.16, 635, 8831, 9.73 \times 10^7, 8.38, 29.1]\%$ for $[R_\infty, R_1, R_2, \alpha_1, \alpha_2, C_1, C_2]$, respectively, with reductions to $[1.22, 0.304, 2.07, 3.20, 5.40, 0.300, 3.18]\%$ after the application of 7 initial guesses with no significant decrease in the error after this point. The use of multiple initial guesses shows reductions from 1 to 7 orders of magnitude for the relative error over the single initial guess and verifies the increased number of initial guesses to maintain the accuracy. The impact of the increasing levels of noise on the relative errors of extracted parameters are given in Table 3.1. Although the noise has a larger impact on the extraction of the double-dispersion parameters than the single-dispersion parameters, it shows less than 5.5% average relative error when the noise is 0.5% for all parameters. The level of noise has the greatest impact on the extraction of the $C_{1,2}$ and α_2 parameters with errors of 14.8%, 9.6%, and 9.25% when there is 2% noise in the dataset. An example of a simulated dataset with 0.5% noise (solid line) compared to the simulation using the extracted parameters (circles) is given in Fig.3.3. From this dataset the datapoints collected at 0.1 μs and 30 s are $v_o(0.1 \mu\text{s}) = 0.0524 \text{ V}$ and $v_o(30 \text{ s}) = 1.533 \text{ V}$, respectively. Therefore, from (3.4) and (3.5) the boundaries for the generation of the initial guesses are $R_\infty \leq 524 \Omega$ and $R_1 + R_2 \geq 14.808 \text{ k}\Omega$. Applying 15 initial guesses to the NLSF yields relative errors of $[0.563, 0.049, 1.06, 0.589, 2.93, 0.093, 1.62]\%$ for $[R_\infty, R_1, R_2, C_1, C_2, \alpha_1, \alpha_2]$, respec-

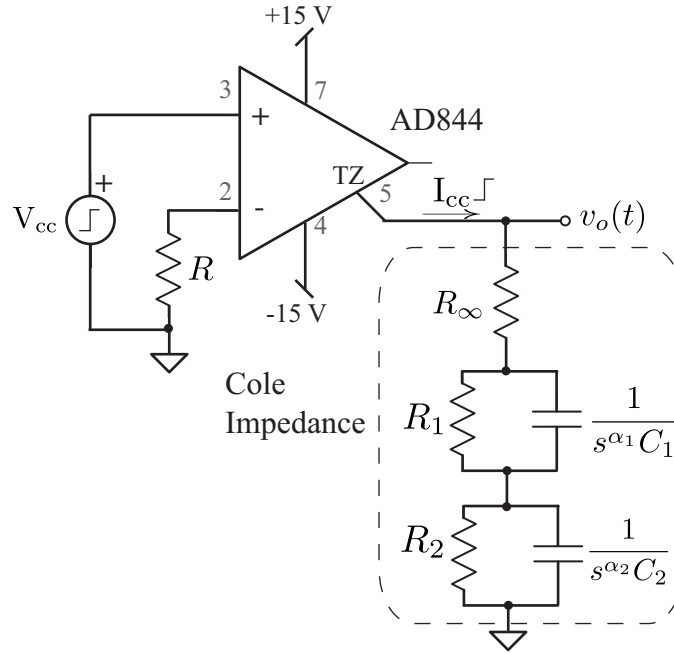


Figure 3.5: Test circuit to apply a current-step input to a double dispersion Cole impedance with the AD844 operating as a current conveyor.

tively. The simulated dataset using the extracted parameters shows less than 0.45% relative error with the simulated noisy dataset over the entire time scale.

3.1.2 Experimental Results

Using the same experimental setup described in Section 2.2.2, a current-step input was applied to 2 apples used as the double-dispersion Cole impedances in the test circuit shown in Fig. 3.5. In this configuration, when an input voltage-step of amplitude V_{cc} is applied it is converted to a current-step of amplitude $I_{cc} = V_{cc}/(R + R_i)$ where R_i is the internal resistance of the AD844, and is approximately $50\ \Omega$. Using this circuit a voltage-step was applied to the AD844 by an Agilent 33250A signal generator to create a step-current of $I_{cc} = 1\text{ V}/(9.92\text{ k}\Omega + 50\Omega) = 0.1\text{ mA}$. The voltage responses, $v_o(t)$, collected using a Tektronix 745D digital oscilloscope from $t = 0.2\ \mu\text{s}$ to $t = 10\text{ s}$ with 72 logarithmically spaced datapoints are given in Fig. 3.6(a) and Fig.3.7(a) for apple 1 and 2, respectively, as solid lines. The parameters extracted using both the single and double dispersion models

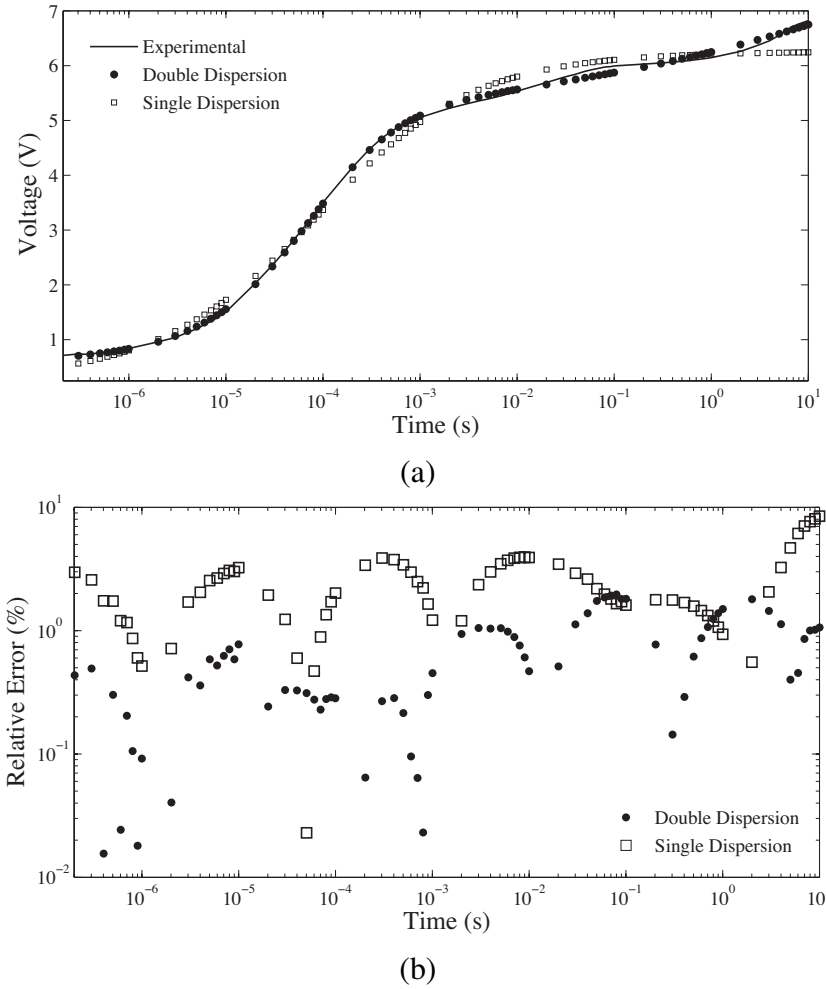


Figure 3.6: (a) Experimental step response of Apple 1 compared to simulated responses using extracted single (rectangles) and double (black circles) dispersion parameters and (b) absolute relative errors.

Fruit/Model		R_{∞} (Ω)	R_1 (Ω)	R_2 (Ω)	C_1 (F)	C_2 (F)	α_1	α_2
Apple 1	Single	5.55k	55.1k	-	92.6n	-	0.6009	-
	Double	7.38k	66.5k	48.4k	219.3 μ	25.8n	0.3755	0.7448
Apple 2	Single	2.28k	60.3k	-	240.3n	-	0.4793	-
	Double	5.60k	61.5k	46.1k	86.0 μ	38.5n	0.2097	0.6899

Table 3.2: Single and double dispersion impedance parameters extracted from step responses of apples 1 and 2 using NLSF.

in the NLSF for both apple 1 and 2 are given in Table 3.2. The MATLAB simulated responses using the single and double dispersion parameters are given in Fig. 3.6(b) and Fig. 3.7(b) as squares and black circles, respectively. The simulations using the double

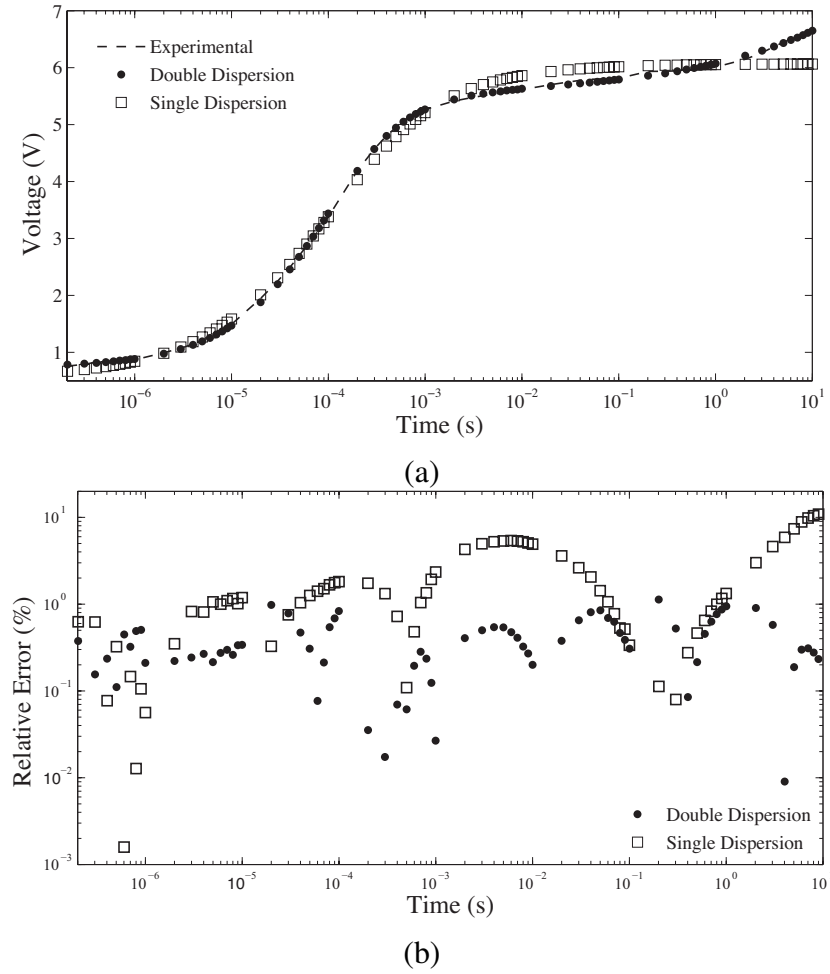


Figure 3.7: (a) Experimental step response of Apple 2 compared to simulated responses using extracted single (rectangles) and double (black circles) dispersion parameters and (b) absolute relative errors.

dispersion parameters shows good agreement with the experimental results with less than 2% and 1% relative error for apple 1 and 2, respectively, over the entire dataset. The single dispersion parameters show much higher relative errors reaching maximums of almost 10% at 10 s. The single dispersion is not able to accurately fit the response above 0.1 s due to the emergence of the second dispersion.

3.2 Least Squares Extraction from Magnitude Response

In Section 2.3 the transfer function of the single-dispersion Cole-impedance model as an element in a simple filter circuit was presented. Here, this method is extended to the double-

Figure 3.8: Theoretical circuit for the collection of the magnitude response of the double dispersion Cole impedance.

Coefficient	Values
X_0	$\omega^{\alpha_1+\alpha_2} \cos\left(\frac{(\alpha_1+\alpha_2)\pi}{2}\right) + \frac{\omega^{\alpha_1}}{C_2 R_2} \cos\left(\frac{\alpha_1 \pi}{2}\right) + \frac{\omega^{\alpha_2}}{C_1 R_1} \cos\left(\frac{\alpha_2 \pi}{2}\right) + \frac{1}{C_1 C_2 R_1 R_2}$
X_1	$\omega^{\alpha_1+\alpha_2} \sin\left(\frac{(\alpha_1+\alpha_2)\pi}{2}\right) + \frac{\omega^{\alpha_1}}{C_2 R_2} \sin\left(\frac{\alpha_1 \pi}{2}\right) + \frac{\omega^{\alpha_2}}{C_1 R_1} \sin\left(\frac{\alpha_2 \pi}{2}\right)$
X_2	$\omega^{\alpha_1+\alpha_2} \cos\left(\frac{(\alpha_1+\alpha_2)\pi}{2}\right) + \omega^{\alpha_1} \frac{R_0+R_2+R_L}{C_2 R_2 (R_0+R_L)} \cos\left(\frac{\alpha_1 \pi}{2}\right) + \omega^{\alpha_2} \frac{R_0+R_1+R_L}{C_1 R_1 (R_0+R_L)} \cos\left(\frac{\alpha_2 \pi}{2}\right) + \frac{R_0+R_1+R_2+R_L}{C_1 C_2 R_1 R_2 (R_0+R_L)}$
X_3	$\omega^{\alpha_1+\alpha_2} \sin\left(\frac{(\alpha_1+\alpha_2)\pi}{2}\right) + \omega^{\alpha_1} \frac{R_0+R_2+R_L}{C_2 R_2 (R_0+R_L)} \sin\left(\frac{\alpha_1 \pi}{2}\right) + \omega^{\alpha_2} \frac{R_0+R_1+R_L}{C_1 R_1 (R_0+R_L)} \sin\left(\frac{\alpha_2 \pi}{2}\right)$

Table 3.3: Magnitude response coefficients of the circuit in Fig. 3.8 given by (3.7).

dispersion Cole impedance model used as a component in the circuit given in Fig. 3.8. The transfer function of this circuit is given by

$$T(s) = \frac{V_o(s)}{V_{in}(s)} = \frac{R_L}{R_\infty + R_L} \cdot \frac{s^{\alpha_1+\alpha_2} + s^{\alpha_1} \frac{1}{C_2 R_2} + s^{\alpha_2} \frac{1}{C_1 R_1} + \frac{1}{C_1 C_2 R_1 R_2}}{s^{\alpha_1+\alpha_2} + s^{\alpha_1} \frac{R_\infty+R_2+R_L}{C_2 R_2 (R_\infty+R_L)} + s^{\alpha_2} \frac{R_\infty+R_1+R_L}{C_1 R_1 (R_\infty+R_L)} + \frac{R_\infty+R_1+R_2+R_L}{C_1 C_2 R_1 R_2 (R_\infty+R_L)}} \quad (3.6)$$

with the magnitude response given by

$$|T(j\omega)| = \frac{R_L}{R_0 + R_L} \cdot \frac{\sqrt{X_0^2 + X_1^2}}{\sqrt{X_2^2 + X_3^2}} \quad (3.7)$$

where the values of the coefficients X_0 , X_1 , X_2 , and X_3 are given in Table 3.3. A MATLAB simulated ideal response of (3.7) when $[R_\infty, R_1, R_2, \alpha_1, \alpha_2, C_1, C_2] = [885 \, \Omega, 899 \, \Omega, 626 \, \Omega, 0.5414, 0.7653, 19 \, \text{nF}, 5.1 \, \mu\text{F}]$ and $R_L = 500 \, \Omega$ is given in Fig. 3.9 as a solid line. For this circuit the magnitude response can be adjusted by changing the value of R_L resulting in an increase or decrease of the range without impacting the trend. Therefore, it is possible to adjust R_L such that the response falls within the most sensitive input range of the collection circuit. The shift in magnitude response when $R_L = 100 \, \Omega$, $200 \, \Omega$, and $500 \, \Omega$ is also given

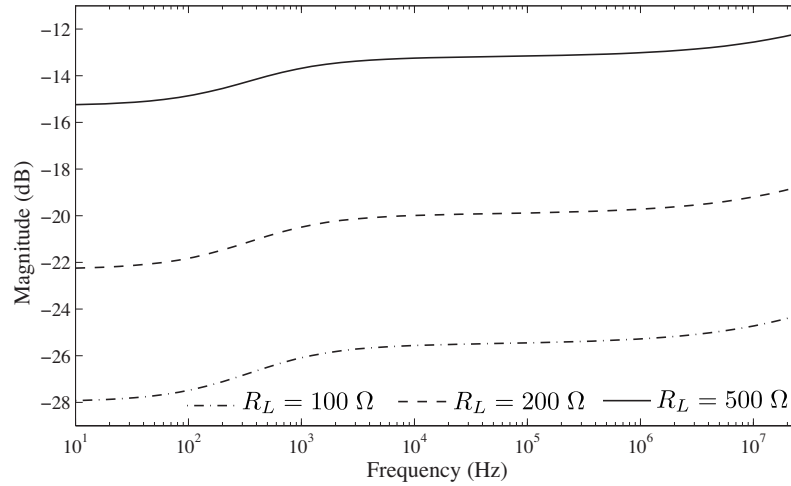


Figure 3.9: MATLAB simulated magnitude response of (3.7) when $[R_\infty, R_1, R_2, \alpha_1, \alpha_2, C_1, C_2] = [885 \, \Omega, 899 \, \Omega, 626 \, \Omega, 0.5414, 0.7653, 19 \, \text{nF}, 5.1 \, \mu\text{F}]$ and $R_L = 100 \, \Omega, 200 \, \Omega$, and $500 \, \Omega$.

in Fig. 3.9. Note, that as R_L increases the magnitude range that the response falls within also rises.

The NLSF method, previously described in Section 2.2 for the step-response extraction method can be applied to the magnitude response of the double-dispersion Cole impedance by modifying (2.21) such that x is the vector of impedance parameters $(R_\infty, R_1, R_2, \alpha_1, \alpha_2, C_1, C_2)$, $T(x)$ is the transfer function (3.7) calculated using x , $ydata$ is the collected frequency response to fit to (3.7), $T(x)_i$ and $ydata_i$ are the simulated response and collected response at frequency ω_i , and n is the total number of data points in the collected frequency response.

Again, characteristics of the magnitude response can be used to create boundaries for the generation of the initial guesses to increase the likelihood that they are close to the solution of the NLSF. We note from (3.7) that at $\omega = 0$ and $\omega = \infty$ the magnitude will be $|T(0)| = R_L / (R_\infty + R_1 + R_2 + R_L)$ and $|T(\infty)| = R_L / (R_\infty + R_L)$. Since the collected magnitude response will not extend from $\omega = 0$ to $\omega = \infty$ but is instead finite in the range $0 < \omega_1 < \omega_n < \infty$ the values collected will only be an approximation of their ideal counterparts. As such, we can use them as boundaries when generating R_∞, R_1 , and R_2 for the

initial guesses such that

$$R_{\infty} \leq \frac{R_L(1 - |T(\omega_n)|)}{|T(\omega_n)|} \quad (3.8)$$

$$R_1 + R_2 \geq \frac{R_L - |T(\omega_1)|(R_{\infty} + R_L)}{|T(\omega_1)|} \quad (3.9)$$

where ω_1 and ω_n are the lowest and highest frequency datapoints, respectively, of the collected magnitude response. Finally, the range of values reported in literature are used to create the bounds to generate the other initial guesses such that $0.5 \leq \alpha_{1,2} \leq 1$ and $0.1 \text{ nF} \leq C_{1,2} \leq 1 \text{ mF}$.

3.2.1 MATLAB Simulation Results

The accuracy of extracting the double dispersion impedance parameters from the magnitude response data is assessed by extracting the parameters from 100 MATLAB simulations of (3.7) with increasing levels of Gaussian white noise with Signal-to-Noise (SNR) ratios from 30 dB to 80 dB in 10 dB steps. For all simulations, the datasets were generated from 10 Hz to 25 MHz with 50 logarithmically spaced datapoints using impedance parameters $R_{\infty} = 42.9 \text{ } \Omega$, $R_1 = 71.6 \text{ } \Omega$, $R_2 = 16.5 \text{ } \Omega$, $\alpha_1 = 0.507$, $\alpha_2 = 0.766$, $C_1 = 3.086 \text{ } \mu\text{F}$, $C_2 = 89.29 \text{ } \mu\text{F}$ which were previously extracted from sheep intestinal tissue in [33]. The evolution of the mean error for each parameter while the NLSF applies 20 initial guesses to the magnitude data are shown in Fig. 3.10. The impact of the number of initial guesses is clear showing a significant decrease in the relative error of each parameter between the 1st and 20th applied initial guesses. After solving using the first initial guess the extracted parameters show relative errors of [57, 43, 5518, 150, 227, 1.05×10^7 , 6.66×10^5]% for $[R_{\infty}, R_1, R_2, \alpha_1, \alpha_2, C_1, C_2]$, respectively, with reductions to [0.165, 0.135, 0.215, 0.133, 0.213, 0.872, 1.18]% after the application of 13 initial guesses with no significant decrease in the error after this point. Note, that the lines in Fig. 3.10 are used to visually track the trend between each datapoint and are not a representation of the average relative error be-

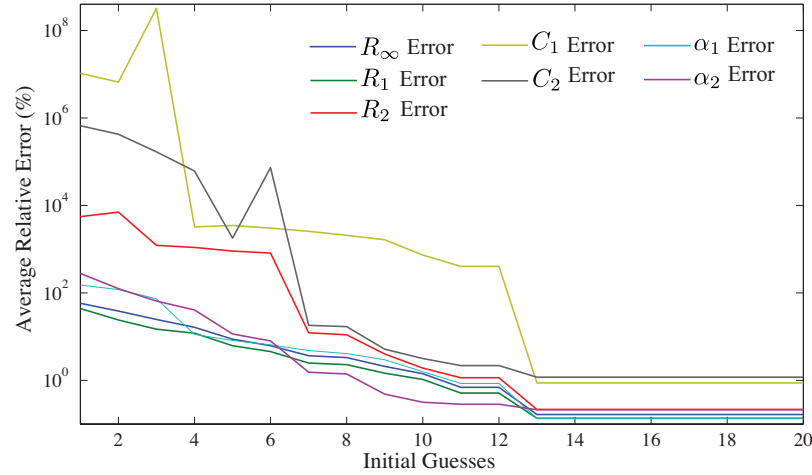


Figure 3.10: Evolution of the average relative error of 100 MATLAB simulations with 20 randomly generated initial guesses applied to the NLSF of the magnitude datasets with impedance parameters $R_\infty = 42.9 \, \Omega$, $R_1 = 71.6 \, \Omega$, $R_2 = 16.5 \, \Omega$, $\alpha_1 = 0.507$, $\alpha_2 = 0.766$, $C_1 = 3.086 \, \mu\text{F}$, $C_2 = 89.29 \, \mu\text{F}$ and 60 dB SNR Gaussian white noise.

SNR (dB)	Relative Error (%)						
	R_∞	R_1	R_2	α_1	α_2	C_1	C_2
30	4.92	3.84	6.25	3.54	5.88	23.6	34.9
40	1.29	1.09	2.06	1.04	1.88	7.02	10.1
50	0.453	0.366	0.641	0.358	0.598	2.44	3.23
60	0.165	0.135	0.215	0.133	0.213	0.872	1.18
70	0.049	0.039	0.063	0.036	0.060	0.240	0.330
80	0.013	0.010	0.017	0.009	0.017	0.062	0.098

Table 3.4: Average relative error of double dispersion Cole impedance parameters extracted from 100 MATLAB simulations of (3.7) with 30 dB to 80 dB SNR Gaussian white noise.

tween these initial guesses (which is not possible to represent since the initial guesses can only ever take positive integer values). The use of multiple initial guesses shows reductions in relative errors from 3 to 7 orders of magnitude over the single initial guess. The impact of increasing noise levels on the relative error of the extracted parameters are given in Table 3.4. When the SNR of the noise decreases to 40 dB there is a significant increase in the relative error of the extracted parameters with all showing larger than 1% relative error compared to the ideal values. The increased noise has the greatest impact on the extraction of the $C_{1,2}$ parameters.

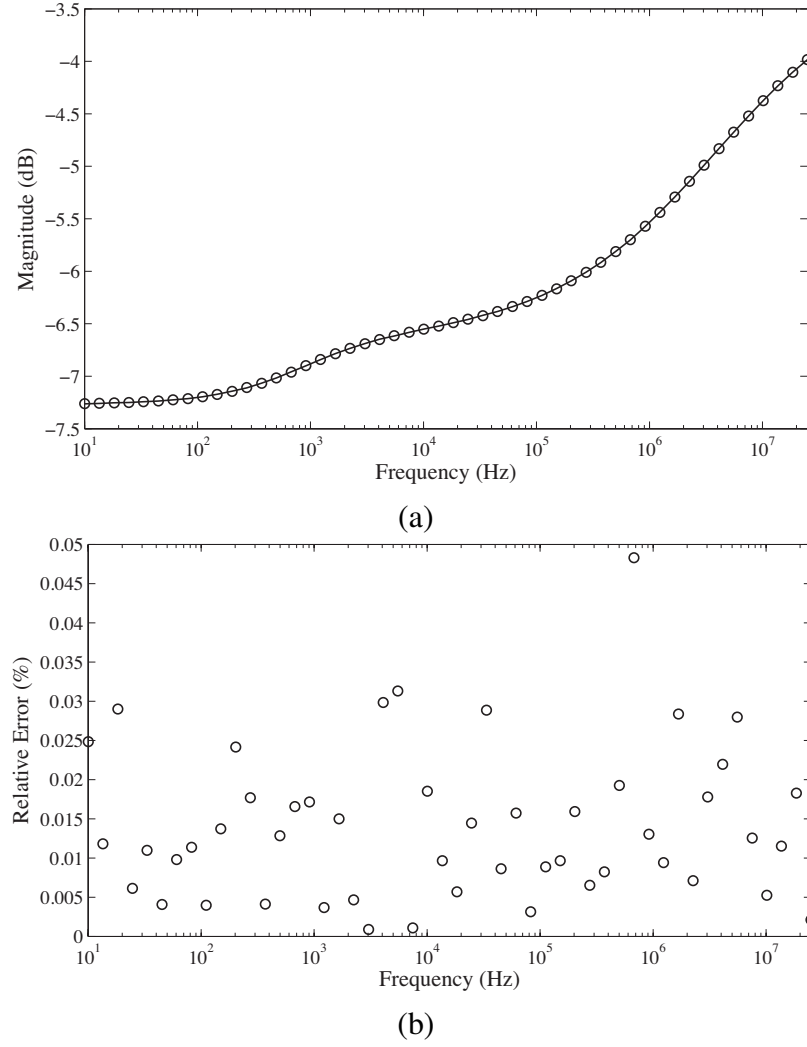


Figure 3.11: MATLAB simulated (a) magnitude and (b) error plots of a double dispersion Cole impedance (solid) with impedance parameters $R_\infty = 42.9 \, \Omega$, $R_1 = 71.6 \, \Omega$, $R_2 = 16.5 \, \Omega$, $\alpha_1 = 0.507$, $\alpha_2 = 0.766$, $C_1 = 3.086 \, \mu\text{F}$, $C_2 = 89.29 \, \mu\text{F}$ when $R_L = 100 \, \Omega$ with 60 dB SNR Gaussian white noise compared to the response using the extracted parameters (circles).

An example of a simulated dataset with 60 dB SNR (solid line) compared to simulations using the extracted parameters (circles) is given in Fig. 3.11(a). From this dataset the datapoints collected at 10 Hz and 25 MHz are $|T(10 \, \text{Hz})| = -7.263 \, \text{dB} = 0.633$ and $|T(25 \, \text{MHz})| = -3.9827 \, \text{dB} = 0.4334$, respectively. Therefore, from (3.8) and (3.9) the boundaries for the generation of the initial guesses are $R_\infty \leq 58.17 \, \Omega$ and $R_1 + R_2 \geq 72.58 \, \Omega$. Applying the NLSF with 20 initial guesses yields relative errors of [0.025, 0.029, 0.204,

0.008, 0.273, 0.095, 1.73]% for $[R_\infty, R_1, R_2, \alpha_1, \alpha_2, C_1, C_2]$, respectively. The simulated dataset using the extracted parameters shows less than 0.05% relative error with the simulated noisy dataset over the entire frequency range and is shown in Fig. 3.11(b).

The impedance parameters previously extracted from simulations were within a small range of resistance values ($R < 100 \Omega$); though it is still possible to extract the impedance parameters from datasets generated with resistances from a larger range. However, to maintain the same level of accuracy for the larger range it is necessary to increase the number of applied initial guesses. The evolution of the mean error for impedance parameter while the NLSF applies 60 initial guesses to 100 magnitude datasets generated such that $R_{\infty,1,2} \leq 1 \text{ k}\Omega$, $0.5 \leq \alpha_{1,2} \leq 1$, $0.1 \text{ nF} \leq C_{1,2} \leq 1 \text{ mF}$ with 60 dB SNR Gaussian white noise are shown in Fig. 3.12(a). An example simulated dataset with parameters $[R_\infty, R_1, R_2, \alpha_1, \alpha_2, C_1, C_2] = [885 \Omega, 899 \Omega, 626 \Omega, 0.5414, 0.7653, 19 \text{ nF}, 5.1 \mu\text{F}]$, $R_L = 100 \Omega$, and 60 dB SNR Gaussian white noise (solid) compared to simulations using the extracted parameters is given in Fig. 3.12(b). Applying the NLSF with 60 initial guesses yields relative errors of [5.44, 5.37, 0.02, 0.36, 0.06, 7.21, 0.36]% for $[R_\infty, R_1, R_2, \alpha_1, \alpha_2, C_1, C_2]$, respectively. This same process can be scaled up to extract the parameters from even larger ranges of impedance values by increasing the number of applied initial guesses to the datasets.

3.2.2 PSPICE Simulation Results

Although there is currently much progress regarding the realization of constant phase elements (or fractional order capacitors) [3, 88–90] there are no commercial devices using these processes available to implement these circuits. Until commercial devices with the desired characteristics become available, integer order approximations must be used to realize fractional circuits. There are many methods to create an approximation of s^α that include Continued Fraction Expansions (CFEs) as well as rational approximation methods [7]. These methods present a large array of approximations with the accuracy and approximated frequency band increasing as the order of the approximation increases. Here,

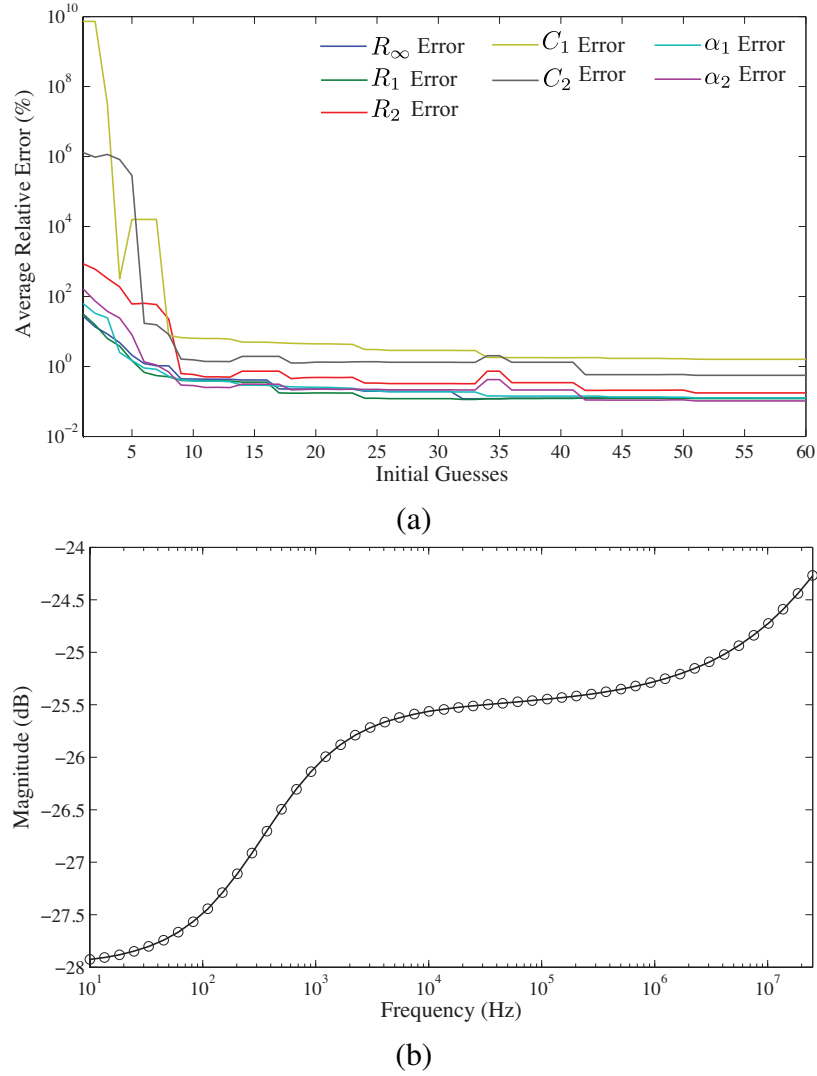


Figure 3.12: (a) Evolution of the average relative error of 100 MATLAB simulations with 60 randomly generated initial guesses applied to the NLSF with magnitude datasets randomly generated such that $R_{\infty,1,2} \leq 1 \text{ k}\Omega$, $0.5 \leq \alpha_{1,2} \leq 1$, $0.1 \text{ nF} \leq C_{1,2} \leq 1 \text{ mF}$ with 60 dB SNR Gaussian white and (b) simulated dataset with parameters $[R_{\infty}, R_1, R_2, \alpha_1, \alpha_2, C_1, C_2] = [885 \Omega, 899 \Omega, 626 \Omega, 0.5414, 0.7653, 19 \text{ nF}, 5.1 \mu\text{F}]$, $R_L = 100 \Omega$ and 60 dB SNR Gaussian white noise (solid) compared to simulations using extracted parameters (circles).

a CFE method [110] was selected to model the fractional order capacitors for PSPICE simulations. Collecting twenty terms of the CFE yields a 10th order approximation of the fractional capacitor that can physically realized using the RC ladder network in Fig. 3.13(a) when $n = 10$. The component values required to realize 10th order approximated CPE with values $C = 3.086 \mu\text{F}$, $\alpha = 0.507$ and $C = 89.29 \mu\text{F}$, $\alpha = 0.766$ centered at $f = 60 \text{ kHz}$

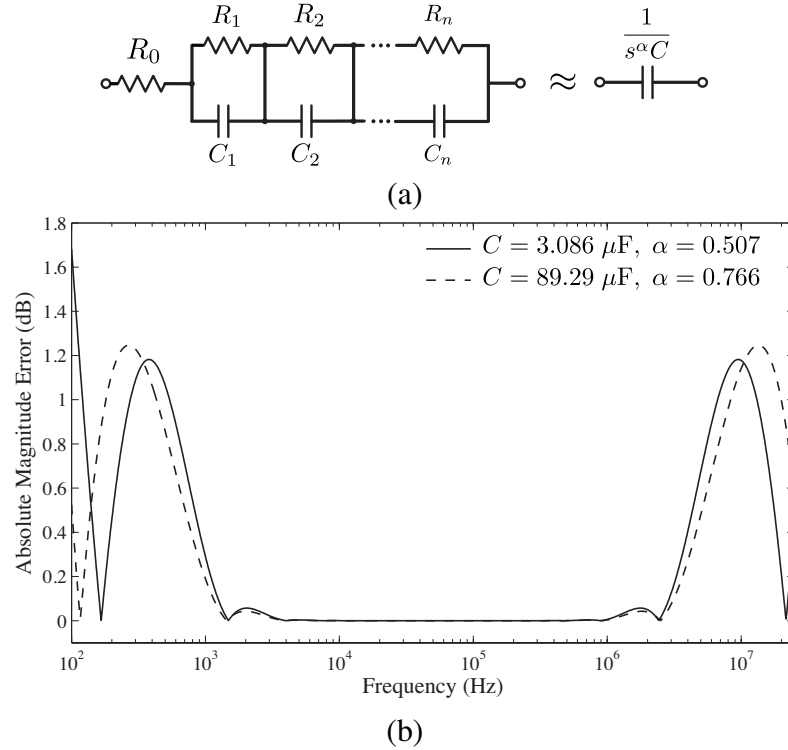


Figure 3.13: (a) RC ladder structure to realize a n^{th} order integer approximation of a CPE and (b) the error of 10th order approximated fractional capacitors with values $C = 3.086 \mu\text{F}$, $\alpha = 0.507$ (solid) and $C = 89.29 \mu\text{F}$, $\alpha = 0.766$ (dashed) centered at $f = 60 \text{ kHz}$.

are given in Table 3.5. The full details regarding the design of this approximated CPE are given in Appendix C. The absolute magnitude error of the approximations compared to the ideal are given in Fig. 3.13(b). Both approximations show less than 0.1 dB over 3 decades but show larger deviations in the frequency bands from 100 Hz to 1410 Hz and 2.4 MHz to 25 MHz; reaching maximums of 1.182 dB at 379 Hz and 9.52 MHz for $C = 3.086 \mu\text{F}$, $\alpha = 0.507$ and 1.246 dB at 265 Hz and 13.4 MHz for $C = 89.29 \mu\text{F}$, $\alpha = 0.766$.

The circuit in Fig. 3.8 with a double-dispersion Cole impedance ($R_\infty = 42.9 \Omega$, $R_1 = 71.6 \Omega$, $R_2 = 16.5 \Omega$, $\alpha_1 = 0.507$, $\alpha_2 = 0.766$, $C_1 = 3.086 \mu\text{F}$, $C_2 = 89.29 \mu\text{F}$) and $R_L = 100 \Omega$ with the CPEs approximated by 10th order RC ladders using the component values in Table 3.5 was simulated in PSPICE using an OPA655 (400 MHz unity gain bandwidth) operational amplifier. This simulated circuit is given in Fig. 3.14. This PSPICE simulation was conducted from 100 Hz to 25 MHz using 55 logarithmically spaced datapoints is given

n	Approximated CPE Component Values			
	$C = 3.086 \mu\text{F}$ $\alpha = 0.507$		$C = 89.29 \mu\text{F}$ $\alpha = 0.766$	
	$R_n (\Omega)$	$C_n (\text{F})$	$R_n (\Omega)$	$C_n (\text{F})$
0	21.9	-	3.88m	-
1	45.8	1.33n	15.5m	4.89 μ
2	49.5	5.12n	23.6m	12.2 μ
3	56.0	11.0n	33.5m	20.2 μ
4	67.0	18.5n	48.2m	27.8 μ
5	85.4	26.8n	72.7m	34.0 μ
6	118.7	35.2n	120m	37.8 μ
7	185.5	43.0n	227m	38.6 μ
8	349.7	49.4n	546m	35.7 μ
9	951.8	53.7n	2.21	28.4 μ
10	8681	55.3n	89.2	12.5 μ

Table 3.5: Values to realize 10th order approximated fractional capacitors with values $C = 3.086 \mu\text{F}$, $\alpha = 0.507$ and $C = 89.29 \mu\text{F}$, $\alpha = 0.766$ centered at $f = 60 \text{ kHz}$.

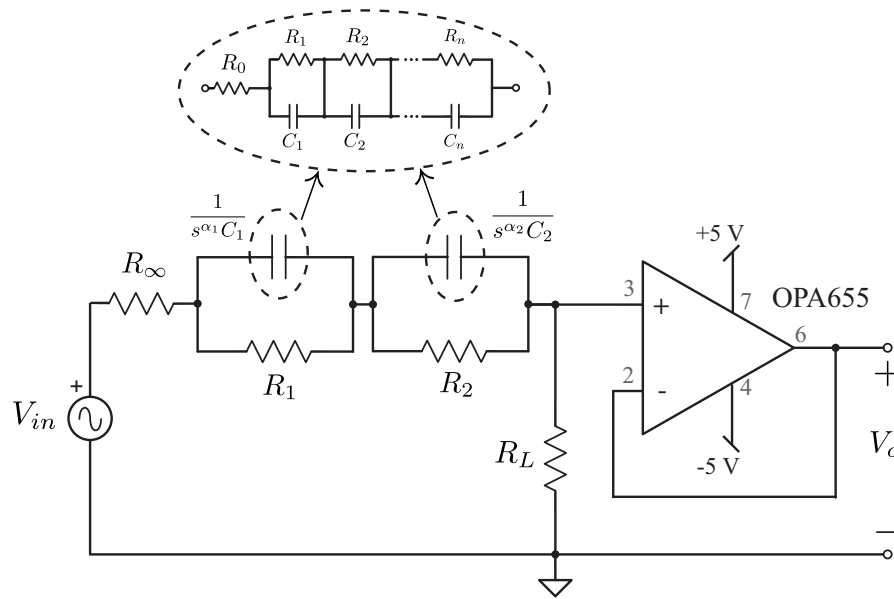


Figure 3.14: Circuit simulated in PSPICE to collect the magnitude response of a double-dispersion Cole impedance parameters implemented using RC ladder approximations of the CPEs.

in Fig. 3.15(a). From the PSPICE simulated response parameters of $[R_\infty, R_1, R_2, \alpha_1, \alpha_2, C_1, C_2]$ were extracted as $[50.3 \Omega, 62.3 \Omega, 17.5 \Omega, 0.588, 0.769, 11.12 \mu\text{F}, 63.53 \mu\text{F}]$ using 20 initial guesses with the NLSF. Compared to the ideal parameters the extracted parameters

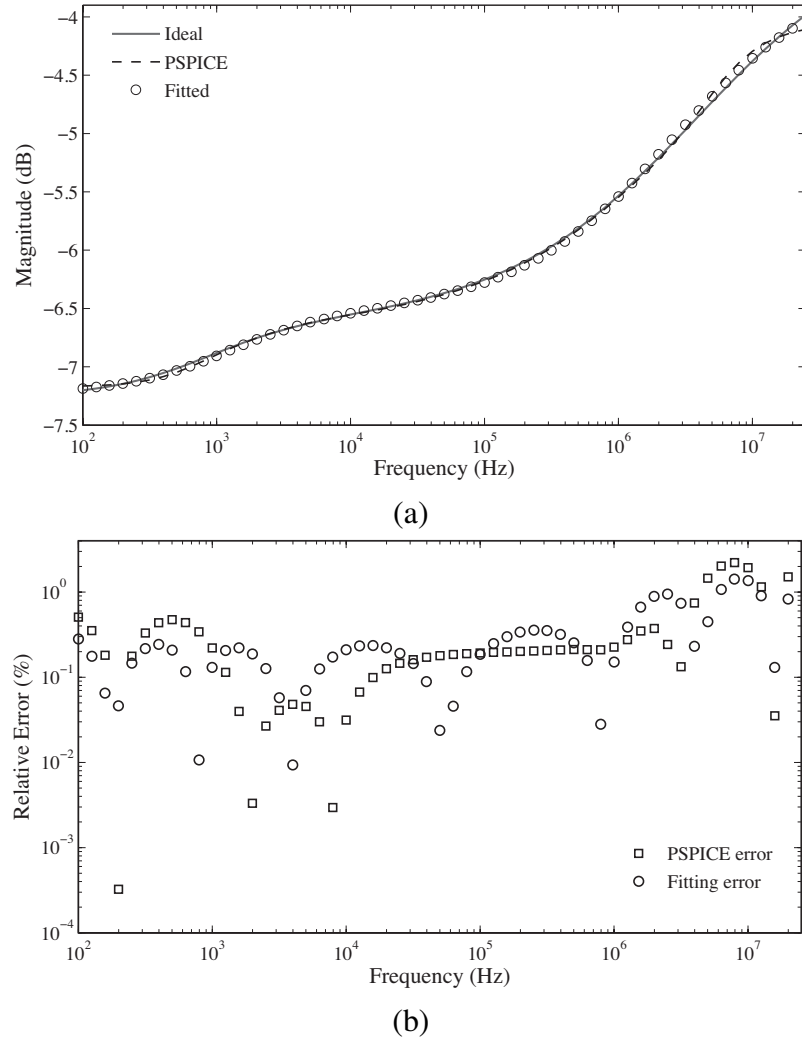


Figure 3.15: (a) Simulated ideal (solid), PSPICE (dashed) magnitude responses when ($R_\infty = 42.9 \, \Omega$, $R_1 = 71.6 \, \Omega$, $R_2 = 16.5 \, \Omega$, $\alpha_1 = 0.507$, $\alpha_2 = 0.766$, $C_1 = 3.086 \, \mu\text{F}$, $C_2 = 89.29 \, \mu\text{F}$) and $R_L = 100 \, \Omega$ compared to the simulated response using the extracted parameters (circles) and (b) relative errors of the PSPICE simulation compared to the ideal (squares) and simulated response using the extracted parameters compared to the PSPICE response (circles).

show relative errors of [17.1, 13.1, 6.09, 16.0, 0.33, 64.0, 28.9]%, respectively. The much larger relative errors of the PSPICE simulation compared to the MATLAB simulations is attributed to the deviations introduced using the approximations of the fractional capacitors. These approximations combined with the non-idealities introduced by the OPA655 result in deviations greater than 0.75% above 4 MHz reaching a maximum of 3.14% at 25.1 MHz. Note though, that the response using the extracted parameters shows a very good fit with

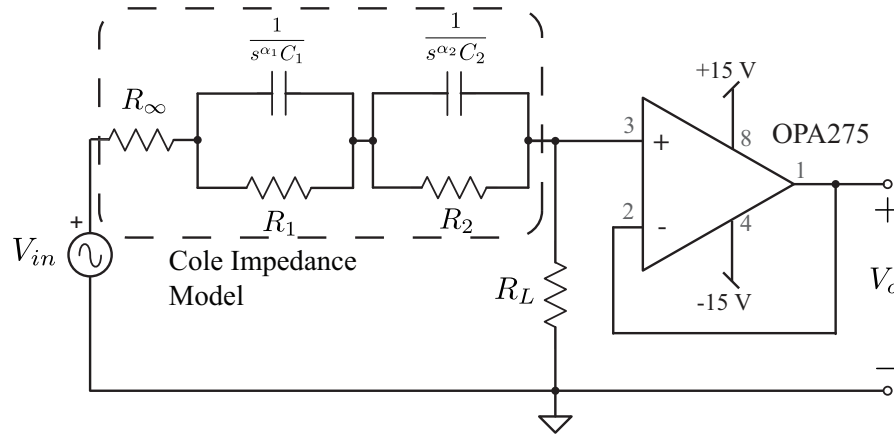


Figure 3.16: Experimental circuit to collect the magnitude response of a double-dispersion Cole impedance parameters using apples as the Cole impedance model.

the PSPICE response showing less than 0.5% error until 1 MHz and less than 2% error over the entire response. The relative errors of the PSPICE response compared to the ideal and the response using the extracted parameters compared to the PSPICE response are given in Fig. 3.15(b) as squares and circles, respectively.

3.2.3 Experimental Results

To validate the extraction method the magnitude response of the circuit in Fig. 3.16 was collected when apples were used as the double dispersion Cole impedances. This magnitude response was collected using an Agilent 54622D mixed signal oscilloscope when a 1 V peak-to-peak sinusoidal waveform with frequencies from 100 mHz to 1 MHz, in 64 logarithmic steps, was applied by a Agilent 33250A. In the experimental setup a OPA275 op amp with 9 MHz gain bandwidth product was used to buffer the output voltage, v_o , when $R_L = 497 \, \Omega$. Note that R_L was selected such that the lowest frequency measurement (at 0.1 Hz) would be greater than 1 mV (the minimum value measurable by the Agilent 54622D). From the experimental magnitude responses parameters $[R_\infty, R_1, R_2, C_1, C_2, \alpha_1, \alpha_2]$ were extracted as $[371 \, \Omega, 5.28 \, \text{k}\Omega, 58.6 \, \text{k}\Omega, 112 \, \text{nF}, 24.2 \, \mu\text{F}, 0.768, 0.762]$ and $[327 \, \Omega, 5.56 \, \text{k}\Omega, 16.8 \, \text{k}\Omega, 95.6 \, \text{nF}, 49.2 \, \mu\text{F}, 0.778, 0.638]$ for apple 1 and 2, respectively, using the NLSF with 30 applied initial guesses. The MATLAB simulated responses using these

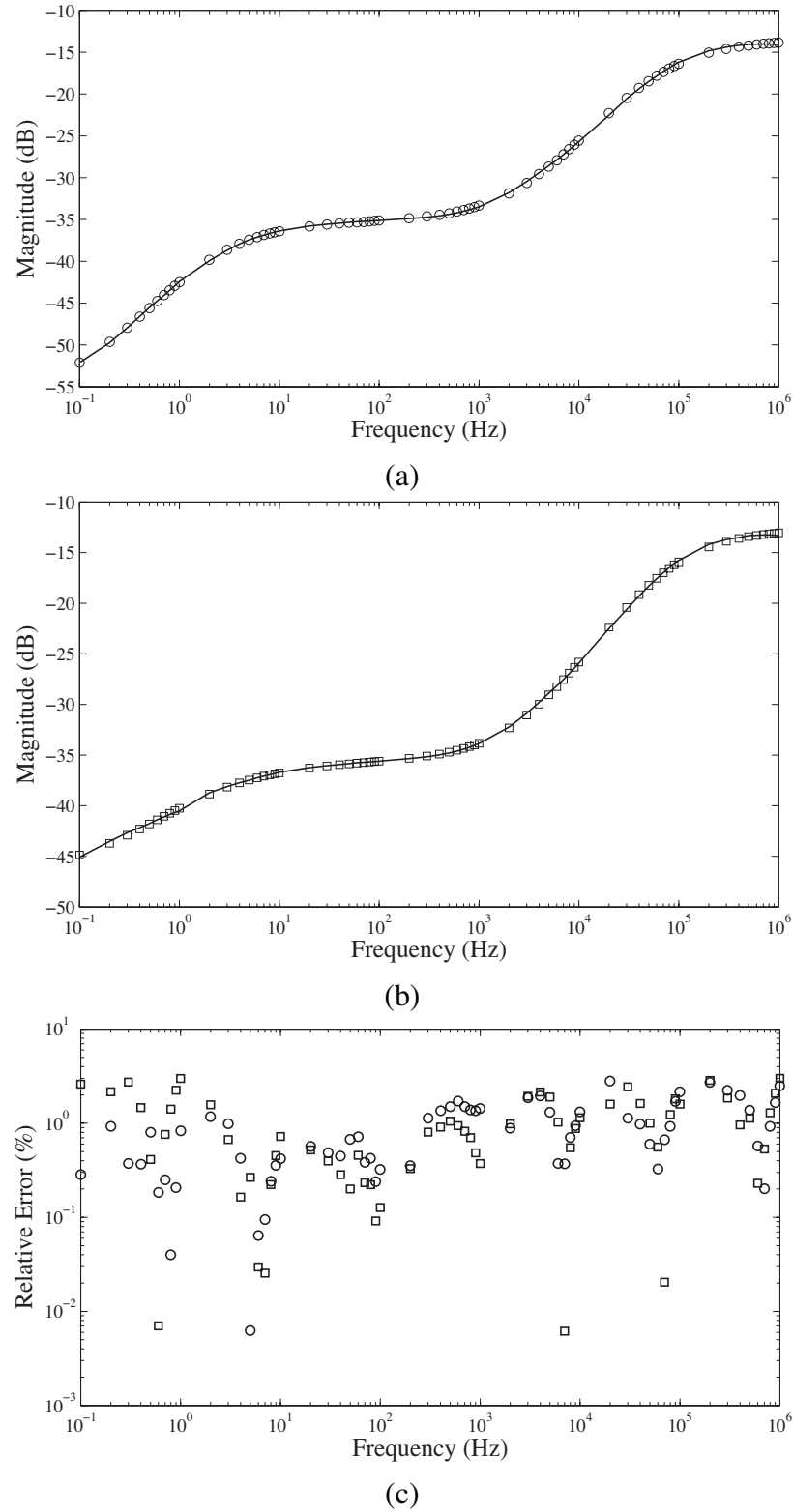


Figure 3.17: Experimentally collected step responses of (a) apple 1 (solid) and (b) apple 2 (dashed) compared to MATLAB simulated responses using extracted impedance parameters (circles and squares) and (c) relative errors of apple 1 (circles) and 2 (squares) simulated responses compared to the experimental.

parameters are given in Fig. 3.17(a) and (b) as circles and squares, respectively. These simulated responses show excellent agreement with the experimental results, with the relative errors between the experimental and simulated datapoints given in Fig. 3.17(c) as solid and dashed lines for apple 1 and apple 2, respectively. The simulated results show less than 3% relative error over the entire collected datasets.

3.3 Contribution

In conclusion, this chapter has presented methods of extracting the double-dispersion Cole impedance model parameters from the current excited step response and magnitude response, without requiring any direct impedance measurements. The summary of the results in this chapter are presented below:

- A non-linear least squares method was applied to the current step response of the double-dispersion Cole impedance model. The application of multiple initial guesses to the numerical solver was introduced to overcome accuracy limitations resulting from potential local solutions. Using MATLAB simulations, this method shows less than 5.5% average relative error when the noise is 0.5% for all parameters. This was further validated experimentally using results collected from an apples which showed less than 2% error over the entire step response between simulations of the extracted parameters and the experimental results. This work was peer reviewed and published in [107].
- A non-linear least squares method was applied to the magnitude response of the double-dispersion Cole impedance model. The application of multiple initial guesses to the numerical solver was introduced to overcome accuracy limitations resulting from potential local solutions. Using MATLAB simulations, this method shows less than 1.2% average relative error for all parameters when the noise had a Signal-to-Noise ratio of 60 dB. This was further validated in PSPICE using approximations of

the constant phase elements which showed less than 2% error over the entire magnitude response between simulations of the extracted parameters and the experimental results.

CHAPTER 4

FRACTIONAL SUPERCAPACITOR IMPEDANCE MODEL

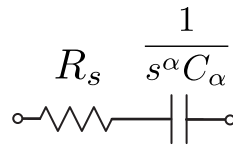


Figure 4.1: Theoretical fractional impedance model of a supercapacitor.

The fractional supercapacitor model shown in Fig. 4.1, previously introduced in Section 1.2.5, has been used to represent the low and high frequency behaviour of the supercapacitors when $\alpha = 1$ and $\alpha = 0.5$, respectively [87]. The impedance of this fractional model is given by

$$Z_c(s) = R_s + \frac{1}{C_\alpha s^\alpha} \quad (4.1)$$

and has been used in [82] to model the impedance in the frequency range from 10 mHz to 1000 Hz and [83] in the frequency range 50 mHz to 215 mHz with $\alpha \approx 1$ and 450 mHz to 100 Hz with $\alpha \approx 0.5$. This model has been selected over other fractional models because of its simplicity and good fit with experimental data at low and high frequencies. Measurement of the fractional impedance parameters that characterize this model (R_s , C_α , α) has required direct measurement of the impedance [83] or frequency response [86] requiring either an impedance or network analyzer. In this chapter an indirect method to extract the impedance parameters from the voltage excited step response of the fractional supercapacitor model using non-linear least squares process is presented. For these methods the underlying circuit theory and process are presented and validated by both simulations

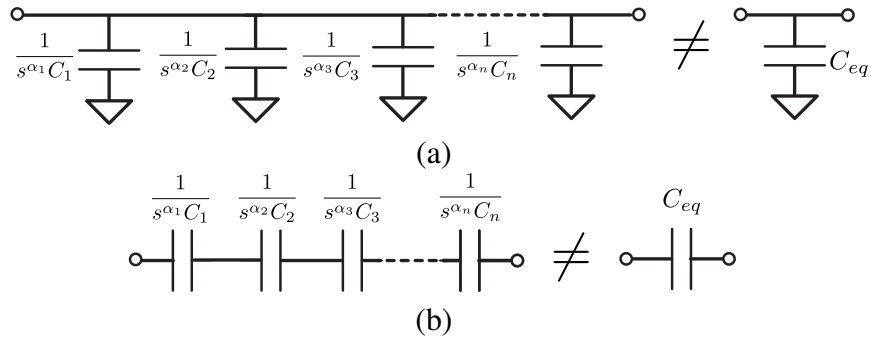


Figure 4.2: (a) Parallel and (b) series connection of n fractional capacitors.

and experimentally collected results from low and high capacity supercapacitors. It should be noted that throughout this chapter the pseudo-capacitance (C_α) units of the fractional supercapacitor model will be described as $F/s^{1-\alpha}$, previously introduced in Section 1.2.5. This is done to prevent confusion between comparisons of the fractional and integer order models whose units of capacitance and pseudo-capacitance, respectively, cannot be directly compared.

4.1 Fractional Capacitors

Traditional capacitors with order $\alpha = 1$ can be combined in parallel and series as shown in Figs. 4.2(a) and (b), respectively, with the resulting capacitance calculated using the well known formulas

$$C_p = \sum_{i=1}^n C_i \quad (4.2)$$

$$\frac{1}{C_s} = \sum_{i=1}^n \frac{1}{C_i} \quad (4.3)$$

where C_p and C_s are the parallel and series equivalent capacitance, respectively, and n is the total number of connected capacitors. However when the capacitors have varying orders we cannot use (4.2) and (4.3) to determine an equivalent capacitance but must look at the equivalent impedance instead. Then the impedance of n connected fractional capacitors in

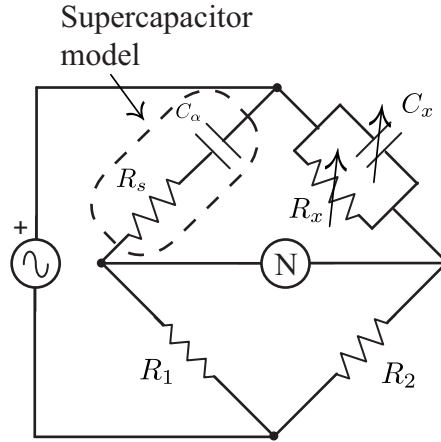


Figure 4.3: Wien bridge circuit to determine the capacitance of series resistance of a capacitor.

parallel and series becomes

$$Z_p(\omega) = \frac{1}{\sum_{i=1}^n \omega^{\alpha_i} C_i \left[\cos\left(\frac{\alpha_i \pi}{2}\right) + j \sin\left(\frac{\alpha_i \pi}{2}\right) \right]} \quad (4.4)$$

$$Z_s(\omega) = \sum_{i=1}^n \frac{1}{\omega^{\alpha_i} C_i \left[\cos\left(\frac{\alpha_i \pi}{2}\right) + j \sin\left(\frac{\alpha_i \pi}{2}\right) \right]} \quad (4.5)$$

where $Z_p(\omega)$ and $Z_s(\omega)$ are the equivalent parallel and series impedance, respectively. The order of each element has a significant effect on the impedance of each fractional capacitor and cannot be neglected when creating an equivalent impedance. It should be noted though, that (4.4) and (4.5) can be simplified to (4.2) and (4.3), respectively, when the orders of all parallel or series capacitors are equal and the resulting equivalent capacitance shares that same order. With fractional capacitors requiring updated equations to determine the equivalent impedance of parallel and series elements it follows that the techniques to measure these quantities also require updating to the fractional domain.

4.1.1 Measurement with a Wien Bridge

The Wien bridge, shown in Fig. 4.3, is a circuit to measure an unknown capacitance and series resistance by balancing them with a branch of known impedance at a fixed frequency.

To balance this circuit at a fixed frequency, the components C_x and R_x are adjusted until the impedance of each branch is equal. When balanced, the unknown quantities, C_α and R_s can be found by solving the equations

$$C_\alpha R_s = \frac{1}{\omega^2 R_x C_x} \quad (4.6)$$

$$R_s = R_x \left(1 - \frac{C_x}{C_\alpha} \right) \quad (4.7)$$

where ω is the frequency at which the impedances are balanced. However, these expressions are based on the assumption that $\alpha = 1$. If we generalize these balanced equations to the fractional domain they become

$$C_\alpha R_s = \frac{\sin\left(\frac{\alpha\pi}{2}\right) - \omega R_x C_x \cos\left(\frac{\alpha\pi}{2}\right)}{\omega^{\alpha+1} R_x C_x} \quad (4.8)$$

$$R_s = R_x \left(1 - \frac{C_x \omega^{1-\alpha} \sin\left(\frac{\alpha\pi}{2}\right)}{C_\alpha} - \frac{\cos\left(\frac{\alpha\pi}{2}\right)}{\omega^\alpha C_\alpha R_x} \right) \quad (4.9)$$

Now, if we measure a supercapacitor in the traditional Wien bridge circuit, the values calculated will not be an accurate representation of the element because the true order is neglected. For example, if fractional capacitors with orders $\alpha = 0.25, 0.5, 0.75$, and 1 are balanced in the Wien bridge at $\omega = 1000$ rad/s when $C_x = 1$ nF and $R_x = 10$ k Ω the unknown quantities will be calculated as $C_\alpha = 10$ μ F and $R_s = 1000$ Ω using (4.6) and (4.7). However, solving (4.8) and (4.9) numerically when the order is known yields the capacitances and series resistance given in Table 4.1. From these values it is clear that using the integer order Wien bridge equations greatly underestimates the value of the fractional capacitor, with the true capacitance two orders of magnitude higher than that calculated with (4.6) and (4.7) for orders less than 0.5. This difference is a natural result of the change in impedance introduced by the order of the fractional capacitor. Therefore, it is not possible to use a traditional Wien bridge circuit to measure the fractional impedance parameters that describe fractional capacitors and new techniques are required for their

	$\alpha = 1$	$\alpha = 0.75$	$\alpha = 0.5$	$\alpha = 0.25$
C_α (μF)	10.0	52.0	223.6	680.6
R_s (Ω)	9999	9958	9899	9758

Table 4.1: Theoretical extractions of capacitance and series resistance of a fractional capacitor in a classic Wien Bridge circuit.

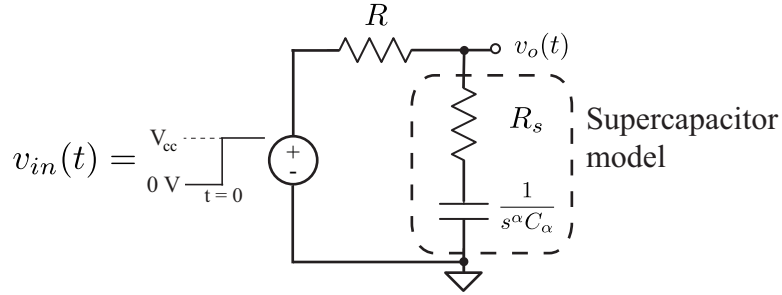


Figure 4.4: Circuit to apply a step-voltage input to the fractional model of a supercapacitor.

correct measurement.

4.2 Charging and Discharging of Supercapacitors

Accurately using supercapacitors in circuits and systems requires both accurate impedance models and expressions for their charging and discharging characteristics. A simple circuit that can be used to obtain the voltage excited step response of a supercapacitor, when modelled as a fractional impedance, is shown in Fig. 4.4. Using the Caputo definition of a fractional derivative, given by (1.1) the output voltage in the s-domain, $V_o(s)$, of Fig. 4.4 with an initial voltage, $v(0)$, on the capacitor when $V_{in}(s)$ is a step function of magnitude V_{cc} , that is $V_{in}(s) = V_{cc}/s$ is given by

$$V_o(s) = \frac{\frac{V_{cc}}{s} \frac{1}{C_\alpha(R+R_s)} + \frac{V_{cc}}{s} s^\alpha \frac{R_s}{C_\alpha(R+R_s)} + v(0) s^{\alpha-1} \frac{R}{C_\alpha(R+R_s)}}{s^\alpha + \frac{1}{C_\alpha(R+R_s)}} \quad (4.10)$$

$$= \frac{1}{R+R_s} \left[\frac{V_{cc}}{C_\alpha} \cdot \frac{s^{-1}}{s^\alpha + 1/C_\alpha(R+R_s)} + V_{cc} R_s \frac{s^{\alpha-1}}{s^\alpha + 1/C_\alpha(R+R_s)} + v(0) R \frac{s^{\alpha-1}}{s^\alpha + 1/C_\alpha(R+R_s)} \right] \quad (4.11)$$

Applying the Laplace transform formula for the Mittag-Leffler function given by (2.4) to (4.11) yields the time domain expression of the output voltage given by

$$v_o(t) = \frac{1}{R + R_s} \left[\frac{V_{cc}}{C_\alpha} t^\alpha E_{\alpha, \alpha+1} \left(\frac{-t^\alpha}{C_\alpha(R + R_s)} \right) + (V_{cc}R_s + v(0)R) E_{\alpha, 1} \left(\frac{-t^\alpha}{C_\alpha(R + R_s)} \right) \right] \quad (4.12)$$

which when there are zero initial conditions ($v(0) = 0$ V) becomes

$$v_o(t) = \frac{V_{cc}}{R + R_s} \left[\frac{t^\alpha}{C_\alpha} E_{\alpha, \alpha+1} \left(\frac{-t^\alpha}{C_\alpha(R + R_s)} \right) + R_s E_{\alpha, 1} \left(\frac{-t^\alpha}{C_\alpha(R + R_s)} \right) \right] \quad (4.13)$$

From the definition of the two-term Mittag-Leffler function we can determine the time-domain expressions with zero initial conditions from (4.13) for the case using standard capacitors, that is when $\alpha = 1$. Substituting both (2.8) and (2.9) into (4.13) we obtain the more familiar expression

$$v_o(t) = V_{cc} \left[1 - \frac{R}{R + R_s} e^{\frac{-t}{(R + R_s)C_\alpha}} \right] \quad (4.14)$$

However, supercapacitors do not behave like standard capacitors and hence the output voltage $v_o(t)$ is accurately given by (4.13) and not by (4.14). MATLAB simulations of (4.13) for $\alpha = 0.25, 0.5, 0.75$, and 1 using the Mittag-Leffler MATLAB function supplied by [101] to an accuracy of 10^{-9} for each datapoint, when $C_\alpha = 1$ F, $R_s = 30 \Omega$, $R = 180 \Omega$, and $V_{cc} = 5$ V are given in Fig. 4.5. Note that the value of α has a significant impact on the charging of the quadripole, with lower values of α reducing the rate at which the supercapacitor charges. To verify that the simulated fractional and integer order time domain expressions are equivalent for the case when $\alpha = 1$, both (4.13) and (4.14) are plotted in Fig. 4.5 as a solid line and circles, respectively, showing perfect agreement with each other.

Similarly, it can be shown that the time-domain expression for the discharging of the

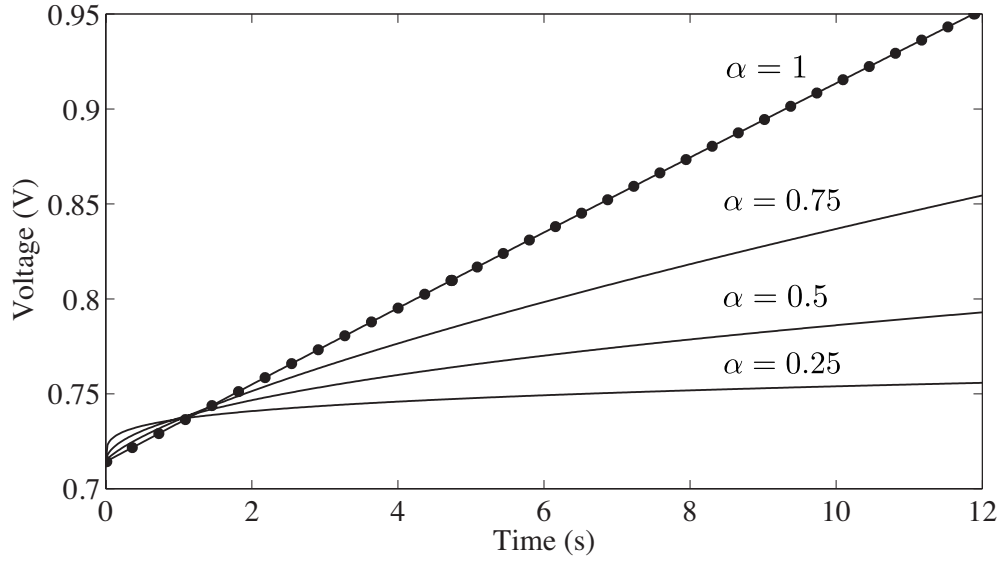


Figure 4.5: MATLAB simulations of the charging of Fig. 4.4 using (4.13) for $\alpha = 0.25$, 0.5, 0.75, and 1 when $C_\alpha = 1$ F, $R_s = 30 \Omega$, $R = 180 \Omega$, $V_{cc} = 5$ V.

supercapacitor in Fig. 4.4 with initial voltage, $v(0)$, when $v_{in}(t) = 0$ is given by

$$v_o(t) = v(0) \frac{R}{(R + R_s)} E_{\alpha,1} \left(\frac{-t^\alpha}{C_\alpha(R + R_s)} \right) \quad (4.15)$$

which when substituting (2.8) into (4.15) for the case when $\alpha = 1$ yields the familiar expression

$$v_o(t) = v(0) \frac{R}{R + R_s} e^{\frac{-t}{C_\alpha(R + R_s)}} \quad (4.16)$$

Using the fractional charging and discharging expressions for a supercapacitor in Fig. 4.4 given by (4.13) and (4.15), we can completely describe the behaviour of a supercapacitor to a step response voltage input.

4.3 Simulation Results

The NLSF method, previously described in Section 2.2 for the step-response extraction method of the single-dispersion model can be modified and applied to the step-response

extraction of the double dispersion model. The general NLSF method is repeated here:

$$\begin{aligned} \min_x \|T(x) - ydata\|_2^2 &= \min_x \sum_{i=1}^n (T(x)_i - ydata_i)^2 \\ s.t. \quad x &> 0 \end{aligned}$$

The extraction of the supercapacitor fractional-order parameters requires that x is the vector of impedance parameters (C_α, R_s, α) , $T(x)$ is the time domain step response (4.13) calculated using x , $ydata$ is the collected step response to fit to (4.13), $T(x)_i$ and $ydata_i$ are the simulated response and collected response at time t_i , and n is the total number of data points in the collected step response.

The impact of noise on the extractions was investigated by applying the NLSF routine to 1000 MATLAB simulated step responses of (4.13) from $t = 0$ to 30 s with 50 linearly spaced datapoints for supercapacitors of orders $\alpha = 0.5, 0.75$, and 1 when $C_\alpha = 1 \text{ F/s}^{1-\alpha}$, $R_s = 30 \text{ } \Omega$, $R = 180 \text{ } \Omega$, $V_{cc} = 5 \text{ V}$, and $v(0) = 0 \text{ V}$. Randomly generated white Gaussian noise with Signal-to-Noise ratios (SNR) of 40 dB to 80 dB in 5 dB steps are added to each response. The average relative error of the 1000 estimated impedance parameters (C_α, R_s, α) for each value of α and SNR are given in Fig. 4.6. This figure displays an overall trend of increasing parameter accuracy with increasing SNR for all orders showing less than 2% error when the noise SNR is greater than 60 dB. Note that the $\alpha = 1$ cases have the least error, regardless of the noise level, which results from using the initial point, $x_0 = [1 \text{ F/s}^{1-\alpha}, 30 \text{ } \Omega, 1]$ in the NLSF. The routine is more likely to solve for an accurate value when x_0 is close to the solution. Though overall these results demonstrate that even in the presence of noise, the NLSF method can accurately extract the fractional impedance parameters from a step response dataset.

Four MATLAB simulations of step responses with 60 dB SNR Gaussian white noise and the simulated responses using the extracted parameters are shown in Fig. 4.7 as dots and squares, respectively, for $\alpha = 0.25, 0.5, 0.75$, and 1. The estimated parameters from

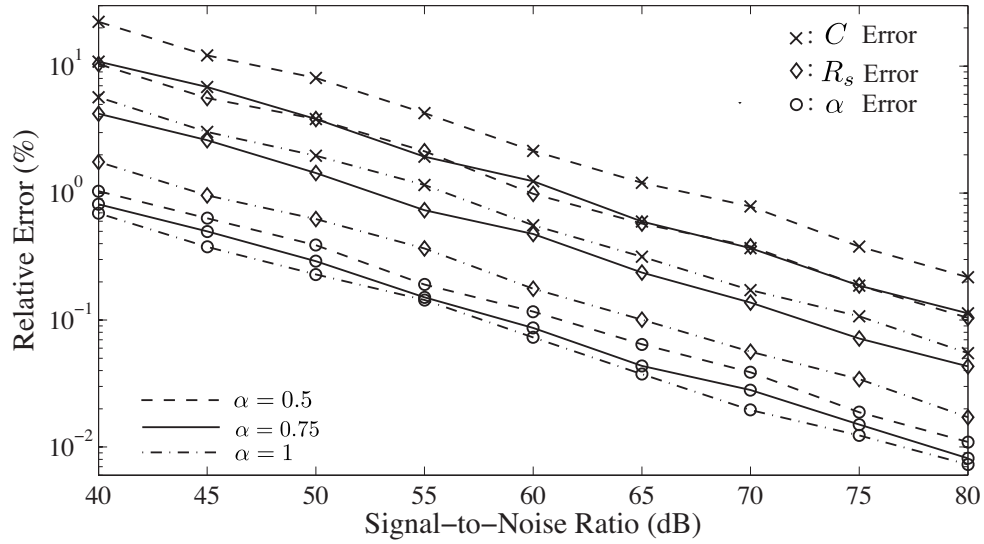


Figure 4.6: Average relative error of extracted parameters from 1000 MATLAB simulated step responses when $C_\alpha = 1 \text{ F/s}^{1-\alpha}$, $R_s = 30 \Omega$, and $\alpha = 0.5, 0.75$, and 1 with 40 to 80 dB SNR Gaussian white noise.

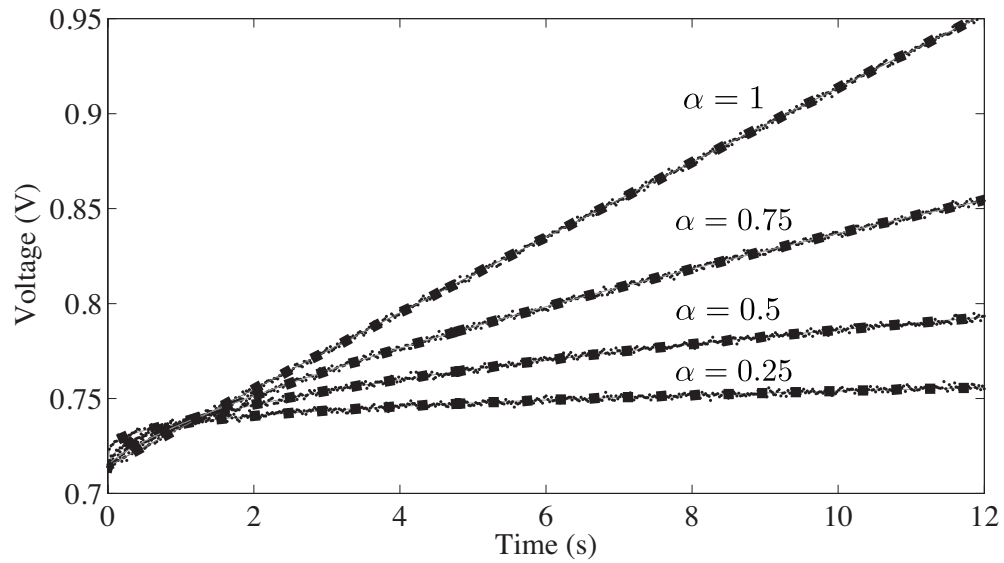


Figure 4.7: MATLAB simulated step responses with 60 dB SNR Gaussian white noise (dots) and simulated response using estimated parameters (squares) for $\alpha = 0.25, 0.5, 0.75$, and 1 when $C_\alpha = 1 \text{ F/s}^{1-\alpha}$, $R_s = 30 \Omega$.

these individual noisy datasets have $(1.27, 0.039, 0.665)\%$, $(-2.02, -0.077, -1.50)\%$, $(-1.84, -0.080, -0.995)\%$, and $(0.256, -0.0001, 0.191)\%$ relative error for (C_α, R_s, α) compared to the ideal values when $\alpha = 0.25, 0.5, 0.75$, and 1 , respectively.

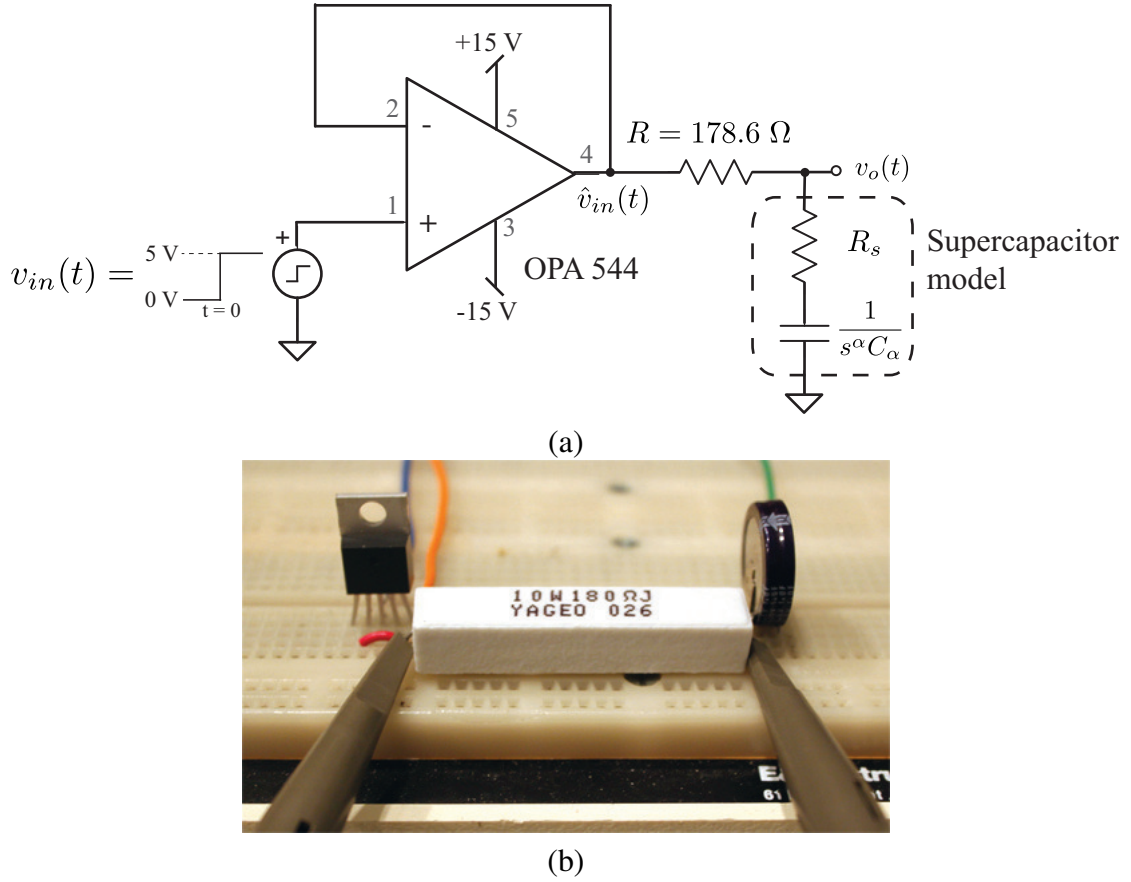


Figure 4.8: (a) Test circuit and (b) physical implementation to apply a step-voltage input to a supercapacitor to collect the output step response.

4.4 Experimental Results

To verify the estimation method the circuit of Fig. 4.8(a) was implemented on a breadboard, shown in Fig. 4.8(b), using an Agilent 33250A waveform generator to apply a pulse with $20 \mu\text{s}$ edge times and 30 s period to the OPA 544 op amp configured as a unity gain buffer. The impact of the edge time can be neglected due to the much larger 30 s time-scale of the collected charging region. This buffered input, $\hat{v}_{in}(t)$, was applied to a supercapacitor through a 178.6Ω resistor. The buffered step input and charging of a 1 F supercapacitor, collected using a Tektronix 745D digital oscilloscope sampling at a rate of 25 S/s, shown in Fig. 4.9, confirms that the op amp is operating in its linear region. As the input step does not introduce any high frequency artifacts the sampling rate is adequate to capture the charging

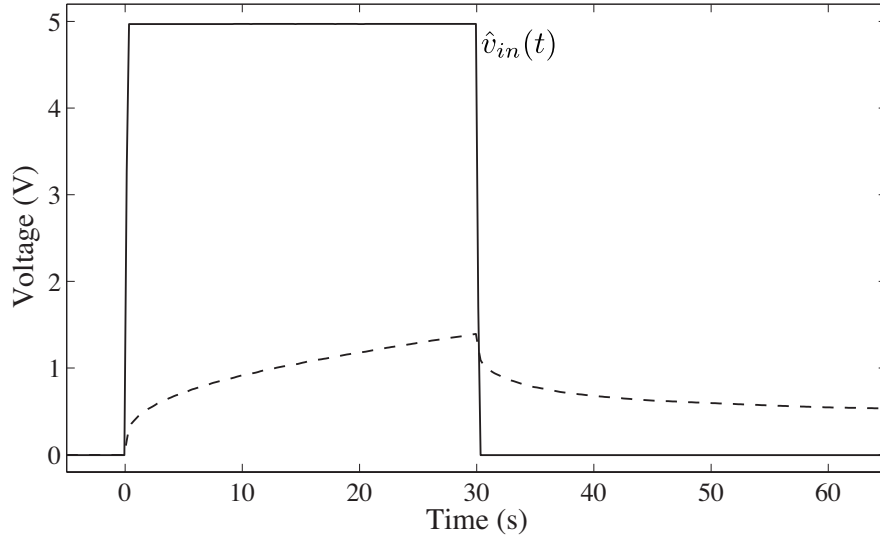
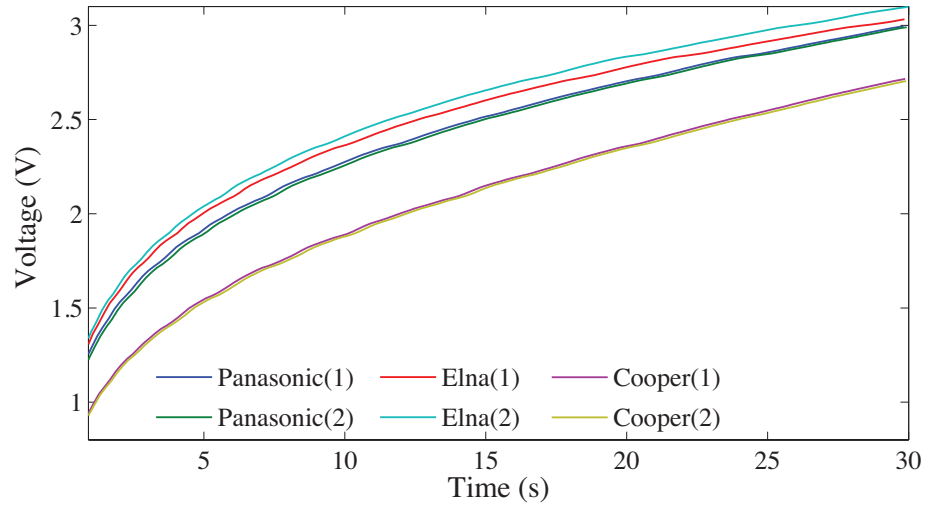


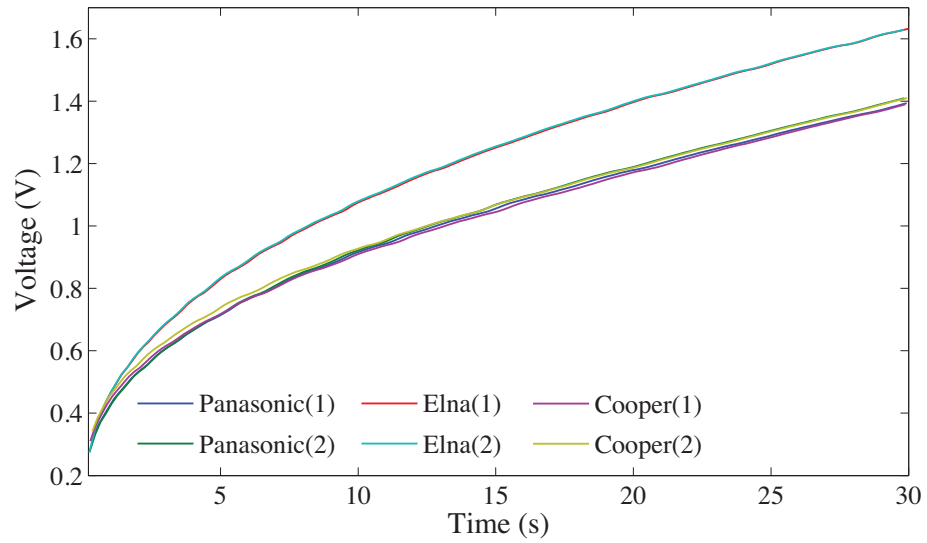
Figure 4.9: Buffered step input $\hat{v}_{in}(t)$ (solid) and charging supercapacitor (dashed) waveforms to validate that the OPA544 op amp is operating in its linear region.

and discharging characteristics for the NLSF. Note the asymmetrical charging response of the 1 F supercapacitor in Fig. 4.9 supporting the results that charge and discharge cycles vary due to irreversible processes and internal resistance [111]. The step responses of six 0.33, 1, and 1.5 F supercapacitors, 2 each from Panasonic, Elna, and Cooper-Bussmann (with all part numbers given in Table 4.2) were collected from the test setup shown in Fig. 4.8(b). The complete set of step responses for the 0.33, 1, and 1.5 F supercapacitors are shown in Figs. 4.10(a), (b), and (c), respectively. Applying the NLSF to each of the collected responses in Fig. 4.10 yields the parameters given in Tables 4.3(a), (b), and (c). The pseudo-capacitances extracted for the fractional model show a significant deviation from the rated capacitances supplied by the manufacturers because the manufacturer values represent the nominal capacity where our extracted values are to represent the transient behaviour. Therefore, a direct comparison between these parameters cannot be made as they are describing different behaviours of the supercapacitors.

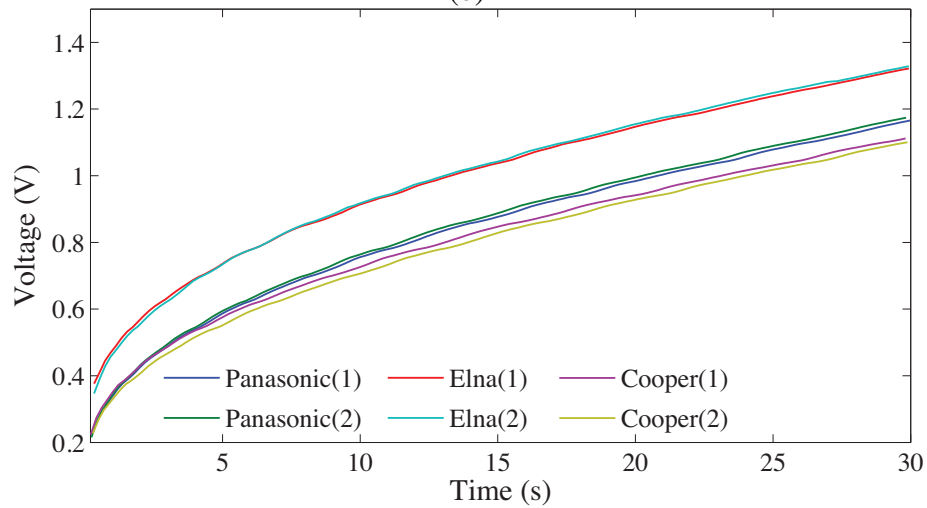
Each of the 3 brands, for all 3 capacitances show similar values to each other, even though each have potentially different manufacturing processes. Of significant note is the fractional order having mean values of $\alpha = 0.56$, 0.56 , and 0.53 for the 0.33, 1, and 1.5



(a)



(b)



(c)

Figure 4.10: Experimentally collected step responses of (a) 0.33, (b) 1, and (c) 1.5 F Panasonic, Elna, and Cooper-Bussmann brand supercapacitors.










Brand	Part Number		
	0.33 F	1 F	1.5 F
Panasonic	 EEC-S0HD334V	 EEC-S5R5105	 EEC-S5R5155
Elna	 DXJ-5R5V334U	 DX-5R5105U	 DB-5R5D155T
Cooper-Bussmann	 KR-5R5V334-R	 KR-5R5V105-R	 KR-5R5V155-R

Table 4.2: Manufacturer part numbers for 0.33, 1, and 1.5 F rated supercapacitors from Panasonic, Elna, and Cooper-Bussmann.

F supercapacitors, respectively. Therefore, in the time scale from 0.2 s to 30 s the high frequency simplification of the porous supercapacitor model to (4.1) with $\alpha \approx 0.5$ is a very good fit. The MATLAB simulation of (4.13) using the estimated parameters of the 1 F, Panasonic(1) supercapacitor in Table 4.3(b) compared to the experimentally collected step response are shown in Fig. 4.11 as black circles and a solid line, respectively. The simulation using the estimated parameters shows a very good fit with the experimental data, with less than 3% relative error over the entire response validating that the extracted fractional parameters do correctly describe the supercapacitor step response in this time scale. For comparison, the parameters from the step response were also extracted using the NLSF assuming $\alpha = 1$ which yields parameters $C_\alpha = 0.645$ F and $R_s = 21.43 \Omega$, the simulated response using these parameters are given in Fig. 4.11 as a dashed line. This response shows a significant error compared to the experimental data reaching a maximum

Brand	0.33 F Rated Capacitance		
	C_α (F/s $^{1-\alpha}$)	R_s (Ω)	α
Panasonic(1)	0.035	28.8	0.536
Panasonic(2)	0.036	28.6	0.544
Elna(1)	0.028	23.7	0.494
Elna(2)	0.029	28.4	0.516
Cooper(1)	0.060	24.6	0.620
Cooper(2)	0.061	24.4	0.623

(a)

Brand	1 F Rated Capacitance		
	C_α (F/s $^{1-\alpha}$)	R_s (Ω)	α
Panasonic(1)	0.131	8.33	0.553
Panasonic(2)	0.127	7.79	0.551
Elna(1)	0.096	6.68	0.542
Elna(2)	0.092	5.81	0.529
Cooper(1)	0.148	10.1	0.579
Cooper(2)	0.146	10.6	0.577

(b)

Brand	1.5 F Rated Capacitance		
	C_α (F/s $^{1-\alpha}$)	R_s (Ω)	α
Panasonic(1)	0.155	5.87	0.540
Panasonic(2)	0.146	5.43	0.529
Elna(1)	0.128	10.1	0.517
Elna(2)	0.114	8.68	0.496
Cooper(1)	0.166	6.68	0.537
Cooper(2)	0.646	6.46	0.555

(c)

Table 4.3: Fractional parameters extracted using NLSF method from supercapacitors with (a) 0.33, (b) 1, and (c) 1.5 F rated capacitance.

of 61% at 0.3316 s, confirming that the fractional model given by (4.1) provides a more accurate fit of the experimental data than its integer order counterpart. The relative errors of the simulated step responses using the estimated parameters in Table 4.3 compared to the experimental results of Fig. 4.10 are given in Fig. 4.12. From these figures, it is clear that all simulated responses using the estimated parameters show very good agreement with the experimental results with maximum errors less than 3% for all responses of the 0.33, 1, and 1.5 F supercapacitors. The majority of simulated datapoints using the estimated parameters show less than 0.3% relative error over the entire dataset with the maximum

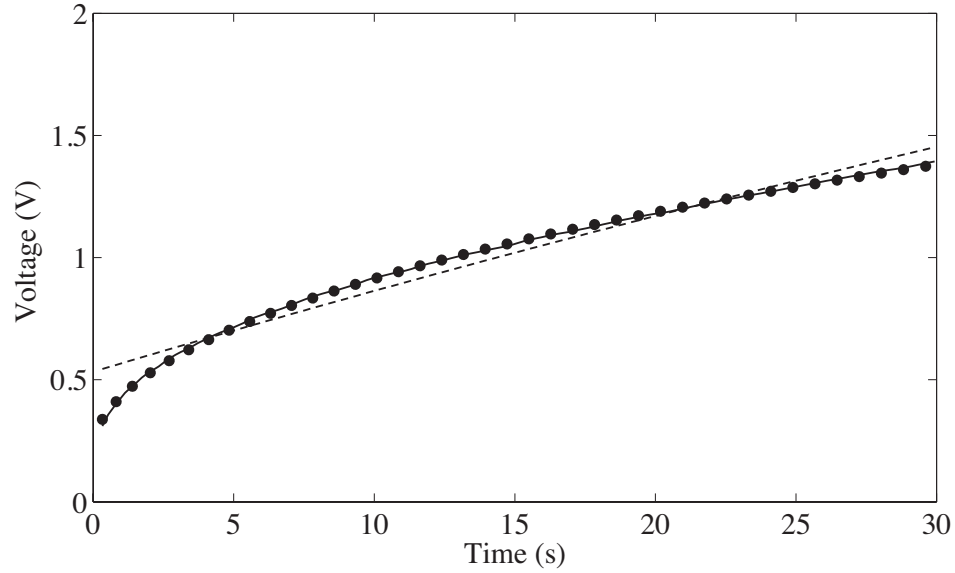
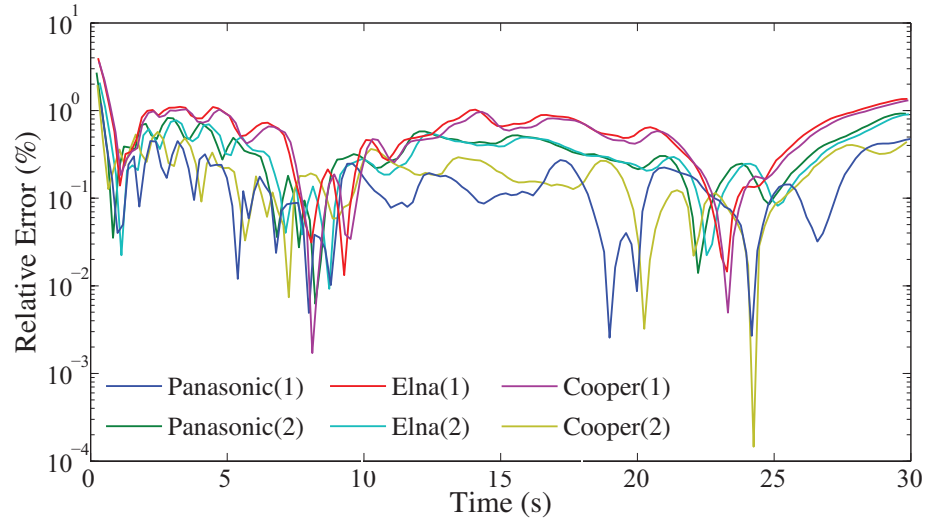


Figure 4.11: Experimentally collected step response of the 1 F, Panasonic(1) supercapacitor (solid) and the MATLAB simulated response using the estimated fractional (black circles) and integer (dashed) parameters.

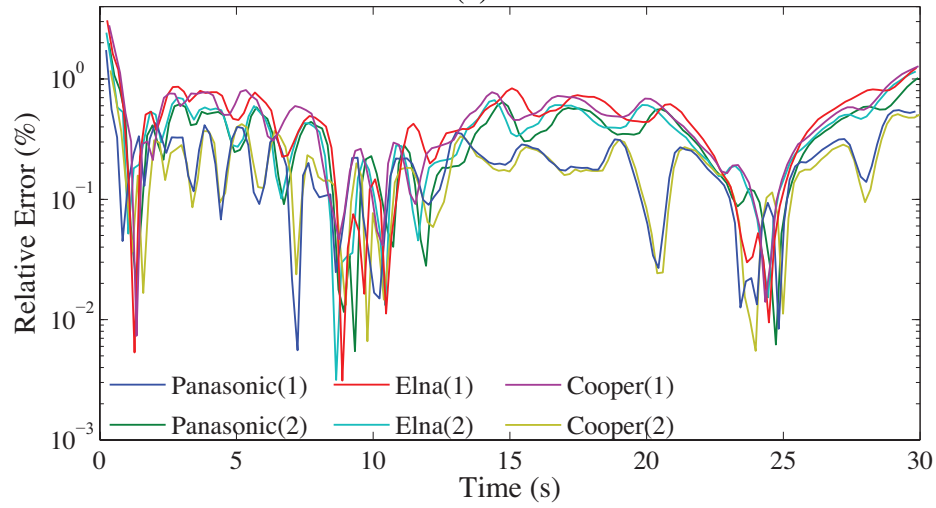
errors occurring at times less than 1 s.

4.4.1 1 F Supercapacitor Comparison

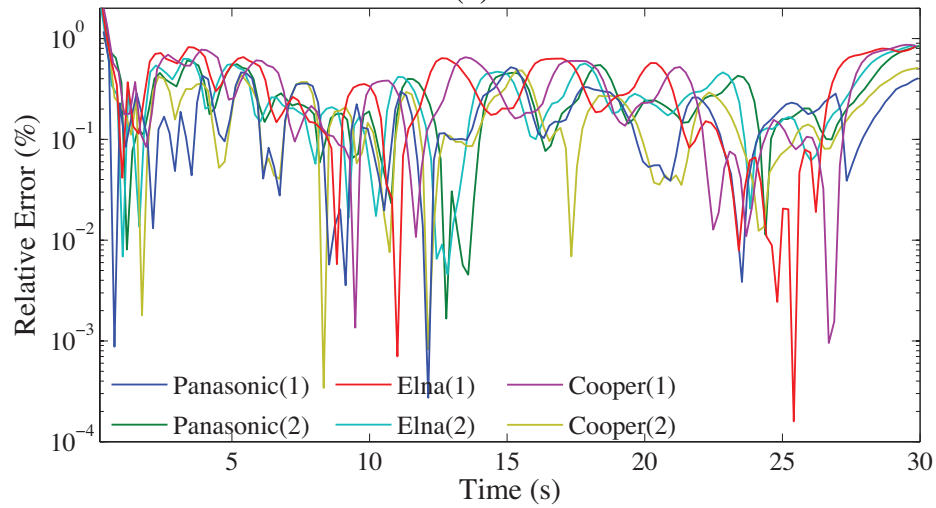
The need for manufacturers to begin using and marketing their supercapacitors having fractional characteristics becomes more apparent when comparing supercapacitors with the same rated capacitance but different part numbers from the same manufacturer. For example, the step responses of 3 different 1 F rated supercapacitors from Cooper-Bussmann having part numbers KR-5R5V105-R, PM-5R0V105-R, and PB-5R0V105-R, collected from the circuit in Fig. 4.8 to an input step of 5 V are given in Fig. 4.13(a). For comparison, a photo of the three types of supercapacitors are given in Fig. 4.13(b). Previously, it was shown that the KR-5R5V105-R supercapacitors possessed fractional parameters of approximately $C_\alpha \approx 0.1 \text{ F/s}^{1-\alpha}$, $R_s \approx 10 \Omega$, and $\alpha \approx 0.53$. However, the NLSF extraction process applied to the step responses of the PM and PB supercapacitors yields parameters $(C_\alpha, R_s, \alpha) = (0.8726 \text{ F/s}^{1-\alpha}, 0.4650 \Omega, 0.9717)$ and $(0.6893 \text{ F/s}^{1-\alpha}, 0.0728 \Omega, 0.9724)$, respectively. The PM and PB models possess parameters very close to those expected by



(a)

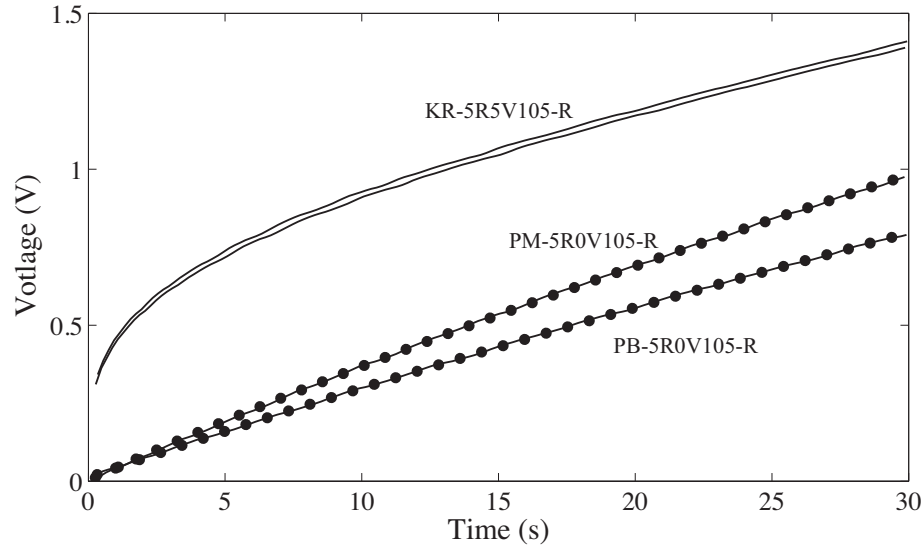


(b)

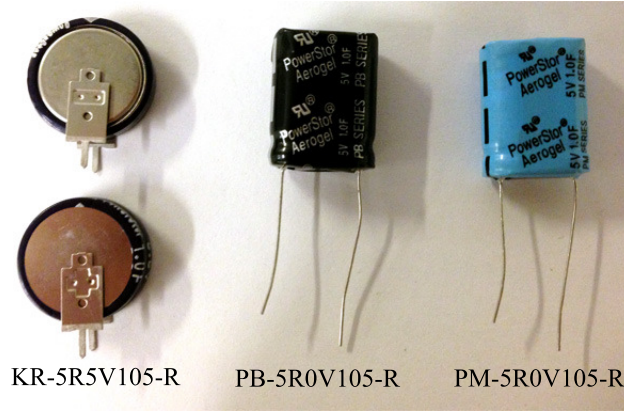


(c)

Figure 4.12: Absolute relative error of the (a) 0.33, (b) 1, and (c) 1.5 F simulated step responses using the estimated parameters in Table 4.3 compared to the experimental results of Fig. 4.10.



(a)



(b)

Figure 4.13: (a) Step responses collected from (b) 1 F rated capacitors from Cooper-Bussmann with part numbers KR-5R5V105-R, PM-5R0V105-R, and PB-5R0V105-R as solid, circle, and square lines, respectively, and

normal capacitors with an order very close to 1 and capacitance value within the expected tolerances. However, the order of the KR model ($\alpha \approx 0.53$) is only half as large as the PB and PM models ($\alpha \approx 1$). However, all three supercapacitor models are marketed with a 1 F rated capacitance even though the KR model has very different charging characteristics than both the PM and PB models. In this time scale, the transient behaviour of the PM and PB models are accurately represented with the low-frequency simplification of the porous model while the KR model is accurately represented by the high-frequency simplification. Therefore, it would be beneficial of manufacturers to adopt fractional models and report

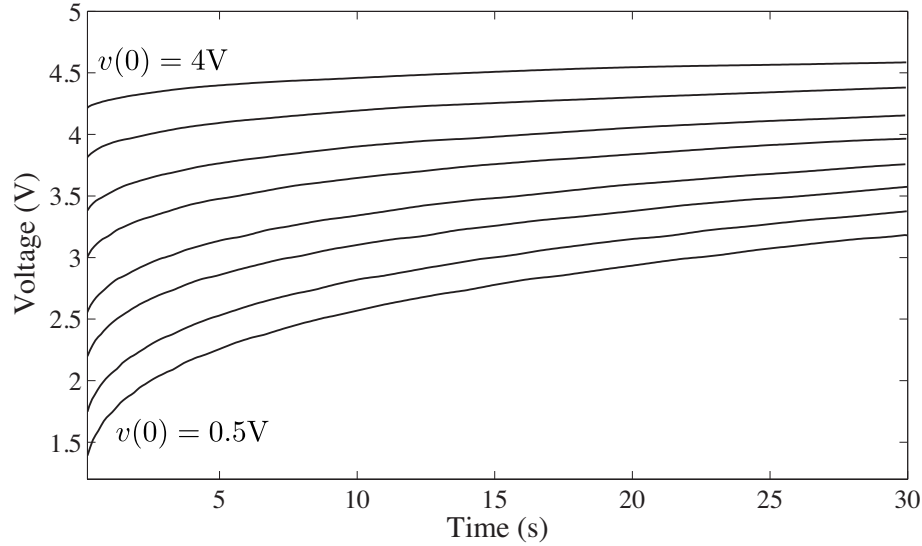


Figure 4.14: Experimental step responses collected from 0.33 F Panasonic supercapacitor from initial voltages of $v(0) = 0.5$ V to 4 V in 0.5 V steps when $V_{cc} = 5$ V.

over which time-scales they are accurate when describing supercapacitor specifications to reflect their transient characteristics.

Regarding Fig. 4.13, the KR supercapacitors appear to have a larger initial voltage than both PB and PM models even though all components were discharged for 15 minutes before testing. This apparent initial voltage results from the large series resistance of the KR model that forms a voltage divider, $R_s/(R + R_s)$, and results in the voltage jump when a step input is initially applied.

4.4.2 Voltage Dependence

The capacitance of supercapacitors has been shown in [111] to depend on the state of charge resulting from the nonlinear response of the molecules at the electrode-electrolyte interface. This behaviour impacts the fractional impedance parameters extracted from the step response of the supercapacitors. The step responses of a 330 mF Panasonic supercapacitor from initial voltages of 0.5 V to 4 V in 0.5 V steps to an input of $V_{cc} = 5$ V are given in Fig. 4.14. Applying the NLSF to each waveform yields the fractional parameters given in Table 4.4. From the extracted impedance parameters there is a trend of decreas-

$v(0)$	C_α (mF/s $^{1-\alpha}$)	R_s (Ω)	α
0.5 V	35.7	34.9	0.536
1 V	36.1	31.2	0.538
1.5 V	35.3	34.2	0.527
2 V	35.8	29.6	0.529
2.5 V	33.6	33.9	0.514
3 V	32.0	29.2	0.497
3.5 V	31.5	35.8	0.499
4 V	31.9	39.8	0.516

Table 4.4: Fractional impedance parameters extracted from 330 mF panasonic supercapacitor from initial voltages of 0.5 V to 4 V in 0.5 V steps.

ing C_α and α as the initial voltage increases. The impact of the inaccuracies introduced in modelling the transient characteristics without accounting for the voltage dependence are highlighted in Fig. 4.15 with the experimental and simulated waveforms of a 330 mF Panasonic supercapacitor shown as solid and dashed lines, respectively. The simulated charging and discharging regions use the fractional parameters $(C_\alpha, R_s, \alpha) = (35 \text{ mF/s}^{1-\alpha}, 28.8 \Omega, 0.536)$ and $(14 \text{ mF/s}^{1-\alpha}, 15.56 \Omega, 0.499)$, respectively, extracted from the initially collected charge and discharge responses in Section 4.4. The initial charging region from 0 s to 10 s shows very good agreement with the simulation, but major errors are introduced between experimental and simulated waveforms in the first discharging region from 10 s to 15 s. This results from the discharging parameters having been extracted after the supercapacitor was charged for 30 s before its discharge which yielded a different initial voltage than that at 10 s in Fig. 4.15. This different initial voltage requires modification of the parameters for this region as a result of their voltage dependence. Without this modification errors are introduced which propagate to subsequent charging and discharging regions and results in the deviations of the simulations from the experimental results. Therefore, to accurately model the transient characteristics in all charge situations, the fractional model must be expanded to account for the dependence of the fractional parameters on the state of charge and voltage. The voltage dependency of the fractional impedance parameters that describe the transient behaviour of supercapacitors warrants future investigation, but is

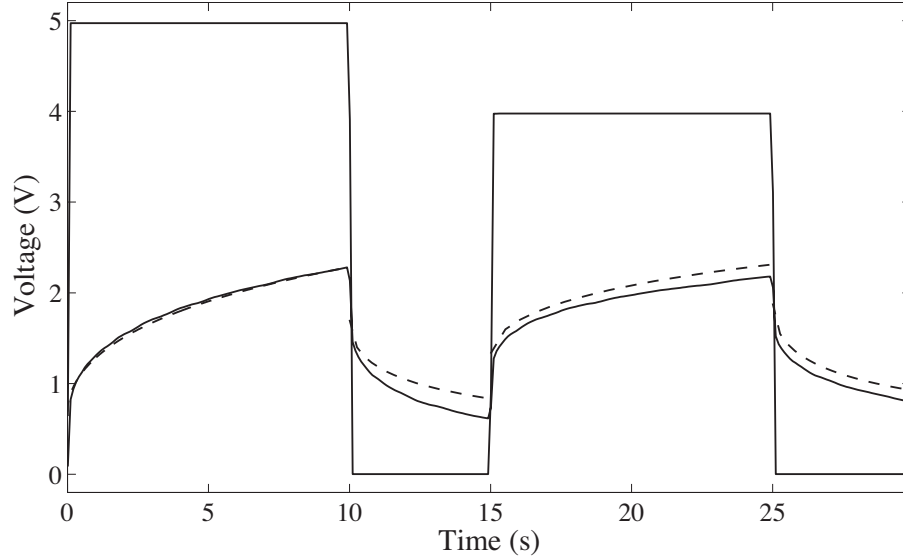


Figure 4.15: Experimental (solid) and simulated (dashed) response to voltage pulses collected from 0.33 F Panasonic supercapacitor.

outside the scope of the main argument presented in this work.

4.4.3 High Capacity Supercapacitors

Supercapacitors with very high capacities are available with rated capacitances upwards of a thousand farads. Two such components are the BCAP1500-P270-K05 and BCAP3000-P270-K05 supercapacitors from Maxwell Technologies Inc., given in Fig. 4.16, with rated capacitances of 1500 and 3000 F, respectively. To extract the fractional parameters of these components a voltage step of 2.5 V was applied to each supercapacitor using the circuit given in Fig. 4.4 when $R = 0.52 \, \Omega$. In this test-setup, fully described in Appendix C, a HP3631A DC power supply was used to generate the step-input with required output current. The relatively slow input step of approximately 300 ms can be neglected due to the much larger 90 s time-scale of the collected dataset. These collected responses are shown in Fig. 4.17 as solid lines. Applying the NLSF extraction process on the BCAP1500-P270-K05 and BCAP3000-P270-K05 datasets yields fractional parameters of $(C_\alpha, R_s, \alpha) = (1003.6 \text{ F}, 0.0179 \, \Omega, 0.9783)$ and $(2095.9 \text{ F}, 0.0223 \, \Omega, 0.9857)$, respectively. The MATLAB simulated step response using the extracted fractional parameters shows very



Figure 4.16: BCAP1500-P270-K05 and BCAP3000-P270-K05 supercapacitors from Maxwell Technologies Inc. with rated capacitances of 1500 and 3000 F, respectively.

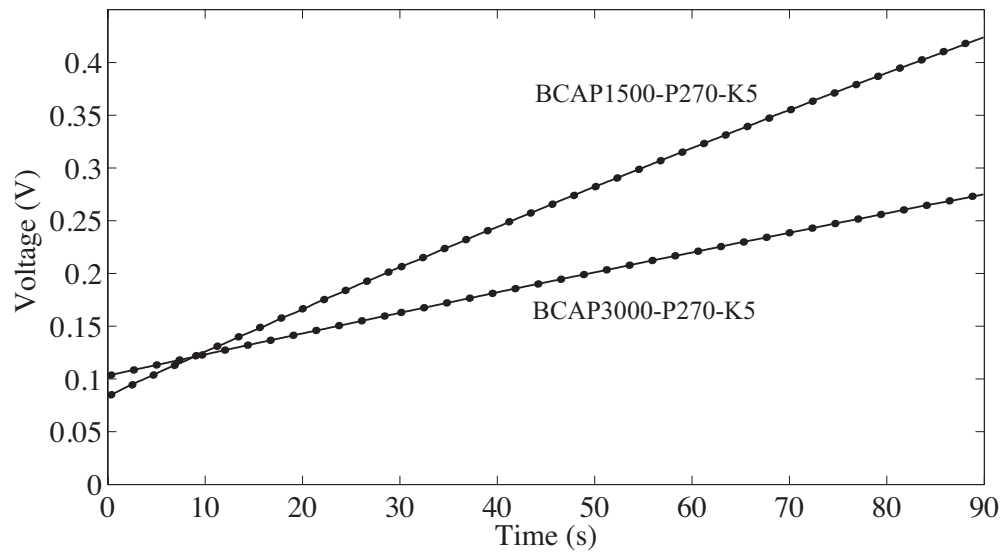


Figure 4.17: Experimental step responses collected from 1500 F (BCAP1500-P270-K05) and 3000 F (BCAP3000-P270-K05) rated capacitors from Maxwell Technologies (solid) compared to MATLAB simulated responses using extracted fractional parameters (circles).

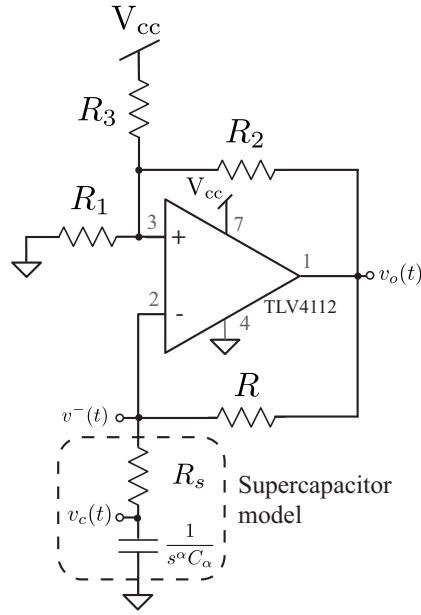
good agreement with the experimental results with less than 0.2% relative error over the entire collected dataset. These simulated responses are given in Fig. 4.17 as circles. These parameters are within the same range as those extracted in [86] and confirm that these supercapacitors behave very closely to the traditional integer order ($\alpha = 1$) capacitor model and are accurately modelled using the low-frequency simplification of the porous model over this limited time scale.

4.5 Fractional Multivibrator

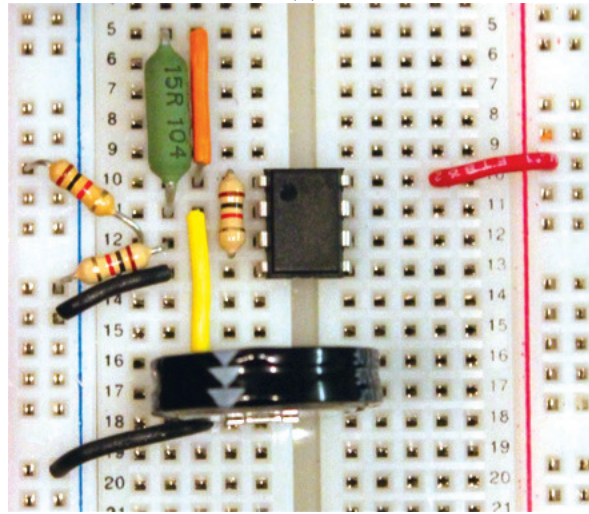
A free-running multivibrator circuit has been previously investigated in [15] examining the effect of using a fractional order capacitor in a single op amp circuit, demonstrating that the fractional order capacitor has the ability to increase the oscillator frequency significantly while using reasonable time constants. However, the physical realization of this circuit in [15] required the use of an approximated fractional capacitor using a RC ladder circuit. Having shown in the previous section that supercapacitors exhibit fractional behaviour in the time domain with an order of approximately 0.5, we employ a supercapacitor in the multivibrator circuit shown in Fig. 4.18 to confirm its fractional behaviour. This circuit utilizes a single supply voltage because the supercapacitor can only accept positive voltages, therefore this circuit will charge and discharge to $2/3 V_{cc}$ and $1/3 V_{cc}$, respectively, at the inverting terminal of the op amp, $v^-(t)$, at which time the output, $v_o(t)$ will toggle from V_{cc} to 0 or vice versa. To predict the oscillator frequency requires accurate modelling of $v^-(t)$ based on the charging and discharging of the supercapacitor. The expressions for these cycles are given by

$$v_C^-(t) = \frac{V_{cc}}{C_\alpha(R+R_s)} t^\alpha E_{\alpha,\alpha+1} \left(\frac{-t^\alpha}{C_\alpha(R+R_s)} \right) + \left[\frac{V_{cc}R + v(0)R}{R+R_s} \right] E_{\alpha,1} \left(\frac{-t^\alpha}{C_\alpha(R+R_s)} \right) \quad (4.17)$$

$$v_D^-(t) = \frac{R}{R+R_s} v(0) E_{\alpha,1} \left(\frac{-t^\alpha}{C_\alpha(R+R_s)} \right) \quad (4.18)$$



(a)



(b)

Figure 4.18: (a) Theoretical and (b) physically implemented fractional multivibrator circuit using a supercapacitor as the fractional element.

where $v_C^-(t)$ and $v_D^-(t)$ are the charging and discharging expressions, respectively, and $v(0)$ is the initial voltage stored on the supercapacitor for that cycle. However, as a result of the series resistance, R_s , of the supercapacitors the initial voltage is not the same as the transition voltages, $2/3 V_{cc}$ and $1/3 V_{cc}$, of typical multivibrators as a result of the voltage divider formed by R and R_s . Therefore, to correctly predict the oscillation frequency and simulate this circuit requires the true voltage on the fractional capacitor for each charge and

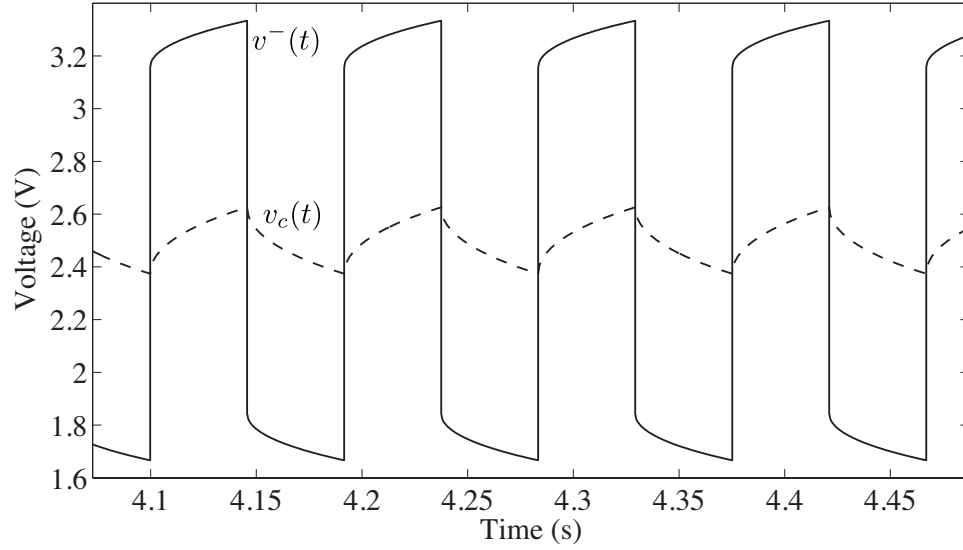


Figure 4.19: MATLAB simulated response of the multivibrator waveforms $v^-(t)$ (solid) and $v_c(t)$ (dashed) using the extracted fractional parameters of 1 F, Panasonic(2) supercapacitor when $V_{cc} = 5$ V.

discharge cycle. The expressions for the voltage on the supercapacitor, shown as $v_c(t)$ in Fig. 4.18, during the charge and discharge cycles are given as

$$v_c^C(t) = \frac{V_{cc}}{C_\alpha(R+R_s)} t^\alpha E_{\alpha,\alpha+1} \left(\frac{-t^\alpha}{C_\alpha(R+R_s)} \right) + v(0) E_{\alpha,1} \left(\frac{-t^\alpha}{C_\alpha(R+R_s)} \right) \quad (4.19)$$

$$v_c^D(t) = v(0) E_{\alpha,1} \left(\frac{-t^\alpha}{C_\alpha(R+R_s)} \right) \quad (4.20)$$

where $v_c^C(t)$ and $v_c^D(t)$ are the voltages during the charging and discharging cycles, respectively.

MATLAB simulations of $v^-(t)$ and $v_c(t)$ using (4.17) and (4.18), respectively, where the initial voltage for the charging/discharging cycle is determined by the previous discharge/charge cycle using (4.20) and (4.19) are given in Fig. 4.19 using the extracted fractional parameters of the 1 F, Panasonic(2) supercapacitor when $V_{cc} = 5$ V and $R = 15$ Ω . We measure an oscillation frequency of 10.98 Hz. For comparison, this simulation was conducted with values $C_\alpha = 1$ F, $R_s = 7.79$ Ω , and $\alpha = 1$, which are the manufacturer's rated values, yielding an oscillation frequency of 0.854 Hz. Therefore, using the fractional

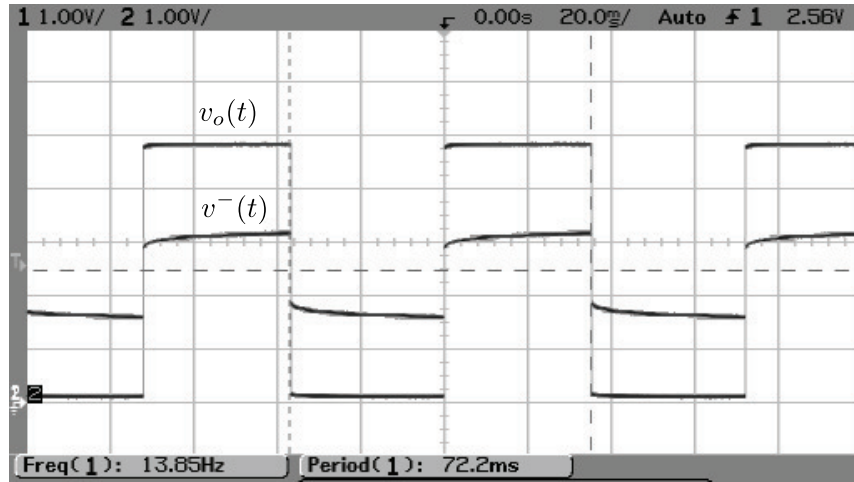


Figure 4.20: Experimental waveforms $v_o(t)$ and $v^-(t)$ using the 1 F, Panasonic(2) supercapacitor collected from the multivibrator circuit of Fig. 4.18.

impedance parameters, which shows a lower pseudo-capacitance and order, results in an oscillation frequency two orders of magnitude higher than predicted by an integer-order model.

The multivibrator circuit in Fig. 4.18(a) was implemented using a TLV4112 op amp with $R_1 = R_2 = R_3 = 1 \text{ k}\Omega$, $R = 15.1 \text{ }\Omega$, and $V_{cc} = 5 \text{ V}$ with the physical realization given in Fig. 4.18(b). The voltages at the non-inverting terminal, $v^-(t)$, and output, $v_o(t)$, collected using a Agilent 54622D mixed signal oscilloscope when the 1 F, Panasonic(2) supercapacitor was used are given in Fig. 4.20. From the waveforms we observe that the multivibrator oscillates at a frequency of 13.85 Hz closer to the value of 10.98 Hz predicted by the MATLAB simulations using the fractional parameters than 0.854 Hz predicted by the integer parameters. Highlighting that the nominal capacitance supplied by manufacturers is not capable of explaining the measured oscillation frequency. While the extracted parameters showed less than 3% error with the experimental step responses in Section 4.4 the predicted oscillation frequency shows an error of 20.7%. This larger error is attributed to using the extracted parameters from an initial voltage $v(0) = 0 \text{ V}$, even though the stored voltage in the multivibrator circuit will be higher as mentioned in Section 4.4.2, this requires further investigation. Also, the same parameters were used for both charging and

discharging cycles even though the supercapacitors were shown not to possess identical charge and discharge cycles in Fig. 4.9.

4.6 Contribution

In conclusion, this chapter has presented methods of extracting the fractional impedance parameters that accurately represent the transient characteristics of a supercapacitor from the voltage excited step response without requiring any direct impedance measurements. The summary of the results in this chapter are presented below:

- The voltage-excited step-response of a fractional model for a supercapacitor is presented with a non-linear least squares method applied to extract the impedance parameters that characterize the model. Using MATLAB simulations, this method shows less than 2% average relative error when the noise had a Signal-to-Noise ratio of 60 dB or greater;
- The non-linear least squares method was validated experimentally using results collected from low capacity supercapacitors with manufacturer ratings of 0.33 F, 1 F, and 1.5 F and high capacity supercapacitors with 1500 F and 3000 F manufacturer ratings. The experimental datasets and those simulated using the extracted parameters show less than 3% relative error for all supercapacitors;
- The fractional time-domain behaviour of the supercapacitors was also highlighted using a supercapacitor in a multivibrator circuit. Using this circuit, the oscillation frequency of the fractional model simulated in MATLAB shows much closer agreement with the experimental results than that predicted by the integer parameters. These results have been peer reviewed and published in [112, 113].

CHAPTER 5

CONCLUSIONS AND FUTURE WORK

5.1 Conclusion

Throughout this work the extraction of fractional-impedance parameters without requiring direct impedance measurements has been investigated. This work has been applied to the single and double dispersion Cole impedance models used extensively in biology and biomedicine and a fractional model applied to supercapacitors.

Concepts from fractional calculus were imported to develop the circuit theory and derive the current and voltage excited step responses and magnitude responses of the single-dispersion Cole impedance model. From the step-excited responses a numerical curve fitting method was developed and applied to extract the impedance parameters that describe this model. To further overcome the accuracy limitations, which are highlighted in MATLAB simulations, a non-linear least squares method is applied to the current and voltage excited step responses with the improvements verified from experimentally collected fruit tissue datasets. The sensitivity of an indirect magnitude extraction method was analyzed with its limitations overcome by the application of a non-linear least squares method. This improved accuracy is verified applying the method to experimentally collected magnitude responses of two apricots and an apple, showing a much better fit using the non-linear least squares parameters.

The concepts from fractional calculus are further applied to the double dispersion Cole impedance model to develop expressions for the current-excited step response and magnitude response of this fractional impedance model. Using these models, non-linear least

squares methods are applied to both frequency and time domain datasets of the double dispersion Cole impedance model to extract the fractional impedance parameters that characterize this model. The extractions are validated by PSPICE simulations for the magnitude response and experimentally collected results from fruit tissues for the current-excited step response.

The impact of using integer-order model techniques to measure a CPE or supercapacitor and how parameters extracted with these methods inaccurately represent the transient characteristics of these devices was analyzed. Fractional circuit theory was applied to a fractional-impedance model applied to supercapacitors to describe the voltage-excited step response of this device. Using this fractional model a non-linear least squares method was applied to the voltage induced step response of supercapacitors to extract the fractional impedance parameters that accurately describe their transient behaviour. This process was verified using experimentally collected step responses from both low and high capacity supercapacitors.

5.2 Contribution

The contributions of this thesis have been to two areas of electrical engineering: circuit theory and signal processing. The first major contribution is the continued development of fractional circuit theory by importing concepts from fractional calculus into circuits and systems. Using this fractional circuit theory expressions for the current and voltage excited step responses and magnitude responses of fractional impedance models have been developed. This continued development is especially important as fractional devices are very close to becoming commercially available, though without the development of the circuit theory regarding their use the benefits they offer will not be immediately available.

The second major contribution of this thesis is the application of signal processing methods to extract the impedance parameters that characterize fractional impedance models without requiring direct impedance measurements. Numerical graph fitting methods and

non-linear least squares fittings have been applied to the step responses of the single and double dispersion impedance models and a fractional supercapacitor model to extract the impedance parameters that characterize these models. The non-linear least-squares fitting has also been applied to the magnitude response of the single and double dispersion Cole impedance model parameters to also extract their impedance parameters.

5.3 Future Work

The continued development of this work shows many interesting applications to continue to explore that include:

- Continued import of fractional calculus into circuit theory to explore possible benefits offered by the fractional-domain generalization of traditional integer order circuits;
- The development of inexpensive and portable instruments that apply the non-linear least squares method to extract the impedance parameters of connected tissues of devices for impedance spectroscopy without requiring direct impedance measurements;
- The investigation of the relationship between the extracted single and double dispersion Cole impedance parameters of fruit tissues to monitor for health, storage viability, or other physiological changes and their physical mechanisms;
- The investigation and comparison of the fractional-impedance parameters extracted using the various indirect methods;
- The development of voltage and time-dependent fractional models to completely describe the behaviour of fruits, vegetables, and supercapacitors long-term transient-time behaviour.

BIBLIOGRAPHY

- [1] K. Oldham and J. Spanier, *The Fractional Calculus: Theory and Applications of Differentiation and Integration to Arbitrary Order*. New York: Academic Press, 1974.
- [2] M. Ortigueira, *Fractional Calculus for Scientists and Engineers*. Springer, 2011.
- [3] T. Haba, G. Ablart, and T. Camps, “The frequency response of a fractal photolithographic structure,” *IEEE Trans. Dielectr. Electr. Insul.*, vol. 4, no. 3, pp. 321–326, 1997.
- [4] T. Haba, G. Ablart, T. Camps, and F. Olivie, “Influence of the electrical parameters on the input impedance of a fractal structure realised on silicon,” *Chaos Solitons Fractals*, vol. 24, no. 2, pp. 479–490, 2005.
- [5] R. Caponetto, G. Dongola, L. Fortuna, A. Gallo, and S. Graziani, “Ipmc actuators non integer order models,” in *New Trends in Nanotechnology and Fractional Calculus Applications* (D. Baleanu, Z. B. Güvenç, and J. A. T. Machado, eds.), pp. 263–272, Springer Netherlands, 2010.
- [6] R. Magin, “Fractional calculus in bioengineering: a tool to model complex dynamics,” in *13th Int. Carpathian Control Conf.*, pp. 464–469, 2012.
- [7] I. Podlubny, I. Petras, B. Vinagre, P. O’Leary, and L. Dorcak, “Analogue realizations of fractional-order controllers,” *Nonlinear Dyn.*, vol. 29, no. 1-4, pp. 281–296, 2002.

- [8] T. Haba, G. Loum, J. Zoueu, and G. Ablart, "Use of a component with fractional impedance in the realization of an analogical regulator of order $1/2$," *J. Applied Sciences*, vol. 8, no. 1, pp. 59–67, 2008.
- [9] J. Machado, I. Jesus, A. Galhano, and J. Cunha, "Fractional order electromagnetics," *Signal Process.*, vol. 86, no. 10, pp. 2637–2644, 2006.
- [10] D. Baleanu, Z. Guvenc, and J. T. Machado, *New Trends in Nanotechnology and Fractional Calculus Applications*, ch. Analysis of the Fractional Dynamics of an Ultracapacitor and its Application to a Buck-Boost Converter, pp. 97–105. Springer Netherlands, 2010.
- [11] P. Varshney, M. Gupta, and G. Visweswaran, "New switched capacitor fractional order integrator," *J. Act. Passive Electron. Dev.*, vol. 2, pp. 187–197, 2007.
- [12] G. Santamaria, J. Valverde, R. Perez-Aloe, and B. Vinagre, "Microelectronic implementations of fractional order integrodifferential operators," *J. Comput. Nonlinear Dyn.*, vol. 3, no. 2, 2008.
- [13] K. Biswas, S. Sen, and P. K. Dutta, "Realization of a constant phase element and its performance study in a differentiator circuit," *IEEE Trans. Circuits Syst. Express Briefs*, vol. 53, no. 9, pp. 802–806, 2006.
- [14] W. Ahmed, R. El-khazali, and A. Elwakil, "Fractional-order wien-bridge oscillator," *Electron. Lett.*, vol. 37, no. 18, pp. 1110–1112, 2001.
- [15] B. Maundy and A. Elwakil, "On a multivibrator that employs a fractional capacitor," *Analog Intergr. Circ. Sig. Process*, vol. 62, no. 1, pp. 99–103, 2010.
- [16] T. Freeborn, B. Maundy, and A. Elwakil, "Field programmable analogue array implementation of fractional step filters," *IET Circuits Devices Syst.*, vol. 4, no. 6, pp. 514–524, 2010.

- [17] B. Maundy, A. Elwakil, and T. Freeborn, "On the practical realization of higher-order filters with fractional stepping," *Signal Process.*, vol. 91, no. 3, pp. 484–491, 2011.
- [18] T. Freeborn, B. Maundy, and A. Elwakil, "Fractional-step tow-thomas biquad filters," *Nonlinear Theory Appl. (IEICE)*, vol. 3, no. 3, pp. 357–374, 2012.
- [19] M. Ortigueira, "An introduction to the fractional continuous-time linear systems: the 21st century systems," *IEEE Circuits Syst. Mag.*, vol. 8, no. 3, pp. 19–26, 2008.
- [20] A. Elwakil, "Fractional-order circuits and systems: An emerging interdisciplinary research area," *IEEE Circuits Syst. Mag.*, vol. 10, no. 4, pp. 40–50, 2010.
- [21] I. Podlubny, *Fractional Differential Equations*. Academic Press, 1999.
- [22] M. Nakagawa and K. Sorimachi, "Basic characteristics of a fractance device," *IEICE Trans. Fundam. Electron. Commun. Comput. Sci.*, vol. E75, pp. 1814–1819, 1992.
- [23] S. Westerlund and L. Ekstam, "Capacitor theory," *IEEE Trans. Dielectr. Electr. Insul.*, vol. 1, no. 5, pp. 826–839, 1994.
- [24] Coilcraft, *Modeling coilcraft RF inductors - Document 158-1*.
- [25] I. Schafer and K. Kruger, "Modelling of lossy coils using fraciton derivatives," *J. Phys. D: Appl.*, vol. 41, 2008.
- [26] A. Shamim, A. Radwan, and K. Salama, "Fractional smith chart theory," *IEEE Mirowave Wireless Compon. Lett.*, vol. 21, no. 3, pp. 117–119, 2011.
- [27] A. Radwan, A. Soliman, and A. Elwakil, "Fractional-order sinusoidal oscillators: design procedure and practical examples," *IEEE Trans. Circuits Syst. I*, vol. 55, no. 7, pp. 2051–2063, 2008.

- [28] A. Radwan and K. Salama, "Fractional order rc and rl circuits," *Circuits Syst. Signal Process.*, vol. 31, no. 6, pp. 1901–1915, 2012.
- [29] K. Moaddy, A. Radwan, K. Salama, S. Momani, and I. Hashim, "The fractional-order modelling and synchronization of electircally coupled neuron systems," *Com-
pute. Math. Appl.*, vol. 64, no. 10, pp. 3329–3339, 2012.
- [30] S. Grimnesand and O. Martinsen, *Bioimpedance and Bioelectricity Basics*. Academic Press, 2000.
- [31] K. Cole, "Permeability and impermeability of cell membranes for ions," in *Proc. Cold Spring Harbor Symp. Quant. Biol.*, vol. 8, pp. 110–112, 1940.
- [32] K. Cole and R. Cole, "Dispersion and absorption in dielectrics i. alternating current characteristics," *J. Chem. Physics*, vol. 9, pp. 341–351, 1941.
- [33] B. Rigaud, L. Hamzaoui, M. Friha, N. Chauveau, and J. Morucci, "In vitro tissue characterization and modelling using electrical impedance measurements in the 100hz-10mhz frequency range," *Physiol. Meas.*, vol. 16, no. 3A, pp. A15–A28, 1995.
- [34] Y. Ulgen and M. Sezdi, "Hematocrit dependence of the cole-cole parameters of human blood," in *Int. Biomed. Eng. Days*, pp. 71–74, 1998.
- [35] M. Sezdi, M. Bayik, and Y. Ulgen, "Storage effects on the cole-cole parameters of erythrocyte suspensions," *Physiol. Meas.*, vol. 27, no. 7, pp. 623–635, 2006.
- [36] S. Kun, B. Ristic, R. Peura, and R. Dunn, "Algorithm for tissue ischemia estimation based on electrical impedance spectroscopy," *IEEE Trans. Biomed. Eng.*, vol. 50, no. 12, pp. 1352–1359, 2003.

- [37] A. Ivorra, M. Genesca, A. Sola, L. Palacios, R. Villa, G. Hotter, and J. Aguilo, "Bioimpedance dispersion width as a paramter to monitor living tissues," *Physiol. Meas.*, vol. 26, no. 2, pp. S165–S173, 2005.
- [38] O. Al-Surkhi, P. Riu, F. Vazquez, and J. Ibeas, "Monitoring cole-cole parameters during haemodialysis (hd)," in *IEEE Int. Conf. Eng. Med. Biol. Soc.*, pp. 2238–2241, 2007.
- [39] C. Tang, F. You, G. Cheng, D. Gao, F. Fu, and X. Dong, "Modeling the frequency dependence of the electrical properties of the live human skull," *Physiol. Meas.*, vol. 30, no. 12, pp. 1293–1301, 2009.
- [40] G. McConnell, R. Butera, and R. Bellamkonda, "Bioimpedance modeling to monitor astrocytic response to chronically implanted electrodes," *J. Neural Eng.*, vol. 6, no. 5, p. 055005, 2009.
- [41] A. Morais, A. Pino, and M. Souza, "A fractional electrical impedance model in detection of occlusal non-cavitated carious," in *IEEE Int. Conf. Eng. Med. Biol. Soc.*, pp. 6551–6554, 2010.
- [42] R. Buendia, R. Gil-Pita, and F. Seoane, "Cole parameter estimation from the modulus of the electrical bioimpedance for assessment of body composition. a full spectroscopy approach.," *J. Electr. Bioimpedance*, vol. 2, pp. 72–78, 2011.
- [43] A. Barrow and S. Wu, "Impedance measurements for cervical cancer diagnosis," *Gynecologic Oncology*, vol. 107, no. 1, pp. S40–S43, 2007.
- [44] S. Laufer, A. Ivorra, V. Reuter, B. Rubinsky, and S. Solomon, "Electrical impedance characterization of normal and cancerous human hepatic tissue," *Physiol. Meas.*, vol. 31, no. 7, pp. 995–1009, 2010.

- [45] W. Gregory, J. Marx, G. Gregory, W. Mikkelsen, J. Tjoe, and J. Shell, "The cole relaxation frequency as a parameter to identify cancer in breast tissue," *Med. Phys.*, vol. 39, no. 7, pp. 4166–4174, 2012.
- [46] C. Wang, M. Li, and M. Yao, "Impedance feature extraction of breast cancer and surrounding tissues," in *Int. Conf. Biomed. Eng. Inf.*, pp. 922–926, 2010.
- [47] A. Keshtkar, Z. Salehnia, A. Keshtkar, and B. Shokouhi, "Bladder cancer detection using electrical impedance technique (tabriz mark 1)," *Pathol. Res. Int*, 2012.
- [48] M. Tuorkey, "Bioelectrical impedance as a diagnostic factor in the clinical practice and prognostic factor for survival in cancer patients: prediction, accuracy and reliability," *J. Biosens. Bioelectron.*, vol. 4, no. 4, 2012.
- [49] D. McRae, M. Esrick, and S. Mueller, "Changes in the noninvasive, in vivo electrical impedance of three xenografts during the necrotic cell-response sequence," *Int. J. Radiation Oncology Biol. Phys.*, vol. 43, no. 4, pp. 849–857, 1999.
- [50] A. Eldarrat, D. Wood, G. Kale, and A. High, "Age-related changes in ac-impedance spectroscopy studies of normal human dentine," *J. Mater. Sci.: Mater. Med.*, vol. 18, no. 6, pp. 1203–1210, 2007.
- [51] A. Elwakil and B. Maundy, "Extracting the cole-cole impedance model parameters without direct impedance measurement," *Electron. Lett.*, vol. 46, no. 20, pp. 1367–1368, 2010.
- [52] B. Maundy and A. Elwakil, "Extracting single dispersion cole-cole impedance model parameters using an integrator setup," *Analog Intergr. Circ. Sig. Process*, vol. 71, pp. 107–110, 2012.
- [53] I. Jesus and J. T. Machado, "Application of integer and fractional models in electrochemical systems," *Math. Prob. Eng.*, 2012.

- [54] I. Jesus, J. Machado, and J. Cunha, "Fractional electrical impedances in botanical elements," *J. Vib. Control*, vol. 14, no. 9-10, pp. 1389–1402, 2008.
- [55] S. Mancuso, "Seasonal dynamics of electrical impedance parameters in shoots and leaves relate to rooting ability of olive (*olea europaea*) cuttings," *Tree Physiol.*, vol. 19, no. 2, pp. 95–101, 1998.
- [56] L. Wu, Y. Ogawa, and A. Tagawa, "Electrical impedance spectroscopy analysis of eggplant pulp and effects of drying and freezing-thawing treatments on its impedance characteristics," *J. Food Eng.*, vol. 87, no. 2, pp. 274–280, 2007.
- [57] M. Tiitta, L. Tomppo, H. Jarnstrom, M. Loija, T. Laakso, A. Harju, M. Venalainen, H. Iitti, L. Paajanen, P. Saranpaa, R. Lappalainen, and H. Viitanen, "Spectral and chemical analyses of mould development on scots pine hardwood," *Eur. J. Wood Prod.*, vol. 67, no. 2, pp. 151–158, 2009.
- [58] T. Repo and M. Zhang, "Modelling woody plant tissues using a distributed electrical circuit," *J. Exp. Bot.*, vol. 44, no. 5, pp. 977–982, 1993.
- [59] T. Repo, G. Zhang, A. Ryypö, and R. Rikala, "The electrical impedance spectroscopy of scots pine (*pinus sylvestris* L.) shoots in relation to cold acclimation," *J. Exp. Bot.*, vol. 51, no. 353, pp. 2095–2107, 2000.
- [60] T. Repo, J. Laukkanen, and R. Silvennoinen, "Measurement of the tree root growth using electrical impedance spectroscopy," *Silva Fennica*, vol. 39, no. 2, pp. 159–166, 2005.
- [61] M. Tiitta and H. Oikkonen, "Electrical impedance spectroscopy device for measurement of moisture gradients in wood," *Rev. Sci. Instrum.*, vol. 73, no. 8, pp. 3093–3100, 2002.

- [62] Y. Yamamoto, H. Harada, K. Yasuhara, and T. Nakamura, "Automatic sensing device of electrical characteristics of living trees," *IEEE Trans. Instrum. Meas.*, vol. 44, no. 3, pp. 729–733, 1995.
- [63] C. Lin, L. Chen, and T. Chen, "The development and application of an electrical impedance spectroscopy measurement system for plant tissues," *Comput. Electron. Agric.*, vol. 82, pp. 96–99, 2012.
- [64] M. Ovadia and D. Zavitz, "The electrode-tissue interface in living heart: equivalent circuit as a function of surface area," *Electroanalysis*, vol. 10, no. 4, pp. 262–272, 1998.
- [65] R. Magin and M. Ovadia, "Modelling the cardiac tissue electrode interface using fractional calculus," *J. Vib. Control*, vol. 14, no. 9-10, pp. 1431–1442, 2008.
- [66] M. Ovadia, E. Fayn, and D. Zavitz, "Impedance experimentation for an electrode interface in human fetal tissue: novel pathological regime of anomalous diffusion," *Chem. Phys. Lett.*, vol. 424, no. 4-6, pp. 285–288, 2006.
- [67] Z. Hantos, B. Daroczy, B. Suki, S. Nagy, and J. Fredberg, "Input impedance and peripheral inhomogeneity of dog lungs," *J. Appl. Physiol.*, vol. 72, no. 1, pp. 168–178, 1992.
- [68] Z. Hantos, A. Adamicz, E. Govaerts, and B. Daroczy, "Mechanical impedances of lungs and chest wall in the cat," *J. Appl. Physiol.*, vol. 73, no. 2, pp. 427–433, 1992.
- [69] C. Ionescu and R. D. Keyser, "Time domain validation of a fractional order model for human respiratory system," in *IEEE Mediterr. Electrotechnical Conf.*, pp. 89–95, 2008.

- [70] C. Ionescu and R. D. Keyser, "Relations between fractional-order model parameters and lung pathology in chronic obstructive pulmonary disease," *IEEE Trans. Biomed. Eng.*, vol. 56, no. 4, pp. 978–987, 2009.
- [71] C. Ionescu, I. Muntean, J. Tenreiro-Machado, and M. A. R. De Keyser, "A theoretical study on modelling the respiratory tract with ladder networks by means of intrinsic fractal geometry," *EEE Trans. Biomed. Eng.*, vol. 57, no. 2, pp. 246–253, 2010.
- [72] A. Beaulieu, D. Bosse, P. Micheau, O. Avoine, J. Praud, and H. Walti, "Measurement of fractional order model parameters of respiratory mechanical impedance in total liquid ventilation," *IEEE Trans. Biomed. Eng.*, vol. 59, no. 2, pp. 323–331, 2012.
- [73] C. Abbey and G. Joos, "Supercapacitor energy storage for wind energy applications," *IEEE Trans. Ind. Appl.*, vol. 43, no. 3, pp. 769–776, 2007.
- [74] M. Glavin, P. Chan, S. Armstrong, and W. Hurley, "A stand-alone photovoltaic supercapacitor battery hybrid energy storage system," in *Power Electron. Motion Control Conf.*, pp. 1688–1695, 2008.
- [75] R. Martinez, Y. Bolea, A. Grau, and H. Martinez, "Lpv model for pv cells and fractional control of dc/dc converter for photovoltaic systems," in *IEEE Int. Symp. Ind. Electron.*, pp. 1069–1074, 2001.
- [76] S. Kim, K. No, and P. Chou, "Design and performance analysis of supercapacitor charging circuits for wireless sensor nodes," *IEEE J. Emerging Sel. Top. Circuits Syst.*, vol. 1, no. 3, pp. 391–402, 2011.
- [77] J. Cao and A. Emadi, "A new battery/ultracapacitor hybrid energy storage system for electric, hybrid, and plug-in hybrid electric vehicles," *IEEE Trans. Power Electron.*, vol. 27, no. 1, pp. 122–132, 2012.

- [78] A. Pandey, F. Allos, A. Hu, and D. Budgett, "Integration of supercapacitors into wirelessly charged biomedical sensors," in *IEEE Int. Symp. Ind. Electron.*, pp. 56–61, 2011.
- [79] L. Shi and M. Crow, "Comparison of ultra capacitor electric circuit models," *IEEE Power and Energy Society General Meeting*, pp. 1–6, 2008.
- [80] R. Martin, J. Quintana, A. Ramos, and I. de la Nuez, "Modeling electrochemical double layer capacitor, from classical to fractional impedance," *IEEE Mediterr. Electrotechnical Conf.*, pp. 61–66, 2008.
- [81] N. Bertrand, J. Sabatier, and J. V. O. Briat, "Fractional non-linear modelling of ultra-capacitors," *Commun. Nonlinear Sc. Numer. Simulat.*, vol. 15, no. 5, pp. 1327–1337, 2010.
- [82] P. Mahon, G. Paul, S. Keshishian, and A. Vassallo, "Measurement and modelling of the higher-power performance of carbon-based supercapacitors," *J. Power Sources*, vol. 91, no. 1, pp. 68–76, 2000.
- [83] J. Quintana, A. Ramos, and I. Nuez, "Identification of the fractional impedance of ultracapacitors," in *Proc. 2nd AFAC Workshop Fractional Differ. Appl.*, pp. 289–293, 2006.
- [84] Y. Wang, T. Hartley, C. Lorenzo, J. Adams, J. Carletta, and R. Veillette, *New Trends in Nanotechnology and Fractional Calculus Applications*, ch. Modeling ultracapacitors as fractional-order systems, pp. 257–262. Springer, 2010.
- [85] A. Dzielinski, G. Sarwas, and D. Sierociuk, "Time domain validation of ultracapacitor fractional order model," *IEEE Conf. Decis. Control*, pp. 3730–3735, 2010.
- [86] A. Dzielinski, G. Sarwas, and D. Sierociuk, "Comparison and validation of integer and fractional order ultracapacitor models," *Adv. Diff. Equ.*, 2011.

- [87] R. Kotz and M. Carlen, "Principles and applications of electrochemical capacitors," *Electrochimica Acta*, vol. 45, no. 15-16, pp. 2483–2498, 2000.
- [88] G. Ablart, T. Haba, and G. Loum, "An analytical expression for the input impedance of a fractal tree obtained by a microelectronic process and experimental measurements of its non-integral dimension," *Chaos Solitons Fractals*, vol. 33, no. 2, pp. 364–373, 2007.
- [89] I. Jesus and J. T. Machado, "Development of fractional order capacitors based on electrolyte processes," *Nonlinear. Dyn.*, vol. 56, no. 1-2, pp. 45–55, 2009.
- [90] M. S. Krishna, S. Das, and B. G. K. Biswas, "Fabrication of a fractional order capacitor with desired specifications: a study on process identification and characterization," *IEEE Trans. Electron. Devices*, vol. 58, no. 11, pp. 4067–4073, 2011.
- [91] T. Freeborn, B. Maundy, and A. Elwakil, "Fractional resonance-based fraction $rl_{\beta}c_{\alpha}$ filters," *Math. Prob. Eng.*, 2013.
- [92] J. MacDonald, "Levm / levwm version 8.12."
- [93] Mathworks, "Matlab version 7.14.0."
- [94] L. Ward, T. Essex, and B. Cornish, "Determination of cole parameters in multiple frequency bioelectrical impedance analysis using only the measurement of impedances," *Physiol. Meas.*, vol. 27, no. 9, pp. 839–850, 2006.
- [95] D. Ayllon, F. Seoane, and R. Gil-Pita, "Cole equation and parameter estimation from electrical bioimpedance spectroscopy measurements - a comparative study," in *IEEE Int. Conf. Eng. Med. Biol. Soc.*, pp. 3779–3782, 2009.
- [96] A. Elwakil and B. Maundy, "Experimental technique for estimating the dispersion coefficient of a constant phase element," in *Eur. Conf. Circuit Theory Des.*, pp. 469–471, 2011.

- [97] H. Solmaz, Y. Ulgen, and M. Tumer, "Design of a micro-controller based cole-cole impedance meter for testing biological tissues," in *World Congr. Med. Phys. Biomed. Eng.*, pp. 488–491, 2009.
- [98] C. Lin, L. Chen, and T. Chen, "The development and application of an electrical impedance spectroscopy measurement system for plant tissues," *Comput. Electron. Agric.*, vol. 82, pp. 96–99, 2012.
- [99] J. Ferreira, F. Seoane, and K. Lindecrantz, "Ad5933-based electrical bioimpedance spectrometer towards textile-enabled applications," in *IEEE. Int. Conf. Eng. Med. Biol. Soc.*, pp. 3282–3285, 2011.
- [100] T. Freeborn, B. Maundy, and A. Elwakil, "Numerical extraction of cole-cole impedance parameters from step response," *Nonlinear Theory Appl. (IEICE)*, vol. 2, no. 4, pp. 548–561, 2011.
- [101] I. Podlubny, "Mittag-leffler function. matlab central file exchange, submission #8738, 17 oct 2005 (updated 7 sept 2012)."
- [102] T. Freeborn, B. Maundy, and A. Elwakil, "Least squares estimation technique of cole-cole parameters from step response," *Electron. Lett.*, vol. 38, no. 13, pp. 752–754, 2012.
- [103] I. Podlubny, I. Petras, and T. Skovranek, "Fitting of experimental data using mittag-leffler function," in *13th Int. Carpathian Control Conf.*, pp. 578–581, 2012.
- [104] D. Sierociuk, I. Podlubny, and I. Petras, "Experimental evidence of variable-order behaviour of ladders and nested ladders," *IEEE Trans. Control. Syst. Technol.*, vol. 21, no. 2, pp. 459–466, 2012.
- [105] T. Coleman and Y. Li, "An interior, trust region approach for nonlinear minimization subject to bounds," *SIAM J. Optim.*, vol. 6, pp. 418–445, 1996.

- [106] T. Freeborn, B. Maundy, and A. Elwakil, "Simplifying cole-impedance extraction from the current-excited step response," *Midwest Symp. Circuits Syst. (MWSCAS)*, pp. 952–955, 2013.
- [107] T. Freeborn, B. Maundy, and A. Elwakil, "Cole impedance extractions from the step-response of a current excited fruit sample," *Comput. Electron. Agric.*, vol. 98, pp. 100–108, 2013.
- [108] A. Sedra and K. Smith, "A second-generation current conveyor and its applications," *IEEE Trans. Circuit Theor.*, vol. 17, no. 1, pp. 132–134, 1970.
- [109] T. Freeborn, B. Maundy, and A. Elwakil, "Improved cole-cole parameter extraction from frequency response using least squares fitting," in *IEEE Int. Symp. Circuits Systems*, pp. 337–340, 2012.
- [110] B. Krishna and K. Reddy, "Active and passive realization of fractance device of order $1/2$," *Act. Passive Electron. Compon.*, 2008.
- [111] P. Kurzweil, M. Chwistek, and R. Galley, "Electrochemical spectroscopic studies on rated capacitance and aging mechanisms of supercapacitors," *2nd Eur. Symp. Supercapacitors Appl. (ESSCAP)*, 2006.
- [112] T. Freeborn, B. Maundy, and A. Elwakil, "Accurate time domain extraction of supercapacitor fractional-order model parameters," *IEEE Int. Symp. Circuits Syst. (ISCAS)*, pp. 2259–2262, 2013.
- [113] T. Freeborn, B. Maundy, and A. Elwakil, "Measurement of supercapacitor fractional-order model parameters from voltage-excited step response," *IEEE J. Emerging Selected Topics Circuits Syst.*, vol. 3, no. 3, 2013.
- [114] D. Stancic, J. Fang, and I. Cosic, "Distributed biological tissue impedance model for spice simulation," in *Int. Symp. Bioelectron. Bioinf.*, pp. 201–205, 2009.

- [115] J. Valsa and J. Vlach, “Rc models of a constant phase element,” *Int. J. Circ. Theor. Appl.*, 2011.

APPENDIX A

EXTRACTION OF IMPEDANCE PARAMETERS IN MATLAB

Included in this appendix are samples of MATLAB code used for the extraction of the fractional impedance parameters that describe the single and double dispersion Cole impedance models for biological tissues as well as the fractional model used to represent supercapacitors.

A.1 Cole Impedance Models

A.1.1 Voltage-Excited Single Dispersion Step Response Numerical Extraction

```
1 % File: SingleColeVoltageStepNumerical.m
2 % Author: Todd Freeborn
3 % Email: todd.freeborn@gmail.com
4 % Description:
5 %     The following code has been used for the extraction of
6 %     the single-dispersion Cole impedance parameters from
7 %     simulated datasets of a Cole impedance to a voltage-input
8 %     step.
9 clear all;
10 close all;
11
12 % Setting the theoretical Cole impedance model values
13 Rinf = 1e3;
14 Rl = 1e3;
15 C = 1e-6;
16 alpha = 0.75;
17 SingleColeParameters = [Rinf Rl C alpha];
18
19 % Set simulation parameters
20 Vcc = 5; % Step-input amplitude
21 R = 1e3;
22 E = 9; % Mittag-Leffler simulation accuracy
23
```

```

24 % Simulating step response to use for future extraction
25 t = logspace(-10, 2, 100);
26 z = -(R+Rinf+R1)/C/R1/(R+Rinf)*t.^alpha;
27 vo1=Vcc*(Rinf+R1)/C/R1/(R+Rinf)*t.^alpha.*mlf(alpha,alpha+1,z,E);
28 vo2 = Vcc*Rinf/(R+Rinf).*mlf(alpha,1,z,E);
29 IdealVo = vo1 + vo2;
30 semilogx(t, IdealVo), hold on;
31
32 % Calculating lower and upper values to use in rise time calculations
33 Lower = Vcc*(Rinf/(R+Rinf));
34 Rise = Vcc*(R*R1/(R+Rinf)/(R+Rinf+R1));
35 upper = Lower+ones(size(t))*0.90*Rise;
36 lower = Lower+ones(size(t))*0.10*Rise;
37
38 % Calculating the experimentally derived values of Rinf and R1
39 Rinf = IdealVo(1)*R/(Vcc-IdealVo(1));
40 R = (IdealVo(length(IdealVo))*R+IdealVo(length(IdealVo))*Rinf- ...
    Vcc*Rinf)/(-IdealVo(length(IdealVo))+Vcc);
41
42 % Determining the rise voltages
43 Lower = IdealVo(1);
44 Upper = IdealVo(length(IdealVo));
45 Rise = Upper-Lower;
46 Middle = Lower+Rise/2;
47
48
49 % Calculating the 10% and 90% times and voltages from the
50 % experimental data
51 for i=1:length(IdealVo)
52     if( IdealVo(i) > Lower+0.1*Rise)
53         v1x = IdealVo(i);
54         t1x = t(i);
55         break;
56     end
57 end
58
59 for j=i:length(IdealVo)
60     if( IdealVo(j) > Lower+0.9*Rise)
61         v2x = IdealVo(j);
62         t2x = t(j);
63         break;
64     end
65 end
66
67 % Calculating the slope based on the rise times and voltages
68 mx = (v2x-v1x)/(log10(t2x)-log10(t1x));
69
70 C2 = 1e-9; alpha2 = 0.5; alphaC = 0.5/2;
71 vError = 10e-9; ErrorLast = 10;
72 iteration = 0;
73 change = alpha2/2;
74
75 % Determining the value of alpha by modifying the alpha of a
76 % simulated step response using the calculated Rinf and R1 until

```

```

77 % the simulation and experimental slopes are equal
78 t = logspace(-20, 2, 100);
79 while(1)
80
81     tNew = t;
82     v1s = 5; v2s = 0;
83     while( abs(v1x-v1s)/v1x > vError)
84         z = -(R+Rinf+R)/C2/R/(R+Rinf)*tNew.^alpha2;
85         part1= Vcc*(Rinf+R)/C2/R/(R+Rinf)*tNew.^alpha2.* ...
            mlf(alpha2, alpha2+1, z, E);
86         part2 = Vcc*Rinf/(R+Rinf).*mlf(alpha2, 1, z, E);
87         ExtractedVo = part1 + part2;
88
89         for i=1:length(ExtractedVo)
90             if( ExtractedVo(i) > v1x)
91                 v1s = ExtractedVo(i);
92                 t1s = tNew(i);
93                 break;
94             end
95         end
96         tNew = linspace(tNew(i-1), tNew(i));
97     end
98
99     tNew = t;
100    while( abs(v2x-v2s)/v2x > vError)
101        z = -(R+Rinf+R)/C2/R/(R+Rinf)*tNew.^alpha2;
102        part1= Vcc*(Rinf+R)/C2/R/(R+Rinf)*tNew.^alpha2.* ...
            mlf(alpha2, alpha2+1, z, E);
103        part2 = Vcc*Rinf/(R+Rinf).*mlf(alpha2, 1, z, E);
104        ExtractedVo = part1 + part2;
105
106        for i=1:length(ExtractedVo)
107            if( ExtractedVo(i) > v2x)
108                v2s = ExtractedVo(i);
109                t2s = tNew(i);
110                break;
111            end
112        end
113        tNew = linspace(tNew(i-1), tNew(i));
114    end
115
116    ms = (v2s-v1s)/(log10(t2s)-log10(t1s));
117    Error = (mx-ms)/mx;
118    if(abs(ErrorLast) > abs(Error))
119        ErrorLast = Error;
120        AlphaError = alpha2;
121    end
122
123    if(abs(Error) < 1e-6 || iteration>20)
124        break;
125    else
126        alphaLast = alpha2;
127        if(Error > 0)
128            alpha2 = alpha2 + change;

```

```

129         else
130             alpha2 = alpha2 - change;
131         end
132         change = abs(alphaLast - alpha2)/2;
133     end
134     iteration = iteration + 1;
135 end
136
137 % Determining the required times to calculate the time shift
138 % constant
139 C2 = C2*10;
140 tNew = t;
141 v3s = 5;
142 while( abs(v1x-v3s)/v1x > vError)
143     z = -(R+Rinf+R)/C2/R/(R+Rinf)*tNew.^alpha2;
144     part1= Vcc*(Rinf+R)/C2/R/(R+Rinf)*tNew.^alpha2.* ...
        mlf(alpha2, alpha2+1, z, E);
145     part2 = Vcc*Rinf/(R+Rinf).*mlf(alpha2, 1, z, E);
146     ExtractedVo = part1 + part2;
147
148     for i=1:length(ExtractedVo)
149         if( ExtractedVo(i) > v1x)
150             v3s = ExtractedVo(i);
151             t3s = tNew(i);
152             break;
153         end
154     end
155     tNew = linspace(tNew(i-1), tNew(i));
156 end
157
158 % Extracting the Capacitance based on the determined time shift
159 % constant
160 decDiv = log10(t3s/t1s);
161 n = log10(t1x/t1s)/decDiv;
162 C2 = (1e-9)*10^n;
163
164 % Calculate step response using extracted parameters
165 z = -(R+Rinf+R)/C2/R/(R+Rinf)*t.^alpha2;
166 part1= Vcc*(Rinf+R)/C2/R/(R+Rinf)*t.^alpha2.* mlf(alpha2, ...
    alpha2+1, z, E);
167 part2 = Vcc*Rinf/(R+Rinf).*mlf(alpha2, 1, z, E);
168 ExtractedVo = part1 + part2;
169
170 SingleColeExtracted = [Rinf R1 C2 alpha2];
171 RelativeErrors = abs(SingleColeParameters- SingleColeExtracted)./ ...
    SingleColeParameters*100;
172 semilogx(t, ExtractedVo, 'o'); xlabel('Time (s)'); ...
    ylabel('Voltage (V)');

```

Listing A.1: MATLAB code for the generation of the voltage-excited step response of the single-dispersion Cole impedance model and the numerical extraction of its parameters

A.1.2 Voltage-Excited Single Dispersion Step Response NLSF Extraction

```

1 % Function: SingleColeVoltageStepResponseRun.m
2 % Author: Todd Freeborn
3 % Email: todd.freeborn@gmail.com
4 % Description:
5 %     This script will generate the output response of a
6 %     voltage-excited single-dispersion Cole impedance and
7 %     extract the parameters from that generated response using
8 %     a least-squares fitting after adding Guassian white noise
9 clear all;
10 close all;
11
12 % Set single-dispersion Cole impedance parameters
13 Rinf = 1e3;
14 Rl = 1e3;
15 C = 1e-6;
16 alpha = 0.75;
17 SingleColeParameters = [Rinf Rl C alpha];
18
19 global E Vcc R
20 Vcc = 5; % Set voltage-step amplitude (Vcc)
21 E = 9; % Set Mittag-Leffler simulation accuracy (E)
22 R = 1e3;
23
24 t = logspace(-6, 1, 50); % Set length in time of simulation
25
26 % Generate ideal step response
27 IdealStepResponse = SingleColeVoltageStepResponse( ...
    SingleColeParameters, t);
28 % Add 60 dB Gaussian white noise to ideal step response
29 NoiseStepResponse = awgn(IdealStepResponse, 60);
30
31 % Configure the optimset for use with lsqcurvefit
32 options = optimset('lsqcurvefit');
33 % Set lower and upper bounds for optimization routine
34 lb = [0 0 0 0];
35 ub = [inf inf inf inf];
36
37 % Generate upper and lower boundaries for creation of initial
38 % guesses
39 v0 = NoiseStepResponse(1);
40 vinf = NoiseStepResponse(length(NoiseStepResponse));
41
42 RinfGuess = v0*R/(Vcc-v0);
43 RlGuess = (vinf*(R+Rinf)-Vcc*Rinf)/(Vcc-v0);
44 lb2 = [0 RlGuess 1e-10 0];
45 ub2 = [RinfGuess 10e3 1e-3 1];
46
47 % Generate initial guesses to be applied to the non-linear least
48 % squares fitting

```



```

49 Guesses = 5;
50 x0 = zeros(Guesses, length(SingleColeParameters));
51 for i = 1:1:Guesses
52     x0(i,1) = RinfGuess;
53     x0(i,2) = R1Guess;
54     x0(i,3) = lb2(3) + (ub2(3)-lb2(3)).*rand(1);
55     x0(i,4) = lb2(4) + (ub2(4)-lb2(4)).*rand(1);
56 end
57
58 % Apply the non-linear least squares fitting to the noisy
59 % step response
60 SingleLSE = inf;
61 for m = 1:1:Guesses
62     [sParam, sError] = lsqcurvefit(@SingleColeVoltageStepResponse ...
        ,x0(m,:),t,NoiseStepResponse,lb,ub,options);
63     if(sError<SingleLSE)
64         SingleLSE = sError;
65         SingleColeExtracted = sParam;
66     end
67 end
68
69 RelativeErrors = abs(SingleColeParameters-SingleColeExtracted)./ ...
    SingleColeParameters*100;
70 semilogx(t, SingleColeVoltageStepResponse(SingleColeParameters,t) ...
    ,t,SingleColeVoltageStepResponse(SingleColeExtracted,t),'o');
71 xlabel('Time (s)'); ylabel('Voltage (V)');

```

Listing A.2: MATLAB code for the generation of the voltage-excited step response of the single-dispersion Cole impedance model and the extraction of its parameters

```

1 % Function: SingleColeCurrentStepResponse.m
2 % Author: Todd Freeborn
3 % Email: todd.freeborn@gmail.com
4 % Description:
5 %     Funciton to generate the step response of a current-
6 %     excited single dispersion Cole impedance model
7 function output = SingleColeCurrentStepResponse(ColeImpedance, t)
8     global Icc E
9     Rinf = ColeImpedance(1);
10    R1 = ColeImpedance(2);
11    C = ColeImpedance(3);
12    alpha = ColeImpedance(4);
13
14    z = -t.^alpha/R1/C;
15    output = Icc*(Rinf+t.^alpha/C.*mlf(alpha, alpha+1, z, E));
16 end

```

Listing A.3: MATLAB function to generate voltage excited step response of a single-dispersion Cole impedance

A.1.3 Current-Excited Single-Dispersion Step Response NLSF Extraction

```

1 % Function: SingleColeCurrentStepResponseRun.m
2 % Author: Todd Freeborn
3 % Email: todd.freeborn@gmail.com
4 % Description:
5 %     This script will generate the output response of a
6 %     current-excited single-dispersion Cole impedance and
7 %     extract the parameters from that generated response using
8 %     a least-squares fitting after adding Guassian white noise
9 clear all;
10 close all;
11
12 % Set single-dispersion Cole impedance parameters
13 Rinf = 1e3;
14 Rl = 1e3;
15 C = 1e-6;
16 alpha = 0.75;
17 SingleColeParameters = [Rinf Rl C alpha];
18
19 global E Icc
20 Icc = 1e-4; % Set current-step amplitude (Icc)
21 E = 9;      % Set Mittag-Leffler simulation accuracy (E)
22
23 t = logspace(-6, 1, 50); % Set length in time of simulation
24
25 % Generate ideal step response
26 IdealStepResponse = SingleColeCurrentStepResponse( ...
    SingleColeParameters, t);
27 % Add 60 dB Gaussian white noise to ideal step response
28 NoiseStepResponse = awgn(IdealStepResponse, 60);
29
30 % Configure the optimset for use with lsqcurvefit
31 options = optimset('lsqcurvefit');
32 % Set lower and upper bounds for optimization routine
33 lb = [0 0 0 0];
34 ub = [inf inf inf inf];
35
36 % Generate upper and lower boundaries for creation of initial
37 % guesses
38 RinfGuess = NoiseStepResponse(1)/Icc;
39 RlGuess = NoiseStepResponse(length(t))/Icc-RinfGuess;
40 lb2 = [0 RlGuess 1e-10 0];
41 ub2 = [RinfGuess 10e3 1e-3 1];
42
43 % Generate initial guesses to be applied to the non-linear least
44 % squares fitting
45 Guesses = 5;
46 x0 = zeros(Guesses, length(SingleColeParameters));
47 for i = 1:1:Guesses
48     x0(i,1) = RinfGuess;

```

```

49     x0(i,2) = R1Guess;
50     x0(i,3) = lb2(3) + (ub2(3)-lb2(3)).*rand(1);
51     x0(i,4) = lb2(4) + (ub2(4)-lb2(4)).*rand(1);
52 end
53
54 % Apply the non-linear least squares fitting to the noisy
55 % step response
56 SingleLSE = inf;
57 for m = 1:1:Guesses
58     [sParam, sError] = lsqcurvefit(@SingleColeCurrentStepResponse ...
59                                   ,x0(m,:),t,NoiseStepResponse,lb,ub,options);
60     if(sError<SingleLSE)
61         SingleLSE = sError;
62         SingleColeExtracted = sParam;
63     end
64 end
65 RelativeErrors = abs(SingleColeParameters- SingleColeExtracted)./ ...
66                   SingleColeParameters*100;
67 semilogx(t, IdealStepResponse, t, SingleColeCurrentStepResponse( ...
68   SingleColeExtracted,t),'o');
69 xlabel('Time (s)'); ylabel('Voltage (V)');

```

Listing A.4: MATLAB code for the generation of the current-excited step response of the single-dispersion Cole impedance model and the extraction of its parameters

```

1 % Function: SingleColeCurrentStepResponse.m
2 % Author: Todd Freeborn
3 % Email: todd.freeborn@gmail.com
4 % Description:
5 %     Funciton to generate the step response of a current-
6 %     excited single dispersion Cole impedance model
7 function output = SingleColeCurrentStepResponse(ColeImpedance, t)
8     global Icc E
9     Rinf = ColeImpedance(1);
10    R1 = ColeImpedance(2);
11    C = ColeImpedance(3);
12    alpha = ColeImpedance(4);
13
14    z = -t.^alpha/R1/C;
15    output = Icc*(Rinf+t.^alpha/C.*mlf(alpha, alpha+1, z, E));
16 end

```

Listing A.5: MATLAB function to generate current excited step response of a single-dispersion Cole impedance

A.1.4 Current-Excited Double-Dispersion Step Response NLSF Extraction

```

1 % Function: DoubleColeCurrentStepResponseRun.m
2 % Author: Todd Freeborn
3 % Email: todd.freeborn@gmail.com
4 % Description:
5 %     This script will generate the output response of a
6 %     current-excited double-dispersion Cole impedance and
7 %     extract the parameters from that generated response using
8 %     a least-squares fitting after adding random noise
9 clear all;
10 close all;
11
12 % Set doubles-dispersion Cole impedance parameters
13 Rinf = 400;
14 R1 = 12e3;
15 R2 = 2.5e3;
16 C1 = 62e-9;
17 C2 = 100e-6;
18 alpha1 = 0.75;
19 alpha2 = 0.55;
20
21 DoubleColeParameters = [Rinf R1 R2 C1 C2 alpha1 alpha2];
22
23 t = logspace(-7, log10(30), 50);
24 global Icc E;
25 Icc = 1e-4;
26 E = 9;
27 Guesses = 15;
28
29 % Generate ideal step response
30 z1 = -t.^alpha1/R1/C1;
31 z2 = -t.^alpha2/R2/C2;
32 IdealStep=DoubleColeCurrentStepResponse(DoubleColeParameters,t);
33 NoiseStep=IdealStep +IdealStep.*(-0.0025+0.005*rand( ...
    size(IdealStep)));
34
35 % Configure the optimset for use with lsqcurvefit
36 options = optimset('MaxFunEvals', 3000, 'Display', 'off', ...
    'TolFun', 1e-9, 'TolX', 1e-9);
37 % Set lower and upper bounds for optimization routine
38 lb = [0 0 0 0 0 0 0];
39 ub = [inf inf inf inf inf inf inf];
40
41 % Generate upper and lower boundaries for creation of initial
42 % guesses
43 RinfGuess = NoiseStep(1)/Icc;
44 R12Guess = NoiseStep(length(t))/Icc-RinfGuess;
45 x0 = zeros(Guesses, length(DoubleColeParameters));
46 lb2 = [0 0 0 1e-12 1e-12 0 0];
47 ub2 = [RinfGuess 2*R12Guess 2*R12Guess 1e-3 1e-3 1 1];

```

```

48
49 x0(1,:) = lb2 + (ub2-lb2).*rand(1, length(DoubleColeParameters));
50
51 while(x0(1,2)+x0(1,3)<R12Guess)
52     x0(1,2) = lb2(2)+(ub2(2)-lb2(2)).*rand(1);
53     x0(1,3) = lb2(3)+(ub2(3)-lb2(3)).*rand(1);
54 end
55
56 DoubleLSE = inf;
57
58 % Extracting impedance parameters using least squares curve
59 % fitting
60 for m = 1:1:Guesses
61     [FitParams, FitError] = lsqcurvefit( ...
        @DoubleColeCurrentStepResponse,x0(m,:),t,NoiseStep,lb,ub, ...
        options);
62
63     if(m<Guesses)
64         if(FitError < DoubleLSE)
65             x0(m+1,:) = FitParams;
66         else
67             x0(m+1,:) =lb2 + (ub2-lb2).*rand(1, ...
                length(DoubleColeParameters));
68
69             while(x0(m+1,2)+x0(m+1,3)<R12Guess)
70                 x0(m+1,2) = lb2(2)+(ub2(2)-lb2(2)).*rand(1);
71                 x0(m+1,3) = lb2(3)+(ub2(3)-lb2(3)).*rand(1);
72             end
73         end
74     end
75
76     if(FitError < DoubleLSE)
77         DoubleColeExtracted = FitParams;
78         DoubleLSE = FitError;
79     end
80
81     BestFitParameters = DoubleColeExtracted;
82     Errors1 = abs(DoubleColeParameters-BestFitParameters) ...
        ./DoubleColeParameters*100;
83     BestFitParameters2 = size(BestFitParameters);
84     BestFitParameters2(1) = BestFitParameters(1);
85     BestFitParameters2(2) = BestFitParameters(3);
86     BestFitParameters2(3) = BestFitParameters(2);
87     BestFitParameters2(4) = BestFitParameters(5);
88     BestFitParameters2(5) = BestFitParameters(4);
89     BestFitParameters2(6) = BestFitParameters(7);
90     BestFitParameters2(7) = BestFitParameters(6);
91     Errors2 = abs(DoubleColeParameters-BestFitParameters2) ...
        ./DoubleColeParameters*100;
92     if(mean(abs(Errors1))<mean(abs(Errors2)))
93         DoubleColeExtracted = BestFitParameters;
94     else
95         DoubleColeExtracted = BestFitParameters2;
96     end

```

```

97 end
98 SingleErrors = abs(DoubleColeParameters-DoubleColeExtracted) ...
    ./DoubleColeParameters*100;
99 semilogx(t, IdealStep, t, DoubleColeCurrentStepResponse( ...
    DoubleColeExtracted,t), 'o');
100 xlabel('Time (s)'); ylabel('Voltage (V)');

```

Listing A.6: MATLAB code for the generation of the current-excited step response of the double-dispersion Cole impedance model and the extraction of its parameters

```

1 % Function: DoubleColeCurrentStepResponse.m
2 % Author: Todd Freeborn
3 % Email: todd.freeborn@gmail.com
4 % Description:
5 %     Function to generate the step response of a current-
6 %     excited double dispersion Cole impedance model
7 function output = DoubleColeCurrentStepResponse(ColeImpedance, t)
8     global Icc E
9     Rinf = ColeImpedance(1);
10    R1 = ColeImpedance(2);
11    R2 = ColeImpedance(3);
12    C1 = ColeImpedance(4);
13    C2 = ColeImpedance(5);
14    alpha1 = ColeImpedance(6);
15    alpha2 = ColeImpedance(7);
16
17    z1 = -t.^alpha1/R1/C1;
18    z2 = -t.^alpha2/R2/C2;
19    output = Icc*(Rinf+t.^alpha1/C1.*mlf(alpha1, alpha1+1, z1, E) ...
        +t.^alpha2/C2.*mlf(alpha2, alpha2+1, z2, E));
20 end

```

Listing A.7: MATLAB function to generate current excited step response of a double-dispersion Cole impedance

A.1.5 Magnitude Single-Dispersion NLSF Extraction

```

1 %   Script: SingleColeMagnitudeRun.m
2 %   Author: Todd Freeborn
3 %   Email: todd.freeborn@gmail.com
4 %   Description:
5 %       this script simulates the magnitude response of an filter
6 %       circuit using a Cole–Cole impedance. From this magnitude
7 %       response, it will extract the parameters using an non-
8 %       linear least squares optimization routine and a direct
9 %       extraction method to compare the accuracies of the
10 %      extracted parameters to the ideal values for both methods
11 clear all;
12 close all;
13 % Setup frequency vectors (100 Hz → 5 MHz)
14 f = logspace(2, log10(5e6), 50);
15 w = 2*pi*f;
16 s = 1i*w;
17 RL = 1e3;
18
19 % Cole–Cole impedance parameters to use [Ro Rinfntity alpha tau]
20 Ro = 12.894e3;
21 Rinf = 0.406e3;
22 alpha = 0.739;
23 tau = 62.34e-6;
24
25 % Setting ideal gains for filter circuit transfer function from
26 % impedance parameters
27 G1 = 1+Ro/RL;
28 G2 = 1+Rinf/RL;
29 SingleColeParameters = [G1 G2 tau alpha];
30
31 % Calculating magnitude response of filter circuit from transfer
32 % function
33 IdealMag = SingleColeMagnitude(SingleColeParameters, w);
34 semilogx(f, IdealMag);
35 NoiseMag = awgn(IdealMag, 60);
36
37 % initial conditions for optimization routine
38 G1guess = 1/NoiseMag(1);
39 G2guess = 1/NoiseMag(length(NoiseMag));
40
41 x0 = [G1guess G2guess 0.75 1e-6];
42 %configure the optimset for use with lsqcurvefit
43 options = optimset('lsqcurvefit');
44
45 % lower and upper bounds for optimization routine
46 lb = [0 0 0 0];
47 ub = [inf inf inf inf];
48 % Extracting impedance parameters using least squares curve fitting

```

```

49 [SingleColeExtracted,error] = lsqcurvefit(@SingleColeMagnitude,x0 ...
    ,w,NoiseMag,lb,ub,options);
50 % Errors of LSQ extracted parameters compared to ideal values
51 RelativeError=(SingleColeParameters-SingleColeExtracted) ...
    ./SingleColeParameters*100;
52 % Plot ideal response vs. extracted response for comparison
53 semilogx(f,NoiseMag,f,SingleColeMagnitude(SingleColeExtracted, ...
    w),'o');

```

Listing A.8: MATLAB code for the generation of the magnitude response of the single-dispersion Cole impedance model and the extraction of its parameters

```

1 % Script: SingleColeMagnitudeRun.m
2 % Author: Todd Freeborn
3 % Email: todd.freeborn@gmail.com
4 % Description:
5 %     this script simulates the magnitude response of an filter
6 %     circuit using a Cole-Cole impedance. From this magnitude
7 %     response, it will extract the parameters using an non-
8 %     linear least squares optimization routine and a direct
9 %     extraction method to compare the accuracies of the
10 %     extracted parameters to the ideal values for both methods
11 clear all;
12 close all;
13 % Setup frequency vectors (100 Hz -> 5 MHz)
14 f = logspace(2, log10(5e6), 50);
15 w = 2*pi*f;
16 s = 1i*w;
17 RL = 1e3;
18
19 % Cole-Cole impedance parameters to use [Ro Rinfntity alpha tau]
20 Ro = 12.894e3;
21 Rinf = 0.406e3;
22 alpha = 0.739;
23 tau = 62.34e-6;
24
25 % Setting ideal gains for filter circuit transfer function from
26 % impedance parameters
27 G1 = 1+Ro/RL;
28 G2 = 1+Rinf/RL;
29 SingleColeParameters = [G1 G2 tau alpha];
30
31 % Calculating magnitude response of filter circuit from transfer
32 % function
33 IdealMag = SingleColeMagnitude(SingleColeParameters, w);
34 semilogx(f, IdealMag);
35 NoiseMag = awgn(IdealMag, 60);
36
37 % initial conditions for optimization routine
38 G1guess = 1/NoiseMag(1);
39 G2guess = 1/NoiseMag(length(NoiseMag));
40

```



```

41 x0 = [G1guess G2guess 0.75 1e-6];
42 %configure the optimset for use with lsqcurvefit
43 options = optimset('lsqcurvefit');
44
45 % lower and upper bounds for optimization routine
46 lb = [0 0 0 0];
47 ub = [inf inf inf inf];
48 % Extracting impedance parameters using least squares curve fitting
49 [SingleColeExtracted,error] = lsqcurvefit(@SingleColeMagnitude,x0 ...
    ,w,NoiseMag,lb,ub,options);
50 % Errors of LSQ extracted parameters compared to ideal values
51 RelativeError=(SingleColeParameters-SingleColeExtracted) ...
    ./SingleColeParameters*100;
52 % Plot ideal response vs. extracted response for comparison
53 semilogx(f,NoiseMag,f,SingleColeMagnitude(SingleColeExtracted, ...
    w),'o');

```

Listing A.9: MATLAB function to generate the magnitude response of a single-dispersion Cole impedance

A.1.6 Magnitude Double-Dispersion NLSF Extraction

```

1 % File:      DoubleColeMagnitudeResponseRun
2 % Author:    Todd Freeborn
3 % Email:     todd.freeborn@gmail.com
4 % Description
5 %           Purpose of this script is to apply a non-linear least
6 %           squares fitting routine on simulated frequency responses
7 %           of the Double Dispersion Cole-Cole impedance model, to
8 %           extract the 7 parameters that characterize it
9 clear all;
10 close all;
11
12 global RL
13 RL = 100;
14
15 % Set up frequency vectors
16 f = logspace(1, log10(25e6), 50);
17 w = 2*pi*f;
18 s = 1i*w;
19
20 % Set double-dispersion Cole impedance parameters
21 Rinf = 885;
22 R1 = 889;
23 R2 = 626;
24 alpha1 = 0.5414;
25 alpha2 = 0.7653;
26 C1 = 19e-9;
27 C2 = 5.1e-6;

```

```

28 DoubleColeParameters = [Rinf R1 R2 alpha1 alpha2 C1 C2];
29
30 % Set number of initial conditions
31 initialConditions = zeros(50, 7);
32 [R, C] = size(initialConditions);
33
34 % Set upper and lower bounds for optimization routine
35 lb2 = [0 0 0 0 0 0 0];
36 ub2 = [inf inf inf inf inf inf inf];
37
38 % Generate ideal step response
39 IdealMag = DoubleColeMagnitudeResponse(DoubleColeParameters,w);
40 NoiseMag = awgn(IdealMag, 60);
41
42 Mag0 = NoiseMag(1);
43 MagInf = NoiseMag(length(NoiseMag));
44 voInfinity = 10^(MagInf/20);
45 voZero = 10^(Mag0/20);
46
47 RinfGuess = RL*(1-voInfinity)/voInfinity;
48 R12Guess = (RL-voZero*(RinfGuess+RL))/voZero;
49
50 lb = [0 0 0 0.5 0.5 1e-9 1e-9];
51 ub = [RinfGuess 2*R12Guess 2*R12Guess 1 1 1e-3 1e-3];
52
53 % Randomly generate values for alpha1, alpha2, C1, and C2 between
54 % the upper and lower bounds
55 for i = 1:1:C
56     initialConditions(:,i) = lb(i) + (ub(i)-lb(i)).*rand(R,1);
57 end
58
59 for i=1:1:R
60     R1 = initialConditions(i,2);
61     R2 = initialConditions(i,3);
62
63     while(R1 + R2 < R12Guess)
64         R1 = lb(2) + (ub(2)-lb(2)).*rand(1,1);
65         R2 = lb(3) + (ub(3)-lb(3)).*rand(1,1);
66     end
67     initialConditions(i,1) = RinfGuess;
68     initialConditions(i,2) = R1;
69     initialConditions(i,3) = R2;
70 end
71
72 % Apply the non-linear least squares fitting to the noisy
73 % step response
74 options = optimset('lsqcurvefit');
75 MinError = inf;
76 for i = 1:1:R
77     [newParameters,error] = lsqcurvefit( ...
78         @DoubleColeMagnitudeResponse,initialConditions(i,:),w,NoiseMag,lb2,ub2, ..
79         options);
78     if(error<MinError)
79         DoubleColeExtracted = newParameters;

```

```

80         MinError = error;
81     end
82 end
83
84 % Vector to quickly visually compare values
85 Errors1 = (DoubleColeExtracted-DoubleColeParameters) ...
            ./DoubleColeParameters*100;
86 BestFitParameters2 = size(DoubleColeExtracted);
87 BestFitParameters2(1) = DoubleColeExtracted(1);
88 BestFitParameters2(2) = DoubleColeExtracted(3);
89 BestFitParameters2(3) = DoubleColeExtracted(2);
90 BestFitParameters2(4) = DoubleColeExtracted(5);
91 BestFitParameters2(5) = DoubleColeExtracted(4);
92 BestFitParameters2(6) = DoubleColeExtracted(7);
93 BestFitParameters2(7) = DoubleColeExtracted(6);
94 Errors2 = (BestFitParameters2-DoubleColeParameters) ...
            ./DoubleColeParameters*100;
95 if (mean(abs(Errors1)) < mean(abs(Errors2)))
96     ErrorsParameters = Errors1;
97 else
98     DoubleColeExtracted = BestFitParameters2;
99     ErrorsParameters = Errors2;
100 end
101
102 RelativeError = abs(DoubleColeParameters-DoubleColeExtracted) ./ ...
                DoubleColeParameters*100;
103 semilogx(f, NoiseMag, f, DoubleColeMagnitudeResponse( ...
                DoubleColeExtracted,w), 'o');

```

Listing A.10: MATLAB code for the generation of the magnitude response of the double-dispersion Cole impedance model and the extraction of its parameters

```

1 %   Function: DoubleColeMagnitudeResponse.m
2 %   Author: Todd Freeborn
3 %   Email: todd.freeborn@gmail.com
4 %   Description:
5 %       Function to generate the magnitude response of the
6 %       double-dispersion Cole impedance model
7 function output = DoubleColeMagnitudeResponse(ColeImpedance,w)
8     global RL
9
10    Rinf = ColeImpedance(1);
11    R1 = ColeImpedance(2);
12    R2 = ColeImpedance(3);
13    alpha1 = ColeImpedance(4);
14    alpha2 = ColeImpedance(5);
15    C1 = ColeImpedance(6);
16    C2 = ColeImpedance(7);
17
18    X0 = (w.^(alpha1+alpha2)*cos((alpha1+alpha2)*pi/2)+ ...
          w.^alpha1/C2/R2*cos(alpha1*pi/2)+ ...
          w.^alpha2/C1/R1*cos(alpha2*pi/2)+1/C1/C2/R1/R2);

```

```

19     X1 = (w.^(alpha1+alpha2)*sin((alpha1+alpha2)*pi/2)+ ...
        w.^alpha1/C2/R2*sin(alpha1*pi/2)+ ...
        w.^alpha2/C1/R1*sin(alpha2*pi/2));
20     X2 = (w.^(alpha1+alpha2)*cos((alpha1+alpha2)*pi/2)+ ...
        w.^alpha1*(Rinf+R2+RL)/C2/R2/(Rinf+RL)*cos(alpha1*pi/2)+ ...
        w.^alpha2*(Rinf+R1+RL)/C1/R1/(Rinf+RL)*cos(alpha2*pi/2)+ ...
        (Rinf+R1+R2+RL)/C1/C2/R1/R2/(Rinf+RL));
21     X3 = (w.^(alpha1+alpha2)*sin((alpha1+alpha2)*pi/2)+ ...
        w.^alpha1*(Rinf+R2+RL)/C2/R2/(Rinf+RL)*sin(alpha1*pi/2)+ ...
        w.^alpha2*(Rinf+R1+RL)/C1/R1/(Rinf+RL)*sin(alpha2*pi/2));
22     output = 20*log10(RL/(Rinf+RL)*sqrt(X0.^2+X1.^2)./ ...
        (sqrt(X2.^2+X3.^2)));
23 end

```

Listing A.11: MATLAB function to generate the magnitude response of a double-dispersion Cole impedance

A.2 Supercapacitor Model

A.2.1 Voltage-Excited Step Response NLSF Extraction

```

1  %   Function: FractionalSupercapVoltageStepRun.m
2  %   Author: Todd Freeborn
3  %   Email: todd.freeborn@gmail.com
4  %   Description:
5  %       This script will generate the output response of a
6  %       voltage-excited fractional supercapacitor impedance model
7  %       and extract the parameters from that generated response
8  %       using a least-squares fitting after adding Guassian white
9  %       noise
10 clear all;
11 close all;
12
13 % Set fractional supercapacitor impedance parameters
14 Rs = 5;
15 C = 0.01;
16 alpha = 0.5;
17 SupercapParameters = [C Rs alpha];
18
19 global E Vcc R
20 Vcc = 5; % Set voltage-step amplitude (Vcc)
21 E = 9; % Set Mittag-Leffler simulation accuracy (E)
22 R = 180;
23
24 t = logspace(-6, 3, 50); % Set length in time of simulation
25
26 % Generate ideal step response

```

```

27 IdealStepResponse = FractionalSupercapVoltageStep( ...
    SupercapParameters, t);
28 % Add 60 dB Gaussian white noise to ideal step response
29 NoiseStepResponse = awgn(IdealStepResponse, 60);
30
31 % Configure the optimset for use with lsqcurvefit
32 options = optimset('lsqcurvefit');
33 % Set lower and upper bounds for optimization routine
34 lb = [0 0 0];
35 ub = [inf inf inf];
36
37 v0 = NoiseStepResponse(1);
38 RsGuess = v0*R/(Vcc-v0);
39 x0 = [RsGuess 30 0.75];
40
41 % Apply the non-linear least squares fitting to the noisy
42 % step response
43 [SuperCapExtracted, sError] = lsqcurvefit( ...
    @FractionalSupercapVoltageStep,x0,t,NoiseStepResponse,lb,ub, ...
    options);
44
45 RelativeErrors = abs(SupercapParameters-SuperCapExtracted)./ ...
    SupercapParameters*100;
46 semilogx(t, FractionalSupercapVoltageStep(SupercapParameters,t),t ...
    ,FractionalSupercapVoltageStep(SuperCapExtracted,t),'o');
47 xlabel('Time (s)'); ylabel('Voltage (V)');

```

Listing A.12: MATLAB code for the generation of the voltage-excited step response of the fractional supercapacitor impedance model and the extraction of its parameters

```

1 % Function: FractionalSupercapVoltageStep.m
2 % Author: Todd Freeborn
3 % Email: todd.freeborn@gmail.com
4 % Description:
5 %     Function to generate the step response of a voltage-
6 %     excited fractional supercapacitor impedance model
7 function output = FractionalSupercapVoltageStep(ColeImpedance, t)
8     global R Vcc E
9     C = ColeImpedance(1);
10    Rs = ColeImpedance(2);
11    alpha = ColeImpedance(3);
12
13    z = -t.^alpha/(R+Rs)/C;
14    output = Vcc/(R+Rs)*(t.^alpha/C.*mlf(alpha, alpha+1,z,E)+ ...
        Rs*mlf(alpha,1,z,E));
15 end

```

Listing A.13: MATLAB function to generate voltage excited step response of a fractional supercapacitor impedance

APPENDIX B

SIMPLIFIED CURRENT-EXCITED STEP-RESPONSE DERIVATION

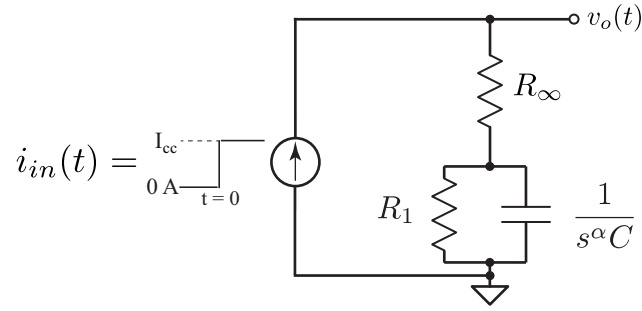


Figure B.1: Theoretical circuit to apply a step-current input to the single-dispersion Cole impedance model.

The initial analysis presented in [100] analyzed the response of the output voltage response of the single-dispersion Cole impedance, given in Fig. B.1, to an input step current of amplitude I_{cc} by applying a nodal analysis in the s -domain, yielding the expression

$$V_o(s) = \frac{I_{cc}}{s} \left[\frac{R_1 + R_\infty + s^\alpha R_\infty R_1 C}{s^\alpha R_1 C + 1} \right] \quad (\text{B.1})$$

From (B.1) the derivation in [100] continues as:

$$\begin{aligned} V_o(s) &= \frac{I_{cc}}{s} \left[\frac{R_1 + R_\infty + s^\alpha R_\infty R_1 C}{s^\alpha R_1 C + 1} \right] \\ &= \frac{I_{cc}}{s} \left[\frac{R_1 + R_\infty}{s^\alpha R_1 C + 1} + \frac{s^\alpha R_\infty R_1 C}{s^\alpha R_1 C + 1} \right] \\ &= I_{cc} \left[\frac{R_1 + R_\infty}{R_1 C} \cdot \frac{s^{-1}}{s^\alpha + \frac{1}{R_1 C}} + R_\infty \frac{s^{\alpha-1}}{s^\alpha + \frac{1}{R_1 C}} \right] \end{aligned}$$

$$v_o(t) = I_{cc} \left[\frac{R_1 + R_\infty}{R_1 C} \cdot t^\alpha E_{\alpha, \alpha+1} \left(\frac{-t^\alpha}{R_1 C} \right) + R_\infty E_{\alpha, 1} \left(\frac{-t^\alpha}{R_1 C} \right) \right] \quad (B.2)$$

which yields the output-voltage expression presented in Section 2.1 by (2.7). Using this expression required simulation of two Mittag-Leffler terms to generate each step response. Though a simplified expression of the output voltage to the current-step excitation was presented in [106] which requires the simulation of only a single Mittag-Leffler term to generate the step response. This expression presented in Section 2.2.2 by (2.23) can also be derived from (B.1) by continuing as:

$$\begin{aligned} V_o(s) &= \frac{I_{cc}}{s} \left[\frac{R_1 + R_\infty + s^\alpha R_\infty R_1 C}{s^\alpha R_1 C + 1} \right] \\ &= \frac{I_{cc}}{s} \left[\frac{R_1 + R_\infty + R_\infty (s^\alpha R_1 C)}{s^\alpha R_1 C + 1} \right] \\ &= \frac{I_{cc}}{s} \left[\frac{R_1 + R_\infty + R_\infty (s^\alpha R_1 C + 1 - 1)}{s^\alpha R_1 C + 1} \right] \\ &= \frac{I_{cc}}{s} \left[\frac{R_1 + \cancel{R_\infty} - \cancel{R_\infty} + R_\infty (s^\alpha R_1 C + 1)}{s^\alpha R_1 C + 1} \right] \\ &= \frac{I_{cc}}{s} \left[\frac{R_1 + R_\infty (s^\alpha R_1 C + 1)}{s^\alpha R_1 C + 1} \right] \\ &= \frac{I_{cc}}{s} \left[\frac{R_1}{s^\alpha R_1 C + 1} + \frac{R_\infty (s^\alpha R_1 C + 1)}{s^\alpha R_1 C + 1} \right] \\ &= \frac{I_{cc}}{s} \left[\frac{R_1}{s^\alpha R_1 C + 1} + R_\infty \right] \\ &= I_{cc} \left[\frac{1}{C} \cdot \frac{s^{-1}}{s^\alpha + \frac{1}{R_1 C}} + \frac{R_\infty}{s} \right] \\ v_o(t) &= I_{cc} \left[\frac{t^\alpha}{C} E_{\alpha, \alpha+1} \left(\frac{-t^\alpha}{R_1 C} \right) + R_\infty \right] \quad (B.3) \end{aligned}$$

MATLAB simulations of (B.2) and (B.3) when $I_{cc} = 1$ mA, $R_\infty = R_1 = 1$ k Ω , $C = 1$ μ F and α is varied from 0.5 to 1 are given in Fig. B.2 as solid lines and black circles, respectively, showing perfect agreement with each other. By simplifying the step-response expression we can significantly reduce the simulation time of the step response. The time required to simulate 1000 instances of (B.2) and (B.3) when $R_\infty = R_1 = 1$ k Ω , $C = 1$ μ F and $\alpha =$

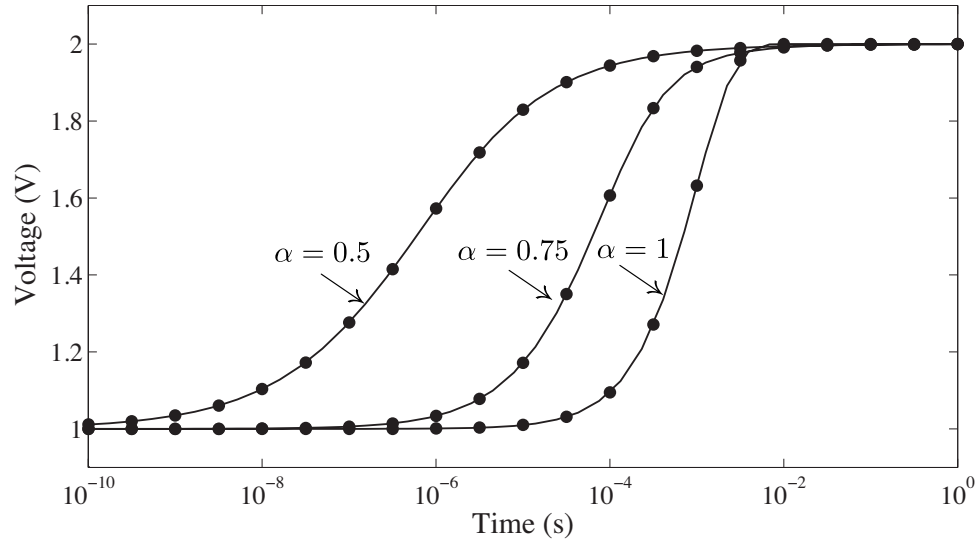


Figure B.2: MATLAB simulations of (B.2) and (B.3) when $R_\infty = R_1 = 1 \text{ k}\Omega$, $C = 1 \text{ }\mu\text{F}$ and α is varied from 0.5 to 1 as solid lines and black circles, respectively.

0.5 from $t = 0.1 \text{ }\mu\text{s}$ to 1 s with 25 logarithmically spaced datapoints with Mittag-Leffler accuracy of 10^{-7} required 34.11 s and 22.19 s, respectively. Showing a decrease of 34.9% in execution time using (B.2) over (B.3) which will also decrease the time required to extract the Cole impedance parameters from a collected step response dataset using a NLSF which requires numerous simulations of the step response.

B.1 MATLAB Simulated Extractions

The accuracy and time required to extract the Cole impedance parameters using both (B.2) and (B.3) in the non-linear least squares fitting applied to MATLAB simulated step responses of an apricot ($R_\infty = 406 \text{ }\Omega$, $R_1 = 12.49 \text{ k}\Omega$, $C = 62.34 \text{ nF}$, $\alpha = 0.739$) [51]. For these simulations an input-step of 0.1 mA was set while varying both the accuracy of the simulated Mittag-Leffler function and the number of initial conditions. When applying non-linear least squares fitting, the solver has the best chance to determine the absolute minimum if the supplied initial condition (x_0) is close to the solution set. We can estimate initial conditions of $R_\infty \approx v_o(1\text{ }\mu\text{s})/I_{cc}$ and $R_1 \approx v_o(1\text{ s})/I_{cc} - R_\infty$ from the collected dataset and randomly generating values such that $0.1 \text{ nF} \leq C \leq 1 \text{ mF}$ and $0.5 \leq \alpha \leq 1$, selected

Mittag-Leffler Accuracy ($10^{-x}\%$)	$(R_{\infty}, R_1, C, \alpha)$ Average Error Average Solving Time (s)			
	1 Initial Condition		5 Initial Conditions	
	(B.3)	(B.2)	(B.3)	(B.2)
$x = 7$	(−4.25, 0.10, −9.28, 1.04)	(−4.61, 0.11, −10.2, 1.13)	(0.06, 0.0001, −0.19, 0.02)	(0.04, 0.0008, −0.28, 0.03)
	3.10	4.95	13.11	20.90
$x = 5$	(−9.33, 0.33, 10.1, 1.02)	(−8.55, 0.31, −9.19, 0.93)	(−0.72, 0.03, −3.37, 0.39)	(−1.22, 0.05, −3.94, 0.46)
	1.25	2.18	5.08	9.67

Table B.1: Average relative errors and extraction times of impedance parameters using (B.3) and (B.2) from 1000 MATLAB simulated step responses of an apricot with 50 dB SNR Gaussian white noise.

based on reported values in literature. However, these random guesses for C and α may not be very close to the solution and yield instead a local minimum and not the absolute minimum. With this in mind multiple initial conditions were applied to the solver to find a more accurate result.

For example, 1 and 5 initial conditions are supplied to the solver for 1000 simulations of the apricot step response with 50 dB SNR Gaussian white noise and Mittag-Leffler accuracies of 10^{-x} where $x = 7$ and 5. The average error of the extracted impedance parameters $(R_{\infty}, R_1, C, \alpha)$ and the extraction time for each set of initial conditions and Mittag-Leffler accuracies are given in Table B.1. For these MATLAB simulations, the datasets consisted of 25 logarithmically spaced datapoints from 1 ns to 1 s and were executed on a 2.4 GHz Core 2 Duo iMac running MATLAB 7.12.0. From the results in Table B.1, the accuracy of the extracted parameters increases with increasing number of initial conditions and increasing accuracy of the simulated Mittag-Leffler function. The average accuracy increases by an order of magnitude when we increase from 1 to 5 initial conditions. Of significant note is the reduction in time required to extract the impedance parameters using (B.3) over (B.2) with negligible impact on the accuracy. From the simulations we see average decreases of 37.3% to 47.4% in the extraction time using (B.3) over (B.2). Confirming the significant decrease in execution time required to extract the impedance parameters by reducing the

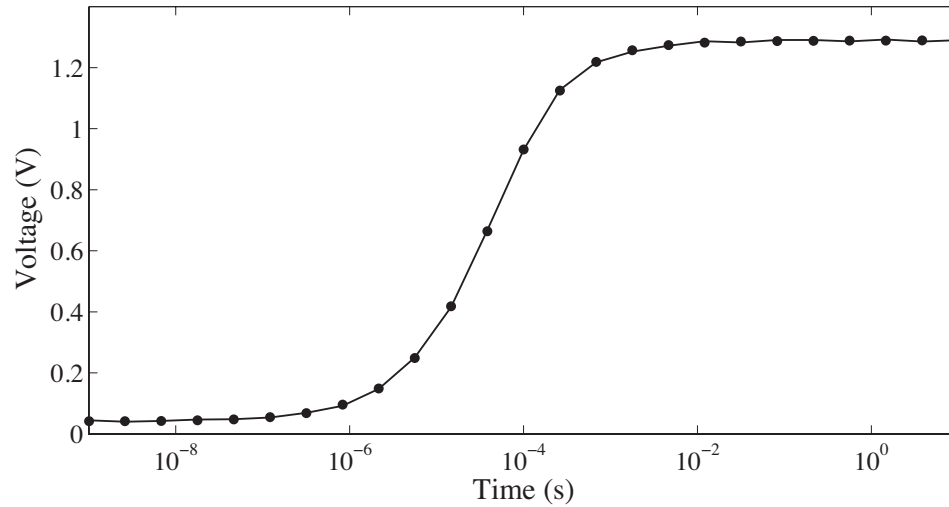


Figure B.3: MATLAB simulated step response of (B.3) using an apricot parameters ($R_{\infty} = 406 \, \Omega$, $R_1 = 12.49 \, \text{k}\Omega$, $C = 62.34 \, \text{nF}$, $\alpha = 0.739$) with 50 dB SNR Gaussian white noise and using extracted parameters as a solid line and black circles, respectively.

number of Mittag-Leffler terms in the step response model for data-fitting. A sample simulated apricot step response with the added noise is given as a solid line in Fig. B.3 with the simulated response using the extracted parameters using (B.3) given as black circles. Using 10 initial conditions and Mittag-Leffler accuracy of 10^{-7} , the extracted impedance parameters have relative errors of $(R_{\infty}, R_1, C, \alpha) = (-1.31, 0.08, 3.31, -0.278)\%$ compared to the ideal and were extracted in 21.9 s. Using (B.2) for the extraction yielded similar relative errors but required 33.8 s, showing a reduction of 35.2% in the extraction time for this case. The accuracy differences between (B.2) and (B.3) likely result from slight numerical differences introduced between simulations requiring two and one simulation of the Mittag-Leffler function, respectively, as well as the optimization routine itself. The *lsqcurvefit* function requires a gradient which, if not provided, is estimated via finite differences which could yield different results and contribute to the deviations between the extracted parameters using the least squares fitting.

APPENDIX C

APPROXIMATED CONSTANT PHASE ELEMENT

While fractional order circuit models show a significant number of applications in biomedicine and biology there are a lack of simulation tools to aid in the simulation of fractional order systems. Fractional circuit models are not currently supported by circuit simulation software packages and instead require integer order approximations typically realized using RC ladder topologies [114, 115]. There are many methods to realize approximations of CPEs that include Continued Fraction Expansions (CFEs) and rational approximation methods [7]. In this work, a CFE method [110] was selected to model the CPEs for PSPICE simulations which begins with the CFE of $(1+x)^\alpha$ given by

$$(1+x)^\alpha = \frac{1}{1 - \frac{\alpha x}{1 + \frac{(1+\alpha)x}{2 + \frac{(1-\alpha)x}{3 + \frac{(2+\alpha)x}{2 + \frac{(2-\alpha)x}{5 + \dots}}}}} \quad (\text{C.1})$$

which after substituting $x = s - 1$ into (C.1) realizes an approximation of s^α , with the order determined by the number of terms that are collected. For example, collecting 8 terms of (C.1) when $\alpha = -0.5$ yields

$$\frac{1}{s^{0.5}} \approx \frac{s^4 + 36s^3 + 126s^2 + 84s + 9}{9s^4 + 84s^3 + 126s^2 + 36s + 1} \quad (\text{C.2})$$

$$\begin{aligned} &\approx \frac{1}{9} + \frac{0.2291313787}{s + 0.03109120413} + \frac{0.2962962975}{s + 0.3333333333} + \frac{1.899696037}{s + 7.548632170} \\ &\quad + \frac{0.5378392488}{s + 1.420276625} \end{aligned} \quad (\text{C.3})$$

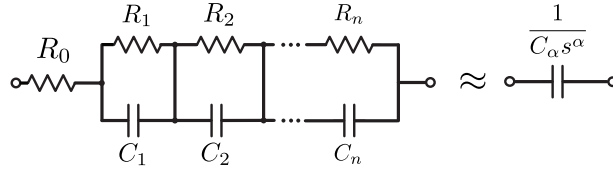


Figure C.1: RC ladder structure to realize a n^{th} order integer approximation of a CPE with pseudo-capacitance C_α .

Note that this creates an approximation of the CPE centered around the frequency 1 rad/s. Next, using the approximation of (C.3) the fractional Laplace transform operator can be physically realized using the RC ladder network in Fig. C.1. The impedance of this RC ladder network is

$$Z = R_0 + \frac{1/C_1}{s + \frac{1}{R_1 C_1}} + \frac{1/C_2}{s + \frac{1}{R_2 C_2}} + \dots + \frac{1/C_n}{s + \frac{1}{R_n C_n}} \quad (\text{C.4})$$

The resistor and capacitor values for the RC ladder in Fig. C.1 can be determined through equating terms of (C.3) to (C.4). Then an approximate CPE with any desired capacitance, C_α , centered around any frequency, ω_c , can be designed by applying magnitude and frequency scaling factors to the component values in the ladder realization. The resistor and capacitor values become

$$R_s = R \cdot k_m \quad (\text{C.5})$$

$$C_s = \frac{C}{k_f k_m} \quad (\text{C.6})$$

where R_s and C_s are the scaled resistor and capacitor values, R and C are the unscaled resistor and capacitor values, $k_m = \frac{1}{C_\alpha \omega_c^\alpha}$ is the magnitude scaling factor (where C_α is the CPE pseudo-capacitance) and $k_f = \omega_c$ is the frequency scaling factor. The component values required for the 4th order approximation of the CPE with capacitance of 12.6 μF and order of $\alpha = 0.5$ using the RC ladder network in Fig. C.1, shifted to a center frequency of 1 kHz, are given in Table C.1. The magnitude and phase of the ideal (solid line) and 4th order approximated (dashed) CPE with pseudo-capacitance 12.6 μF and order $\alpha = 0.5$,

n	0	1	2	3	4
$R_n (\Omega)$	111.1	251.7	378.7	888.9	7369.7
C_n (nF)	-	68.9	296	537	695

Table C.1: Component values to realize 4th order approximations of fractional order capacitors with a center frequency of 1 kHz.

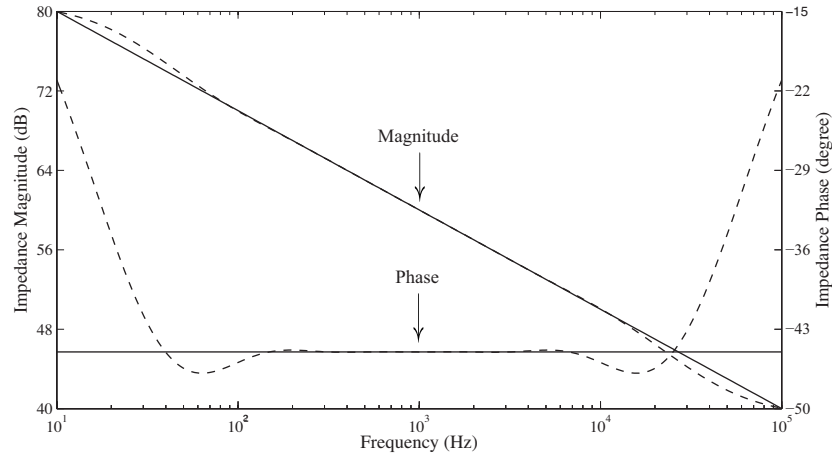


Figure C.2: Magnitude and phase response of the approximated fractional order capacitor (dashed) compared to the ideal (solid) with capacitance of $12.6 \mu\text{F}$ and order $\alpha = 0.5$ after scaling to a center frequency of $f_c = 1 \text{ kHz}$.

shifted to a center frequency of $f_c = \frac{\omega_c}{2\pi} = 1 \text{ kHz}$, are presented in Fig. C.2. From this figure we observe that the approximation is very good over almost 4 decades, from 200 Hz to 70 kHz, for the magnitude and almost 2 decades, from 200 Hz to 6 kHz, for the phase. In these regions, the deviation of the approximation from ideal does not exceed 1.23 dB and 0.23° for the magnitude and phase, respectively. The MATLAB script that generated the CPE approximation and component values to realize it with the RC ladder circuit is given in Program Listing C.1. This script requires that MATLAB is configured to use the MAPLE symbolic engine as it is a further generalization of a previously designed MAPLE script that realized the CPE.

```

1 % File: CPEscriptInitial.m
2 % Author: Todd Freeborn
3 % Email: todd.freeborn@gmail.com
4 % Description:
5 % To convert Dr. Maundy's MAPLE script that computes the
6 % resistor and capacitor values of a distributed RC tree to
7 % approximate a Constant Phase Element (CPE) to a Matlab
8 % script.
9 clear all;
10 close all;
11 % Set the parameters for the RC ladder that is to be built
12 alpha = 0.5;
13 C = 12.6e-6;
14 order = 4;
15 fo = 1e3;
16
17 % Values to be used in scaling the approximation
18 wo = 2*pi*fo;
19 kf = wo;
20 km = 1/C/(wo^alpha);
21 n = order*2;
22
23 % Direct conversion of Maple code to be executed using the MAPLE
24 % symbolic engine inside MATLAB (note: this requires the MAPLE
25 % symbolic engine to be incorporated with MATLAB)
26 s = sym('s'); x = sym('x'); b = sym('beta');
27
28 maple('with(numtheory):');
29 out1 = maple('cfrac', (1+x)^b, x, n, 'simple');
30 out1 = subs(out1, x, s-1);
31
32 sa_h = maple('cfrac', out1);
33 total = sa_h;
34 total = maple('normal', total, 'expanded');
35 total = maple('sort', total, s, 'descending');
36 s_alpha = collect(total, s);
37
38 s_alpha = subs(s_alpha, b, -alpha);
39 s_alpha = maple('normal', s_alpha);
40 s_alpha = maple('simplify', s_alpha);
41
42 num = maple('numer', s_alpha);
43 num = maple('collect', num, s);
44
45 % Conversion of the coefficients calculated in MAPLE to double
46 % values that can be turned into vectors for use in MATLAB
47 mainCoeff = maple('coeff', num, s, order);
48 coeff = zeros(order+1, 1);
49 for i = 1:length(coeff);
50     coeff(i) = maple('coeff', num, s, i-1)/mainCoeff;
51 end
52 coeff(order+1, 1) = 1;
53 numTest = ones(1, order+1); denTest = ones(1, order+1);

```

```

54 for i = 1:1:length(numTest)
55     denTest(1,i) = coeff(i);
56     numTest(1,i) = coeff(length(numTest)+1-i);
57 end
58
59 % Calculating the residues of the approximated expression
60 [R, P, K] = residue(numTest, denTest);
61 Rin = K*km;
62
63 % Calculating the required capacitor and resistor values to build
64 % approximated CPE
65 Cap = zeros(size(R)); Res = zeros(size(R));
66 for i = 1:1:length(R)
67     Cap(i) = 1/R(i)/kf/km;
68     Res(i) = -R(i)/P(i)*km;
69 end
70
71 exponent = 0;
72 while( fo > 1)
73     exponent = exponent + 1;
74     fo = fo/10;
75 end
76 f = logspace(exponent-4, exponent+4, 201);
77 w = 2*pi*f; s = 1i*w;
78 Z = Rin;
79 for i= 1:1:length(R)
80     Z = Z + (1/Cap(i))./(s+1/Res(i)/Cap(i));
81 end
82
83 % Plotting the ideal FC vs. the approximated
84 Ideal = 1./(s.^alpha)/C;
85 magIdeal = 20*log10(abs(Ideal)); magApprox = 20*log10(abs(Z));
86
87 phaseIdeal = 180/pi*unwrap(angle(Ideal));
88 phaseApprox = 180/pi*unwrap(angle(Z));
89
90 subplot(2,1,1); semilogx(f, magIdeal, f, magApprox, '—');
91 title('Impedance Magnitude of Ideal and Approximated FC');
92 ylabel('Magnitude Impedance (dB)'); xlabel('Frequency (Hz)');
93 subplot(2,1,2); semilogx(f, phaseIdeal, f, phaseApprox, '—');
94 title('Impedance Phase of Ideal and Approximated FC');
95 ylabel('Impedance Phase (degrees)'); xlabel('Frequency (Hz)');
96 values = [Rin; Res; Cap];

```

Listing C.1: MATLAB code for the generation of the approximated CPE by an RC ladder structure.

APPENDIX D

SUPERCAPACITOR STEP-RESPONSE TEST CIRCUITS

To test the high capacity supercapacitors required the design and manufacture of a custom test fixture resulting from their terminals being aluminum which is not easily soldered. In this design, two printed circuit boards (PCBs) were used to contact both the positive and negative terminals of the supercapacitors with electrical connections then easily made to test equipment with peripheral hardware on the PCBs. The design files for these two boards are given in Fig. D.1(a) with the manufactured boards (sponsored by AP Circuits) given in Fig. D.1(b). This board implements the circuit shown Fig. 4.4 allowing a step input to be applied directly from a DC power supply with high current output to the supercapacitor through a resistor with high power rating. This direct, rather than buffered, connection was done to apply a current upwards of 5 A to the supercapacitors.

The two PCBs were held in contact with the supercapacitor terminals by using elastic bands to apply pressure from each board to the terminals which provided a secure connection for the tests and provided flexibility to change supercapacitors which had significantly different heights based on the capacity. Four $\frac{1}{4}$ " wooden dowels were used to stabilize the PCBs around the supercapacitor. This test fixture connected to a HP3631A DC power supply is given in Fig. D.2. The components and part numbers to populate the test PCBs and their descriptions are given in Table D.1.

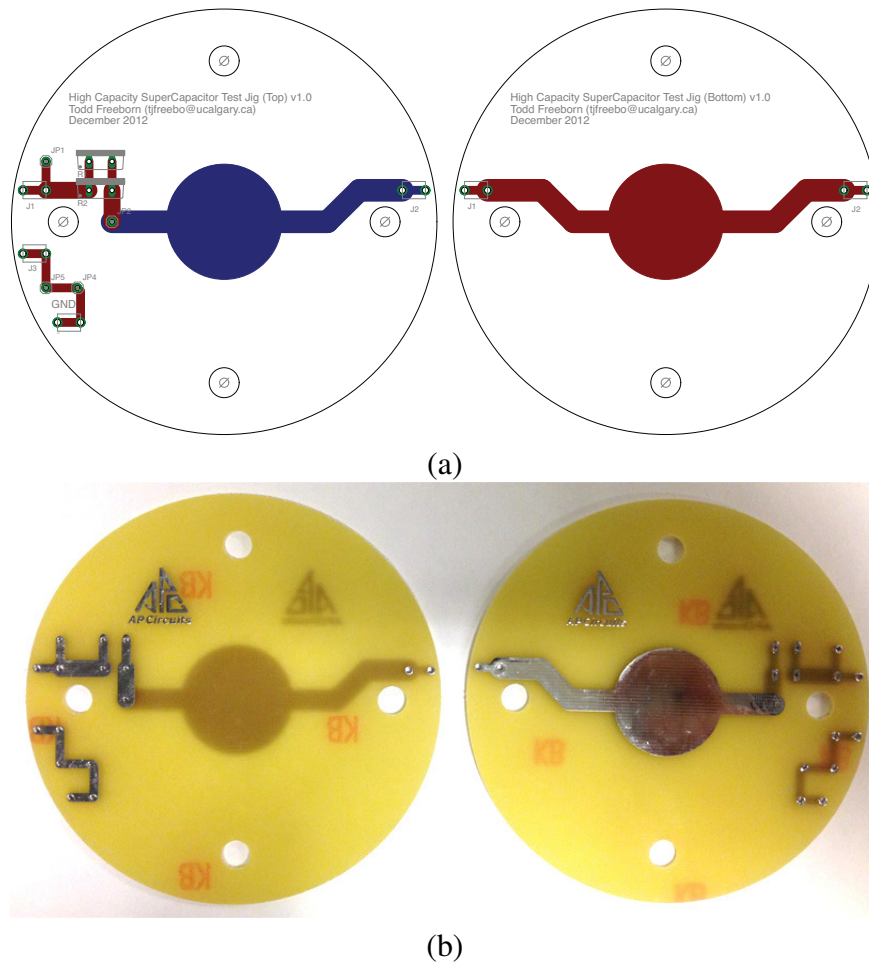


Figure D.1: (a) Designed and (b) manufactured PCBs to build high capacity supercapacitor step-response test fixture.

Designator	Digi-Key P/N	Description
J1	J576-ND	Red, horizontal, insulated mini-jack connector
J2	J575-ND	White, horizontal, insulated mini-jack connector
J3, J4	J577-ND	Black, horizontal, insulated mini-jack connector
JP1, JP2, JP3, JP4	929647-09-04-EU-ND	4-position, 0.1", straight, breakaway connector
R1, R2	PWR221T-30-1R00F-ND	1 Ω , $\pm 1\%$, 30 W resistor

Table D.1: Components, part-numbers, and descriptions of components to populate high capacity supercapacitor test PCBs.



Figure D.2: BCAP1500-P270-K05 supercapacitor from Maxwell Technologies Inc. installed between the high capacity supercapacitor test PCBs.